2017

Characterization of Cellulose Synthesis Complexes in *Physcomitrella patens*

Xingxing Li
University of Rhode Island, xingxing_li@my.uri.edu

CHARACTERIZATION OF CELLULOSE SYNTHESIS COMPLEXES IN PHYSCOMITRELLA PATENS

BY

XINGXING LI

A DISSERTATION SUBMITTED IN PARTIAL FULFILLMENT OF THE REQUIREMENTS FOR THE DEGREE OF

DOCTOR OF PHILOSOPHY

IN

XINGXING LI

UNIVERSITY OF RHODE ISLAND

2017

DOCTOR OF PHILOSOPHY DISSERTATION

OF

XINGXING LI

APPROVED:

Dissertation Committee:

Major Professor Alison Roberts

Joanna Norris

Gongqin Sun

Steven Irvine

Nasser H. Zawia
DEAN OF THE GRADUATE SCHOOL

UNIVERSITY OF RHODE ISLAND
2017

ABSTRACT

Due to the enormous economic value and significance of cellulose in human consumption and plant cell walls, production of cellulose microfibrils is considered to be one of the most critical biochemical processes in plant biology. In the past decades, cellulose biosynthesis has been extensively studied in vascular plants. More and more fundamental questions related to this key process are being answered. One such question is: What are the protein components of the enzymatic complex for cellulose synthesis? In seed plants, membrane-embedded rosette Cellulose Synthesis Complexes (CSCs) producing cellulose microfibrils are obligate hetero-oligomeric, being assembled from three functionally distinct and non-interchangeable cellulose synthase (CESA) isoforms. For instance, *Arabidopsis* has two types of CSCs. One contains AtCESA1, AtCESA3, and AtCESA6, involved in cellulose synthesis in primary cell walls; the other consists of AtCESA4, AtCESA7, and AtCESA8, specialized for secondary cell wall deposition. Recently, the stoichiometry for the three *Arabidopsis* CESAs forming a CSC was determined to be a 1:1:1 molecular ratio. The constructive neutral evolution hypothesis has been proposed as a mechanism for evolution of these hetero-oligomeric complexes.

Physcomitrella patens, a non-vascular plant, is one of the most popular models for genetics studies. A relatively small genome, dominant haploid phase, and high rate of homologous recombination make *P. patens* a simple and efficient system for genetic manipulation. Seven CESA genes (*PpCESA3, PpCESA4, PpCESA5, PpCESA6, PpCESA7, PpCESA8,* and *PpCESA10*) were identified in the *P. patens* genome, but proteins encoded by these genes are not orthologs of functionally distinct seed plant

CESAs according to phylogenetic studies. The similar rosette-type of CSCs were observed in *P. patens* by freeze-fracture electron microscopy. It is not yet known whether the *P. patens* CSCs are homo-oligomeric complexes consisting of only a single type of CESA, or hetero-oligomeric complexes assembled by different CESAs like those in seed plants. Knowing this information would be helpful for understanding the roles of different CESAs that compose seed plant CSCs. Furthermore, answers to this question potentially will be useful for testing the constructive neutral evolution hypothesis, since moss CESAs diversified independently from seed plant CESAs.

In this study, I generated PpCESA knock out (KO) mutants. Morphological analyses were carried out to identify mutant phenotypes of these KOs together with several previously made KO mutants. Cellulose defects in these mutants were also analyzed using quantitative methods. Reverse transcriptase PCR (RT-qPCR) was performed to examine the expression of all seven PpCESAs in KO lines to identify co-expressed PpCESAs that potentially reside within the same CSCs as the deleted PpCESA. Immunoblot analysis using specific monoclonal antibodies was used as an additional method to detect co-expression based on the accumulation of the protein products of these *PpCESA* genes. Finally, I carried out Co-immunoprecipitation (Co-IP) assays to identify potential physical interactions between different PpCESA isoforms. The results show that functionally distinct CESA isoforms have evolved in the moss *P. patens* independently from seed plants, and CSCs synthesizing cellulose microfibrils in secondary cell walls of *P. patens* gametophore leaves are obligate hetero-oligomeric complexes. Meanwhile, our research also suggests that PpCESA5 alone is able to form

homo-oligomeric CSCs, making *P. patens* an intriguing model in which to study the evolution of cellulose synthase.

ACKNOWLEDGMENTS

Special thanks to my major advisor, Dr. Alison Roberts, and co-advisor, Dr. Joanna Norris, for giving me an opportunity to join their lab and guiding me on all of my projects. During the four and half years of my graduate school, not only I learned lab techniques from Dr. Roberts and Dr. Norris, but also I learned scientific thinking from them which will be important for my future career. As an international student whose native language is not English, I really appreciate the kind assistance of my advisors in writing of my manuscripts. I would like to thank my committee members, Dr. Gongqin Sun and Dr. Steve Irvine, for their valuable time and comment for my projects and dissertation. I would like to thank the lab members, Mai Tran, Arielle Chaves, and Tess Scavuzzo-Duggan, for teaching me lab skills, helping me with trouble shooting, and providing insights into my projects. I especially appreciate Dr. Jodi Camberg, Dr. Niall Howlett, Dr. Gongqin Sun, Dr. Steve Irvine and their students for allowing me to use their equipment, sharing their protocols, and helping me setup experiments. Finally, I would like to thank my parents for being supportive financially and spiritually throughout these years of my life in the United States.

PREFACE

Manuscript format is used in this dissertation.

Chapter 2 is a manuscript published in *Plant Physiology* 175:210-222 on August 2, 2017 in collaboration with Joanna H. Norris, Mai L. Tran, Bailey Mallon, Danielle Mercure, and Arielle M. Chaves at the University of Rhode Island; Shixin Huang and Seong H. Kim from the Pennsylvania State University; Ashley Tan and Rachel A. Burton from University of Adelaide, Australia; and Allison M.L. Van de Meene and Monika L. Doblin from University of Melbourne, Australia. In this manuscript, I did the phenotypic analysis for some *PpCESAs* knockout (KO) mutants and quantitative PCR analysis for expression of the PpCESA genes in the KO mutants. Results of these experiments lead to a hypothesis: obligate hetero-oligomeric Cellulose Synthesis Complexes (CSCs) are involved in the *P. patens* secondary cell wall deposition.

Chapter 3 is a manuscript that that describes work done in collaboration with Mai L. Tran and Joanna H. Norris at the University of Rhode Island. This manuscript includes morphological analysis for several *PpCESA* KO mutants that identified roles for PpCESA4 and PpCESA10 in tip-growing protonema. In this manuscript, I generated the quadruple *ppcesa4/6/7/10*KO mutants. I also did most of the morphological assays, except the assays for *ppcesa6/7*KOs and *ppcesa3/8*KOs.

Chapter 4 is a manuscript that includes work done in collaboration with John McManus from the University of Pennsylvania State University. In this manuscript, the hypothesis proposed in Chapter 1 is directly tested by reverse transcriptase PCR and Co-immunoprecipitation. In this manuscript, the majority of the work was done by me, except the creation of antibodies. The manuscript is currently being prepared for

submission. Mass spectrometry (M.S.) data will be added to the manuscript before submission. Currently, the M.S. data will be collected and analyzed with our collaboration with Ian S. Wallace and Tori Speicher at University of Nevada, Reno.

TABLE OF CONTENTS

ABSTRACT ..... **ii**

ACKNOWLEDGMENTS ..... **v**

PREFACE ..... **vi**

TABLE OF CONTENTS ..... **viii**

LIST OF TABLES ..... **xi**

LIST OF FIGURES ..... **xii**

CHAPTER 1 ..... **1**

Introduction 1

Cellulose synthesis complex (CSC) 1

Cellulose synthase catalytic subunits (CESAs) 1

Interactions between CESAs 3

Other components of the CSC 4

The moss *Physcomitrella patens* 5

Thesis outline 6

References cited 10

CHAPTER 2 (Manuscript 1) **15**

Short title: CESA functional specialization in *Physcomitrella* 15

Abstract 18

Introduction 19

Results 21

PpCESA3 and PpCESA8 function in secondary cell wall deposition 21

Secondary cell wall microfibrils are helically oriented and laterally aggregated 24

PpCESA proteins are functionally specialized 27

Discussion 29

PpCESA3 and PpCESA8 function redundantly in cellulose deposition in stereid secondary cell walls. 29

CESA evolution in both *P. patens* and Arabidopsis involve sub-functionalization and neo-functionalization. 30
Secondary cell wall microfibrillar texture is similar in mosses and vascular plants. 32
Mosses and vascular plants have acquired similar secondary cell walls through convergent evolution..... 33
Materials and methods..... 35
Vector construction..... 35
Culture and transformation of *P. patens*..... 37
Genotype analysis..... 38
Phenotype analysis..... 38
Cell wall analysis..... 40
High pressure freezing-freeze substitution and transmission electron microscopy 41
Sum Frequency Generation spectroscopy..... 42
Reverse transcription quantitative PCR..... 42
Statistical analysis..... 43
Supplemental Materials..... 43
Acknowledgements 44
References cited: 53
CHAPTER 3 (Manuscript 2) 72
Short title: Identify functions of CESAs in *Physcomitrella* 72
Abstract 73
Introduction 74
Results 76
Genotyping and morphological analysis (rhizoid, caulonema, and gametophore) of *ppcesa4/6/7/10*KO..... 76
Cellulose deposition of the secondary cell wall in *ppcesa4/6/7/10*KO 77
Morphological analysis of protonema colonies..... 78
Discussion 79
Materials and methods..... 82
Transformation and genotyping..... 82

Polarization microscopy of cell wall birefringence 83
Pontamine fast scarlet 4B (S4B) fluorescence histochemistry 83
Analysis of caulonema and rhizoid development 84
Protonema colony morphology assay 84
Statistical analysis 85
Supplemental Materials 85
Acknowledgments 85
References cited: 91
CHAPTER 4 (Manuscript 3) 99
Short title: *Physcomitrella* has hetero-oligomeric Cellulose Synthesis Complexes 99
Abstract 101
Introduction 102
Results 104
Expression levels of *PpCESAs* in the knockout mutants by RT-qPCR 104
Characterization of the PpCESA antibodies 105
Protein expression profiling of the PpCESAs 106
Interactions between the PpCESAs 106
Discussion 108
Materials and methods 112
Culture conditions 112
Vector construction and transformation 112
RNA extraction and Real-time quantitative PCR (RT-qPCR) 113
Generation of monoclonal anti-PpCESAs 114
Protein expression profiling of the PpCESAs 115
Co-immunoprecipitation 115
Statistical analysis 116
Supplemental Materials 117
Acknowledgments 117
References cited: 122

LIST OF TABLES

TABLE PAGE

Manuscript 1

Table 1. Caulonema length for wild type and *ppcesa3/8*KOs grown on vertical plates in the dark. 45

Table S1. Primers used for vector construction and genotype analysis. 59

Manuscript 2

Table S1. Primers designed for knockout vector construction and genotyping. 95

Table S2. Data of morphological analysis of protonema colonies. 96

Manuscript 3

Table S1. Primers for amplification of HA-tagged *PpCESAs*. 127

Table S2. Peptide antigens, designed to regions of each PpCESA, used to raise specific antibodies for each PpCESA isoform. 128

LIST OF FIGURES

TABLE PAGE

Manuscript 1

Figure 1: Phenotypes of *ppcesa3/8*KO, *ppcesa3*KO, and *ppcesa8*KO compared to wild type *Physcomitrella patens*. 46

Figure 2: Quantitative analysis of S4B fluorescence intensity in leaf midribs of *P. patens* wild type, *ppcesa*KO, and rescue lines. 47

Figure 3: Polarized light microscopy with first order retardation plate. 48

Figure 4: Transmission electron microscopy images of leaf midribs of *P. patens*. 49

Figure 5: Sum Frequency Generation (SFG) spectroscopy of *P. patens* leaves. 50

Figure 6: RT-qPCR analysis of *PpCESA3* and *PpCESA8* expression in wild type, *ppcesa3*KOs, and *ppcesa8*KOs. 51

Figure 7: Quantitative analysis of S4B fluorescence intensity in leaf midribs. 52

Fig. S1. Genotype analysis of *ppcesa8*, *ppcesa3* and *ppcesa3/8* KO lines. 62

Fig. S2: Phenotype analysis of a *ppcesa3/*8 double KO line. 63

Fig. S3. Transmission electron microscopy images of leaf cell walls from wild type and *cesa*KO lines of *P. patens*. 64

Fig. S4. Thickness of outer cell walls measured from transmission electron microscopy images. 65

Fig. S5: *P. patens* wild type and KO lines cultured on medium containing 1 μM naphthalene acetic acid (auxin) to induce rhizoid initiation and inhibit leaf initiation 66

Fig. S6: *P. patens* wild type and KO lines cultured in the dark on vertically oriented plates containing medium supplemented with 35 mM sucrose to test for caulonema gravitropism. 67

Fig. S7. Western blot analysis of protein expression for *P. patens* lines. 68

Fig. S8: PCR-based genotyping of *ppcesa6/7* KO lines. 69

Fig. S9: PCR-based genotyping of *ppcesa4/10* KO lines. 70

Fig. S10: Quantification method for S4B fluorescence. Representative paired DIC....52

Manuscript 2

Figure 1: PCR-based genotyping of *ppcesa4/6/7/10*KO lines. 86

Figure 2: B clade PpCESAs are not required for gametophore development. 87

Figure 3: Quantitative analysis of S4B fluorescence intensity in leaf midribs of wild-type *P. patens* and B clade *PpCESA* knockout (KO) mutants. 88

Figure 4: Representative micrographs showing morphologies of B clade PpCESA knockout (KO) mutants protonemal colonies undergoing tip growth 89

Figure 5: Protonemal colonies of knockout (KO) mutant lines and wild-type *P. patens* line were analyzed for area, circularity, and solidity. 90

Figure S1: B clade PpCESAs are not required for rhizoid development. 97

Figure S2: B-clade PpCESAs are not required for caulonema development and gravitropism. 98

Manuscript 3

Figure 1: Heat map of *PpCESA* expression in *PpCESA* knockout (KO) mutants. 118

Figure 2: Antibody specificity test 119

Figure 3: PpCESA protein expression in wild-type *P. patens*. 120

Figure 4: Co-immunoprecipitation (Co-IP) of PpCESAs. 121

Figure S1: RT-qPCR analysis of *PpCESA* expression in the KO mutants. 129

Figure S2: Quantitative analysis of S4B fluorescence intensity in leaf midribs of *P. patens* wild-type (Gd11), *ppcesa8*KO-lox16 (*8*KO), and *PpCESA8pro::HA-PpCESA8* (HA-CESA8). 130

Figure S3: Quantitative analysis of S4B fluorescence intensity in leaf midribs of *P. patens* wild-type (Gd11), *ppcesa6/7*KO-lox23 (6/7KO), and *PpCESA7pro::HA-PpCES7* (HA-CESA7). 131

CHAPTER 1

Introduction

Cellulose synthesis complex (CSC)

Cellulose is a biopolymer of β(1,4)-linked glucose that forms the microfibrils essential in most plant cell walls. It is extensively used for a variety of commercial and industrial purposes including lumber and textiles. The synthesis of cellulose in plants is catalyzed by enzymatic complexes called cellulose synthesis complexes (CSCs) located in plasma membrane (Delmer et al., 1999; Somerville et al., 2006; McFarlane et al., 2014). The membrane-bound CSCs were first observed to have a "rosette" structure and to be associated with the ends of microfibrils in freeze-fracture electron microscopy studies on maize (Mueller & Brown, 1980). By searching a cotton fiber EST library for sequences similar to a bacterial cellulose synthase gene, the first putative plant gene encoding a cellulose synthase catalytic subunit (CESA) was identified (Pear et al., 1996). Antibodies against cotton CESAs were later produced to label the rosettes in freeze-fractured bean hypocotyls indicating CESAs are components of the multi-protein complexes inserted into the plasma membrane (Kimura et al., 1999).

Cellulose synthase catalytic subunits (CESAs)

Among currently identified protein components in CSCs, CESAs are implicated by all sorts of evidence (Delmer et al., 1999; Somerville et al., 2006; McFarlane et al., 2014) to be the only functional subunits that produce individual glucan chains. Recently, a

heterologously-expressed CESA isoform, PttCESA8, from *Populus* tremula x tremuloides (hybrid aspen), was reconstituted in liposomes and shown to be functional for cellulose microfibril formation in vitro (Purushotham et al., 2016) for the first time.

The CESA family is contained within the glycosyltransferase-2 (GT-2) superfamily characterized by an eight-transmembrane-helix topology and conserved cytosolic substrate binding and catalytic site (McFarlane et al., 2014). The site for substrate binding and catalysis consists of a D, DxD, D, QxxRW motif and is predicted to be in the loop bounded by transmembrane helix 2 and 3 (Pear et al., 1996). In this motif, the first two conserved aspartic acid residues are predicted to bind the substrate, UDP-glucose. This was supported by the results of mutational analysis (Pear et al., 1996). The functions of these residues have been confirmed by x-ray crystallography of bacterial cellulose synthase (Morgan et al., 2013). The third aspartic acid is thought to be involved in the addition of UDP-glucose to the existing glucan, and the QxxRW region is predicted to be a binding site for the growing glucan chain (Morgan et al., 2013). Compared with bacterial cellulose synthase, plant CESAs are larger. That is because the plant CESA also contains an extended N-terminal Zn-binding RING finger domain, a plant-conserved domain within the N-terminal cytoplasmic loop, and a class-specific domain within the central cytoplasmic loop in addition to the conserved catalytic region (Pear et al., 1996). These domains are specific to plants, hence they are thought to be important for the interactions between the CESA subunits and presumably involved in the formation of the rosette CSCs (McFarlane et al., 2014).

Interactions between CESAs

CESA genes are members of multigene families in plants. For example, *Arabidopsis* has 10 *CESA* genes from which distinct combinations are required for primary and secondary cell wall synthesis (McFarlane et al., 2014). The *AtCESA4*, *AtCESA7*, and *AtCESA8* genes were first shown to be specifically involved in secondary cell wall deposition (Turner & Somerville, 1997; Taylor et al., 1999; Taylor et al., 2000; Taylor et al., 2003). The mRNAs of the three genes are found to be coregulated in microarray analysis (Brown et al., 2005; Persson et al., 2005a). Proteins encoded by the three genes physically interact and are exclusively required for assembly of CSCs in cells with thickened secondary walls (Taylor et al., 2000; Taylor et al., 2003).

Mutations in *AtCESA1*, *AtCESA3*, and *AtCESA6* cause primary cell wall defects (Arioli et al., 1998; Fagard et al., 2000; Burn et al., 2002; Robert et al., 2004). AtCESA3 and AtCESA6 interact with each other according to results of in vitro pull-down assays, and Bimolecular Fluorescence Complementation (BiFC) experiments show that AtCESA1, AtCESA3, and AtCESA6 can interact in vivo (Desprez et al., 2007). *AtCESA2* and *AtCESA5* were shown to be closely related and partially functionally redundant with *AtCESA6* (Desprez et al., 2007). In *Arabidopsis*, therefore, a primary wall CSC might consist of AtCESA1, AtCESA3, and one or perhaps several AtCESA6 like AtCESAs (McFarlane et al., 2014).

Characterization of CSCs has also been carried out in another vascular plant model, *Populus trichocarpa*. Two types of CSCs are identified in the xylem of *Populus* by co-immunoprecipitation (Co-IP) experiments: one type contains PdxtCESA7A and PdxtCESA8B; the other one contains PdxtCESA1A and PdxtCESA3 (Song et al.,

2010a). Altogether, current evidence suggests that vascular plant CSCs are obligately hetero-oligomeric. A theory known as constructive neutral evolution addresses how homo-oligomer complexes are driven towards hetero-oligomeric by neutral processes during evolution. According to this theory, in the initial complex assembled from multiple copies of the same subunit, additional obligate subunits could be evolved by gene duplication followed by relatively high frequency degenerative mutations causing specific interaction sites among them to be lost (Doolittle, 2012; Finnigan et al., 2012). A study showed that the extant Vo complex of the fungi V-ATPase proton pump which is composed of three obligate subunits, evolved from an ancient two-subunit complex by a gene duplication and subsequent complimentary loss of specific interfaces on each daughter isoforms on which they rely to interact with other subunits in the complex (Finnigan et al., 2012). So far, this is the only study that provided convincible experimental evidence. Hence, the generality of this hypothesis needs to be further tested. Plant CSCs are similar to the fungal Vo complex, which are also composed by paralogous CESA isoforms sharing a considerable amount of similarities. Thus, characterizing the CESAs in plant CSCs will be helpful for continuing testing this theory.

Other components of the CSC

Other than CESAs, several other protein components (Endo et al., 2009; Gu et al., 2010) of seed plant CSCs have been identified successively by Co-IP and BiFC. For instance, a putative endo-1,4-β-D-glucanase, KORRIGAN1 (KOR1), was identified to be a part of the primary cell wall CSCs in *Arabidopsis* (Vain et al., 2014). A microtubule-binding protein, Cellulose synthase interactive protein 1 (CSI1), was

discovered to associate with CSCs and serve as a linker protein between CSCs and microtubule (Li et al., 2012). Genetic evidence and the observed size of the cytosolic portion of the rosette demonstrated in electron micrographs (Bowling & Brown, 2008) imply that more other proteins related to cellulose synthesis might also participate in assembly of CSCs.

The moss *Physcomitrella patens*

Physcomitrella patens, a moss species, has also been shown to have rosette CSCs, but not members of the CESAs clades that contain the functionally distinct isoforms of the hetero-oligomeric CSCs in seed plants (Roberts et al., 2012). The *PpCESA* family includes seven members that cluster in two clades (Roberts & Bushoven, 2007). The A-clade contains *PpCESA3*, *PpCESA5*, and *PpCESA8*. The B-clade contains *PpCESA4*, *PpCESA6*, *PpCESA7*, and *PpCESA10*. Currently, the functions of these *P. patens* CESAs are still under investigation. It is also not yet known if *P. patens* and other mosses have homo-oligomeric or hetero-oligomeric CSCs. Understanding whether or not the PpCESAs serve distinct functions from those of the seed plant CESAs and determining the organization of *P. patens* CSCs will provide insight into the roles of the different CESA isoforms forming CSCs in seed plants, and possibly allow us to test the constructive neutral evolution hypothesis. *Physcomitrella patens* has many advantages as a research model for studying genetics, including a relatively small and fully sequenced genome and predominate haploid phase (Rensing et al., 2008; Zimmer et al., 2013). More importantly, *P. patens* is capable of being genetically manipulated as a result of its high rate of homologous recombination (Reski & Frank, 2005; D. G. Schaefer & Zrÿd, 1997) . Taking advantage of this

unique property, functions of genes of interest can be identified by knockout (KO) mutations (Schaefer, 2002).

Thesis outline

*ppcesa5*KOs have cellulose defects in primary cell walls affecting gametophore bud development and resulting in a "no leafy gametophore" phenotype (Goss et al., 2012). However, other single *PpCESA* KOs do not show obvious phenotypic changes. To investigate functions for the other *PpCESAs*, double *PpCESAs* KO mutants (*ppcesa3/8*KO, *ppcesa6/7*KO, and *ppcesa4/10*KO) were generated. In manuscript 1, we show that *ppcesa3/8*KOs has defects in secondary cell wall deposition in gametophore leaf midribs (Norris et al., 2017). I used reverse transcription quantitative PCR (RT-qPCR) analysis to measure the expression of *PpCESA3* and *PpCESA8* in corresponding *PpCESA* KO mutants. The results show that *PpCESA8* is up-regulated for the loss of *PpCESA3*, suggesting these two PpCESAs are partially functionally redundant. My phenotypic analysis of other double KO mutants revealed that *ppcesa6/7*KOs also have significantly decreased cellulose deposition in the midribs of gametophore leaves. This indicates that *PpCESA3*, *PpCESA8, PpCESA6,* and *PpCESA7* are all involved in cellulose deposition during secondary cell wall formation in gametophore leaves and may be members of the same CSCs. *Ppcesa4/10*KOs showed slightly but significantly decreased cellulose content in the midribs of gametophore leaves, suggesting a minor role of these two PpCESAs during secondary cell wall deposition. Together, this study provided important clues for characterization of composition and function of *P. patens* CSCs.

On the protein sequence level, PpCESAs within the same clade are highly similar, compared to lower similarity between the clade A and B PpCESAs. For instance, the clade B PpCESAs are 90-99% similar to each other and PpCESA6 and PpCESA7 differ by only three amino acids in protein sequence (Wise et al., 2010; Norris et al., 2017). This indicates that PpCESAs from this clade may have overlapping functions, which can mask potential phenotypic defects when carrying out mutational analysis. In manuscript 2, I show that quadruple *ppcesa4/6/7/10*KOs in which all B-clade PpCESAs are knocked out have dramatically reduced cellulose deposition in the midribs of gametophores as expected. However, overall morphology of leafy gametophores is normal in these quadruple KOs indicating the clade B PpCESAs are not required for gametophore morphogenesis. Since *ppcesa3/8*KOs also produce normal looking gametophores (Norris et al., 2017), current results of mutational analyses are consistent with the hypothesis that PpCESA5 forms homo-oligomeric CSCs responsible for cellulose deposition in primary cell walls during gametophore bud development.

In manuscript 2, I used quantitative analysis of colony morphology, to show that quadruple KOs are defective in tip-growth of protonemal filaments indicated by significantly increased circularity and solidity of protonema colonies regenerated from single protoplasts. Later, I found that knocking out *PpCESA4* and *PpCESA10* together is enough to cause this phenotype. *Ppcesa6/7*KOs are not different from wild-type in protonema colony morphology. Different phenotypes of *ppcesa6/7*KOs and *ppcesa4/10*KOs might be related to different gene expression patterns. As shown by previous studies, *PpCESA6* and *PpCESA7* are expressed in leafy gametophores at

higher levels, while *PpCESA4* and *PpCESA10* have higher expression in protonema filaments (Hiss et al., 2014; Tran & Roberts, 2016). The mutant phenotype of *ppcesa4/10*KOs indicates the PpCESA4 and PpCESA10 play some roles in tip-growing protonema cells, supporting the idea that cellulose is an essential cell wall component in cells undergoing tip growth (Newcomb & Bonnett, 1965; Emons & Wolters-Arts, 1983; Emons, 1994; Cosgrove, 2005; Park et al., 2011).

Results of mutational analyses suggest that CSCs involved in cellulose deposition in *P. patens* secondary cell walls might be hetero-oligomeric, consisting of PpCESAs from both A-clade and B-clade and I tested this hypothesis in manuscript 3. First, I measured expression of all seven PpCESAs by RT-qPCR analysis in knockout mutants in order to identify which PpCESAs are downregulated, as predicted for those that reside within the same CSC as the deleted PpCESA. Results show that gene expression of *PpCESA3*, *PpCESA8*, and *PpCESA7* are co-regulated. Western blot analysis of the microsomal proteins isolated from wild-type *P. patens* showed that PpCESA3, PpCESA8, and PpCESA6/7 are highly expressed in gametophores which is consistent with cellulose defects in secondary cell walls of corresponding KO mutants. The Co-immunoprecipitation (Co-IP) experiments show that PpCESA3 and PpCESA8 can both interact with PpCESA6/7 *in planta*. Taken together, these results are consistent with the hypothesis that PpCESA3, PpCESA8, PpCESA6, and PpCESA7 form obligate hetero-oligomeric CSCs that produce cellulose microfibrils during secondary cell wall deposition in *P. patens* gametophore leaves.

To summarize, my work reveals: 1) In the moss *P. patens*, CSCs that synthesize cellulose in secondary cell walls are obligate hetero-oligomeric, with members from

clade A and clade B; 2) PpCESA4 and PpCESA10 function in elongating protonemal implying important role of cellulose in tip growth; 3) Clade B PpCESAs are not required for gametophore morphogenesis, which also means PpCESA5 possibly can form homo-oligomeric CSCs. Taken together, these discoveries indicate that functional specialization of CESAs occurred independently in mosses and seed plants through both subfunctionalization and neofunctionalization, which are consistent with the theory of constructive neutral evolution providing a possible mechanism for the convergent evolution of plant CSCs.

References cited

Arioli, T., Peng, L., Betzner, A. S., Burn, J., Wittke, W., Herth, W., … Williamson, R. E. (1998). Molecular Analysis of Cellulose Biosynthesis in Arabidopsis. *Science*, *279*(5351), 717–720. https://doi.org/10.1126/science.279.5351.717

Bowling, A. J., & Brown, R. M. (2008). The cytoplasmic domain of the cellulose-synthesizing complex in vascular plants. *Protoplasma*, *233*(1–2), 115. https://doi.org/10.1007/s00709-008-0302-2

Brown, D. M., Zeef, L. A. H., Ellis, J., Goodacre, R., & Turner, S. R. (2005). Identification of Novel Genes in Arabidopsis Involved in Secondary Cell Wall Formation Using Expression Profiling and Reverse Genetics. *The Plant Cell*, *17*(8), 2281–2295. https://doi.org/10.1105/tpc.105.031542

Burn, J. E., Hocart, C. H., Birch, R. J., Cork, A. C., & Williamson, R. E. (2002). Functional Analysis of the Cellulose Synthase GenesCesA1, CesA2, and CesA3 in Arabidopsis. *Plant Physiology*, *129*(2), 797–807. https://doi.org/10.1104/pp.010931

Cosgrove, D. J. (2005). Growth of the plant cell wall. *Nature Reviews. Molecular Cell Biology*, *6*(11), 850–861. https://doi.org/10.1038/nrm1746

Delmer, D. P. (1999). CELLULOSE BIOSYNTHESIS: Exciting Times for A Difficult Field of Study. *Annual Review of Plant Physiology and Plant Molecular Biology*, *50*(1), 245–276. https://doi.org/10.1146/annurev.arplant.50.1.245

Desprez, T., Juraniec, M., Crowell, E. F., Jouy, H., Pochylova, Z., Parcy, F., … Vernhettes, S. (2007). Organization of cellulose synthase complexes involved in primary cell wall synthesis in Arabidopsis thaliana. *Proceedings of the National Academy of Sciences*, *104*(39), 15572–15577. https://doi.org/10.1073/pnas.0706569104

Emons, A. M. C. (1994). Winding threads around plant cells: a geometrical model for microfibril deposition. *Plant, Cell & Environment*, *17*(1), 3–14. https://doi.org/10.1111/j.1365-3040.1994.tb00261.x

Emons, Anne Mie C., & Wolters-Arts, A. M. C. (1983). Cortical microtubules and microfibril deposition in the cell wall of root hairs ofEquisetum hyemale. *Protoplasma*, *117*(1), 68–81. https://doi.org/10.1007/BF01281786

Endo, S., Pesquet, E., Yamaguchi, M., Tashiro, G., Sato, M., Toyooka, K., … Demura, T. (2009). Identifying New Components Participating in the Secondary Cell Wall Formation of Vessel Elements in Zinnia and Arabidopsis. *The Plant Cell*, *21*(4), 1155–1165. https://doi.org/10.1105/tpc.108.059154

Fagard, M., Desnos, T., Desprez, T., Goubet, F., Refregier, G., Mouille, G., … Höfte, H. (2000). PROCUSTE1 Encodes a Cellulose Synthase Required for Normal Cell Elongation Specifically in Roots and Dark-Grown Hypocotyls of Arabidopsis. *The Plant Cell*, *12*(12), 2409–2423.

Goss, C. A., Brockmann, D. J., Bushoven, J. T., & Roberts, A. W. (2012). A CELLULOSE SYNTHASE (CESA) gene essential for gametophore morphogenesis in the moss Physcomitrella patens. *Planta*, *235*(6), 1355–1367. https://doi.org/10.1007/s00425-011-1579-5

Gu, Y., Kaplinsky, N., Bringmann, M., Cobb, A., Carroll, A., Sampathkumar, A., … Somerville, C. R. (2010). Identification of a cellulose synthase-associated protein required for cellulose biosynthesis. *Proceedings of the National Academy of Sciences of the United States of America*, *107*(29), 12866–12871. https://doi.org/10.1073/pnas.1007092107

Hiss, M., Laule, O., Meskauskiene, R. M., Arif, M. A., Decker, E. L., Erxleben, A., … Rensing, S. A. (2014). Large-scale gene expression profiling data for the model moss Physcomitrella patens aid understanding of developmental progression, culture and stress conditions. *The Plant Journal*, *79*(3), 530–539. https://doi.org/10.1111/tpj.12572

Kimura, S., Laosinchai, W., Itoh, T., Cui, X., Linder, C. R., & Brown, R. M. (1999). Immunogold Labeling of Rosette Terminal Cellulose-Synthesizing Complexes in the Vascular Plant Vigna angularis. *The Plant Cell*, *11*(11), 2075–2085. https://doi.org/10.1105/tpc.11.11.2075

Li, S., Lei, L., Somerville, C. R., & Gu, Y. (2012). Cellulose synthase interactive protein 1 (CSI1) links microtubules and cellulose synthase complexes. *Proceedings of the National Academy of Sciences*, *109*(1), 185–190. https://doi.org/10.1073/pnas.1118560109

McFarlane, H. E., Döring, A., & Persson, S. (2014). The Cell Biology of Cellulose Synthesis. *Annual Review of Plant Biology*, *65*(1), 69–94. https://doi.org/10.1146/annurev-arplant-050213-040240

Morgan, J. L. W., Strumillo, J., & Zimmer, J. (2013). Crystallographic snapshot of cellulose synthesis and membrane translocation. *Nature*, *493*(7431), 181–186. https://doi.org/10.1038/nature11744

Mueller, S. C., & Brown, R. M. (1980). Evidence for an intramembrane component associated with a cellulose microfibril-synthesizing complex in higher plants. *The Journal of Cell Biology*, *84*(2), 315–326.

Newcomb, E. H., & Bonnett, H. T. (1965). CYTOPLASMIC MICROTUBULE AND WALL MICROFIBRIL ORIENTATION IN ROOT HAIRS OF RADISH. *The Journal of Cell Biology*, *27*(3), 575–589.

Norris, J. H., Li, X., Huang, S., van de Meene, A., Tran, M. L., Killeavy, E., … Roberts, A. W. (2017). Functional specialization of cellulose synthase isoforms in a moss shows parallels with seed plants. *Plant Physiology*. https://doi.org/10.1104/pp.17.00885

Park, S., Szumlanski, A. L., Gu, F., Guo, F., & Nielsen, E. (2011). A role for CSLD3 during cell-wall synthesis in apical plasma membranes of tip-growing root-hair cells. *Nature Cell Biology*, *13*(8), 973–980. https://doi.org/10.1038/ncb2294

Pear, J. R., Kawagoe, Y., Schreckengost, W. E., Delmer, D. P., & Stalker, D. M. (1996a). Higher plants contain homologs of the bacterial celA genes encoding the catalytic subunit of cellulose synthase. *Proceedings of the National Academy of Sciences of the United States of America*, *93*(22), 12637–12642.

Pear, J. R., Kawagoe, Y., Schreckengost, W. E., Delmer, D. P., & Stalker, D. M. (1996b). Higher plants contain homologs of the bacterial celA genes encoding the catalytic subunit of cellulose synthase. *Proceedings of the National Academy of Sciences of the United States of America*, *93*(22), 12637–12642.

Persson, S., Wei, H., Milne, J., Page, G. P., & Somerville, C. R. (2005). Identification of genes required for cellulose synthesis by regression analysis of public microarray data sets. *Proceedings of the National Academy of Sciences of the United States of America*, *102*(24), 8633–8638. https://doi.org/10.1073/pnas.0503392102

Purushotham, P., Cho, S. H., Díaz-Moreno, S. M., Kumar, M., Nixon, B. T., Bulone, V., & Zimmer, J. (2016). A single heterologously expressed plant cellulose synthase isoform is sufficient for cellulose microfibril formation in vitro. *Proceedings of the National Academy of Sciences*, *113*(40), 11360–11365. https://doi.org/10.1073/pnas.1606210113

Rensing, S. A., Lang, D., Zimmer, A. D., Terry, A., Salamov, A., Shapiro, H., … Boore, J. L. (2008). The *Physcomitrella* Genome Reveals Evolutionary Insights into the Conquest of Land by Plants. *Science*, *319*(5859), 64–69. https://doi.org/10.1126/science.1150646

Reski, R., & Frank, W. (2005). Moss (Physcomitrella patens) functional genomics--Gene discovery and tool development, with implications for crop plants and human health. *Briefings in Functional Genomics & Proteomics*, *4*(1), 48–57.

Robert, S., Mouille, G., & Höfte, H. (2004). The mechanism and regulation of cellulose synthesis in primary walls: lessons from cellulose-deficient Arabidopsis mutants. *Cellulose*, *11*(3–4), 351–364. https://doi.org/10.1023/B:CELL.0000046415.45774.80

Roberts, A. W., & Bushoven, J. T. (2006). The cellulose synthase (CESA) gene superfamily of the moss Physcomitrella patens. *Plant Molecular Biology*, *63*(2), 207–219. https://doi.org/10.1007/s11103-006-9083-1

Roberts, A. W., Roberts, E. M., & Haigler, C. H. (2012). Moss cell walls: structure and biosynthesis. *Plant Physiology*, *3*, 166. https://doi.org/10.3389/fpls.2012.00166

Schaefer, D. G., & Zrÿd, J. P. (1997). Efficient gene targeting in the moss Physcomitrella patens. *The Plant Journal: For Cell and Molecular Biology*, *11*(6), 1195–1206.

Schaefer, Didier G. (2002). A new moss genetics: targeted mutagenesis in Physcomitrella patens. *Annual Review of Plant Biology*, *53*, 477–501. https://doi.org/10.1146/annurev.arplant.53.100301.135202

Somerville, C. (2006). Cellulose Synthesis in Higher Plants. *Annual Review of Cell and Developmental Biology*, *22*(1), 53–78. https://doi.org/10.1146/annurev.cellbio.22.022206.160206

Song, D., Shen, J., & Li, L. (2010). Characterization of cellulose synthase complexes in Populus xylem differentiation. *New Phytologist*, *187*(3), 777–790. https://doi.org/10.1111/j.1469-8137.2010.03315.x

Taylor, N. G., Howells, R. M., Huttly, A. K., Vickers, K., & Turner, S. R. (2003). Interactions among three distinct CesA proteins essential for cellulose synthesis. *Proceedings of the National Academy of Sciences of the United States of America*, *100*(3), 1450–1455. https://doi.org/10.1073/pnas.0337628100

Taylor, N. G., Laurie, S., & Turner, S. R. (2000). Multiple Cellulose Synthase Catalytic Subunits Are Required for Cellulose Synthesis in Arabidopsis. *The Plant Cell*, *12*(12), 2529–2539. https://doi.org/10.1105/tpc.12.12.2529

Taylor, N. G., Scheible, W.-R., Cutler, S., Somerville, C. R., & Turner, S. R. (1999). The irregular xylem3 Locus of Arabidopsis Encodes a Cellulose Synthase Required for Secondary Cell Wall Synthesis. *The Plant Cell*, *11*(5), 769–779. https://doi.org/10.1105/tpc.11.5.769

Tran, M. L., & Roberts, A. W. (2016). Cellulose synthase gene expression profiling of Physcomitrella patens. *Plant Biology*, *18*(3), 362–368. https://doi.org/10.1111/plb.12416

Turner, S. R., & Somerville, C. R. (1997). Collapsed xylem phenotype of Arabidopsis identifies mutants deficient in cellulose deposition in the secondary cell wall. *The Plant Cell*, *9*(5), 689–701. https://doi.org/10.1105/tpc.9.5.689

Vain, T., Crowell, E. F., Timpano, H., Biot, E., Desprez, T., Mansoori, N., … Vernhettes, S. (2014). The Cellulase KORRIGAN Is Part of the Cellulose Synthase Complex. *Plant Physiology*, *165*(4), 1521–1532. https://doi.org/10.1104/pp.114.241216

Wise, H. Z., Saxena, I. M., & Brown, R. M. (2010). Isolation and characterization of the cellulose synthase genes PpCesA6 and PpCesA7 in Physcomitrella patens. *Cellulose*, *18*(2), 371–384. https://doi.org/10.1007/s10570-010-9479-6

Zimmer, A. D., Lang, D., Buchta, K., Rombauts, S., Nishiyama, T., Hasebe, M., … Reski, R. (2013). Reannotation and extended community resources for the genome of the non-seed plant Physcomitrella patens provide insights into the evolution of plant gene structures and functions. *BMC Genomics*, *14*, 498. https://doi.org/10.1186/1471-2164-14-498

Manuscript 1

Published in *Plant physiology*, September 2017

Short title: CESA functional specialization in *Physcomitrella*

Corresponding author:

Alison W. Roberts, Department of Biological Sciences, University of Rhode Island, 120 Flagg Road, Kingston RI 02881 USA, email: aroberts@uri.edu, telephone: 401-874-4098, ORCID ID: 0000-0002-7775-5589

Title: Functional specialization of cellulose synthase isoforms in a moss shows parallels with seed plants

Joanna H. Norris[a], Xingxing Li[a], Shixin Huang[b], Allison M.L. Van de Meene[c], Mai L. Tran[a], Erin Killeavy[a], Arielle M. Chaves[a], Bailey Mallon[a], Danielle Mercure[a], Hwei-Ting Tan[d], Rachel A. Burton[d], Monika S. Doblin[c], Seong H. Kim[b], Alison W. Roberts[a]

[a]Department of Biological Sciences, University of Rhode Island, Kingston RI 02881, USA

[b]Department of Chemical Engineering, The Pennsylvania State University, University Park, PA 16802, USA

[c]ARC Centre of Excellence in Plant Cell Walls, Plant Cell Biology Research Centre, School of BioSciences, The University of Melbourne, Victoria 3010, Australia.

[d]ARC Centre of Excellence in Plant Cell Walls, School of Agriculture, Food and Wine, University of Adelaide, Waite Campus, Glen Osmond, South Australia 5064, Australia

One sentence summary: Regulatory uncoupling of primary and secondary cellulose synthases occurred independently in mosses and seed plants, and is associated with convergent evolution of secondary wall structure.

List of author contributions: J.H.N. and A.W.R. conceived the project, and supervised and performed experiments; X.L., S.H., A.M.L.VdM., and M.L.T. designed and performed experiments, and analyzed the data; A.M.C., E.K., B.M., D.M. and H-T.T. performed experiments; S.H.K. supervised experiments; A.W.R. wrote the manuscript with contributions from J.H.N., S.H., A.M.L.V., S.H.K., R.A.B. and M.S.D. All authors read and approved the manuscript.

Funding information: This work was supported primarily by National Science Foundation Award IOS-1257047. Analysis of mutants by SFG spectroscopy was supported as part of The Center for LignoCellulose Structure and Formation, an Energy Frontier Research Center funded by the U.S. Department of Energy, Office of Science, Office of Basic Energy Sciences under Award Number DE-SC0001090. CBM3a affinity cytochemistry and freeze substitution transmission electron microscopy were supported by the Australian Research Council Centre for Excellence in Plant Cell Walls Grant CE1101007. High pressure freezing and transmission electron microscopy was undertaken at the Melbourne Advanced Microscopy Facility at the Bio21 Institute and the Biosciences Microscopy Unit at The University of Melbourne. DNA sequencing and qPCR were conducted using the Rhode Island Genomics and Sequencing Center, a Rhode Island NSF EPSCoR research facility, supported in part by the National Science Foundation EPSCoR Cooperative Agreement EPS-1004057.

Present addresses: BM, Neuroimaging Research Branch, National Institutes of Health, Baltimore, MD 21224, USA; DM, Pfizer Inc., Groton, CT 06340, USA; H-T Tan, Centre for Tropical Crops and Biocommodities, Queensland University of Technology, Brisbane, QLD 4000, Australia

Abstract

The secondary cell walls of tracheary elements and fibers are rich in cellulose microfibrils that are helically oriented and laterally aggregated. Support cells within the leaf midribs of mosses deposit cellulose-rich secondary cell walls, but their biosynthesis and microfibril organization have not been examined. Although the *Cellulose Synthase* (*CESA*) gene families of mosses and seed plants diversified independently, *CESA* knockout analysis in the moss *Physcomitrella patens* revealed parallels in CESA functional specialization of Arabidopsis and *P. patens*, with roles for both sub-functionalization and neo-functionalization. The similarities include regulatory uncoupling of the CESAs that synthesize primary and secondary cell walls, a requirement for two or more functionally distinct CESA isoforms for secondary cell wall synthesis, interchangeability of some primary and secondary CESAs, and some CESA redundancy. The cellulose-deficient midribs of *ppcesa3/8* knockouts provided negative controls for structural characterization of stereid secondary cell walls in wild type *P. patens*. Sum frequency generation spectra collected from midribs were consistent with cellulose microfibril aggregation, and polarization microscopy revealed helical microfibril orientation only in wild type leaves. Thus, stereid secondary walls are structurally distinct from primary cell walls, and they share structural characteristics with the secondary walls of tracheary elements and fibers. We propose a mechanism for convergent evolution of secondary walls in which deposition of aggregated and helically oriented microfibrils is coupled to rapid and highly localized cellulose synthesis enabled by regulatory uncoupling from primary wall synthesis.

Introduction

In vascular plants, cellulose is a major component of both primary cell walls that are deposited during cell expansion and secondary cell walls that are deposited after expansion has ceased (Carpita and McCann 2000). Secondary cell walls of water-conducting tracheary elements and supportive fibers are rich in cellulose with microfibrils arranged in helices that vary in angle according to developmental stage and environmental conditions (Barnett and Bonham 2004). Secondary cell wall microfibrils are also more aggregated than those of primary cell walls (Donaldson 2007; Fernandes et al. 2011; Thomas et al. 2014). Recently, Sum Frequency Generation (SFG) spectroscopy has been used to compare the mesoscale structure of cellulose microfibrils in primary and secondary cell walls. Both high cellulose content and microfibril aggregation contribute to a strong secondary cell wall signature in SFG spectra of mature angiosperm tissues (Barnette et al. 2012; Lee et al. 2014; Park et al. 2013).

Cellulose microfibrils are synthesized by cellulose synthase (CESA) proteins that function together as cellulose synthesis complexes (CSCs) in the plasma membrane (Delmer 1999; Kimura et al. 1999). Recent analyses of CSC and microfibril structure indicate that the rosette CSCs of land plants most likely contain 18 CESA subunits (Fernandes et al. 2011; Jarvis 2013; Newman et al. 2013; Nixon et al. 2016; Oehme et al. 2015; Thomas et al. 2014; Vandavasi et al. 2016) in a 1:1:1 ratio (Gonneau et al. 2014; Hill et al. 2014). Seed plants have six phylogenetic and functional classes of CESA proteins, three required for primary cell wall synthesis (Desprez et al. 2007; Persson et al. 2007) and three required for synthesis of the lignified secondary cell

walls of tracheary elements and fibers (Taylor et al. 2003). Mutation of any of the secondary CESAs results in a distinctive irregular xylem phenotype characterized by collapsed xylem tracheary elements and weak stems (Taylor et al. 2004). The secondary cell wall CESAs of Arabidopsis are regulated by master regulator NAC domain transcription factors that also activate genes required for the synthesis of other secondary cell wall components, such as xylan and lignin (Schuetz et al. 2013; Yang and Wang 2016; Zhong and Ye 2015).

The moss *Physcomitrella patens* (Hedw.) B. S. G. has seven *CESA* genes (Goss et al. 2012; Roberts and Bushoven 2007). Phylogenetic analysis has revealed that the *P. patens* CESAs do not cluster with the six CESA clades shared by seed plants (Roberts and Bushoven 2007). Like other mosses, *P. patens* lacks the lignified secondary cell walls that are characteristic of vascular plant tracheary elements and fibers. However, mosses do have support cells (stereids) with thick unlignifed cell walls (Kenrick and Crane 1997) and water-conducting cells (hydroids) that have thin cell walls and undergo programmed cell death like tracheary elements (Hebant 1977). Although the stereid cell walls of *P. patens* are known to contain cellulose (Berry et al. 2016), the mesoscale structure has not been examined. Only one of the seven *P. patens* CESAs has been characterized functionally. When *PpCESA5* was disrupted, gametophore buds failed to develop into leafy gametophores, instead forming irregular cell clumps. The associated disruption of cell expansion and cell division are consistent with an underlying defect in primary cell wall deposition (Goss et al. 2012). Recently it was shown that *PpCESA3* expression is regulated by the NAC transcription factor *PpVNS7*, along with thickening of stereid cell walls (Xu et al. 2014).

Here we show that PpCESA3 and PpCESA8 function in the deposition of stereid cell walls in the gametophore leaf midribs of *P. patens* and are sub-functionalized with respect to PpCESA5. We also used polarization microscopy and SFG to reveal similarities in the mesoscale organization of the microfibrils synthesized by PpCESA3 and PpCESA8 and those in the secondary cell walls of vascular plants. Finally, we propose a mechanism through which uncoupling of primary and secondary CESA regulation played a role in independent evolution of secondary cell walls with aggregated, helically arranged cellulose microfibrils in the moss and seed plant lineages.

Results

PpCESA3 and PpCESA8 function in secondary cell wall deposition

Cellulose synthase genes *PpCESA3* and *PpCESA8* were independently knocked out by homologous recombination in an effort to examine their roles in development and cell wall biosynthesis in *P. patens*. Stable antibiotic resistant lines generated by transforming wild type *P. patens* with CESA3KO or CESA8KO vectors were tested for integration of the vector and deletion of the target gene by PCR (Fig. S1). Integration was verified for five *ppcesa8*KO lines recovered from two different transformations, line 8KO5B from a transformation of the GD06 wild type line and lines 8KO4C, 8KO5C, 8KO7C and 8KO10C from a transformation of the GD11 wild type line (Fig. S1). Integration was verified for three *ppcesa3*KO lines recovered from a single transformation of GD11 and three double *ppcesa3/8*KO lines recovered from a single transformation of the *ppcesa8*KO5B line with the CESA3KO vector (Fig. S1).

The GD06 and GD11 lines are from independent selfings of the same haploid wild type line, as described in Materials and Methods.

The colonies that developed from wild type and KOs consisted of protonemal filaments and leafy gametophores (Fig. 1). Whereas wild type, *ppcesa3*KO, and *ppcesa8*KO gametophores grew vertically, the gametophores on *ppcesa3*/*8*KO colonies were unable to support themselves and adopted a horizontal orientation. Superficially *ppcesa3*/*8*KO colonies appeared to produce fewer gametophores (Fig. 1), but dissection revealed similar numbers of horizontal gametophores that had been overgrown by protonemal filaments. Thus, PpCESA3 and PpCESA8 are not required for gametophore initiation or morphogenesis, but they appear to contribute to structural support.

When examined with polarized light microscopy, the wild type gametophore leaves exhibited strong cell wall birefringence in the midribs and margins (Fig. 1). In contrast, the leaves produced by *ppcesa3/8*KOs lacked strong birefringence in these cells, consistent with reduced crystalline cellulose content. The *ppcesa3*KO leaves appeared similar to wild type leaves (Fig. 1) and *ppcesa8*KO leaves had an intermediate phenotype. Staining with the fluorescent cellulose binding dye Pontamine Fast Scarlet (S4B) (Anderson et al. 2010) produced similar results with strong fluorescence in the midribs of wild type and *ppcesa3*KO leaves, weak fluorescence in *ppcesa3*/*8*KO leaves, and intermediate fluorescence in *ppcesa8*KO leaves (Fig. 1). Cellulose Binding Module (CBM) 3a provides a third method for detecting cellulose and can be used to probe thin sections (Blake et al. 2006). In sections from fully expanded wild type leaves, the walls of the lamina cells were labeled relatively weakly

with CBM3a, whereas the thickened cell walls of the central midrib and bundle sheath cells were strongly labeled (Fig. 1). The same was true for *ppcesa3*KO leaves. However, midrib and bundle sheath cell labeling was nearly absent in *ppcesa3/8*KO and diminished in *ppcesa8*KO (Fig. 1) compared to wild type and *ppcesa3*KO. Differential interference contrast microscopy of the same sections showed enhanced contrast in wild type and *ppcesa3*KO midribs (Fig. 1). Partial cell collapse occurred during embedding in *ppcesa3/8*KO leaves (Fig. 1).

The cellulose content of the leaf midribs in wild type and single and double *ppcesa*KO mutants was quantified by measuring the intensity of S4B fluorescence. Statistical analysis confirmed that the S4B fluorescence was significantly reduced in double KOs, but not in *ppcesa3*KOs (Fig. 2). The intermediate phenotype of the *ppcesa8*KOs was confirmed and shown to be significantly different from both wild type and the double KOs (Fig. 2). Updegraff analysis showed that cellulose content of cell walls from whole *ppcesa3/8*KO gametophores (mean ±S.E. of three genetic lines = 33.8 ±0.034%) was reduced significantly ($p = 0.004$) compared to wild type (GD06, mean ±S.E. of three independent cultures = 60.1 ±0.030%).

To confirm that the observed *ppcesa3/8*KO phenotype was due to the absence of PpCESA3 and PpCESA8, the selection cassette was removed from *ppcesa3/8*KO-86 by Cre-mediated recombination of flanking *lox-p* sites (Vidali et al. 2010) to allow transformation with vectors that drive expression of PpCESA3 or PpCESA8 with their native promoters (Fig. S2). Stable antibiotic resistant lines selected for the presence of numerous erect gametophores were examined with polarization microscopy (Fig. S2). For the transformation with *proCESA8::CESA8*, 13 lines were examined, 6 of these

had strong midrib birefringence, and the first 3 were used for further analysis. For the transformation with *proCESA3::CESA3*, the first three lines examined had strong midrib birefringence and were used for further analysis. S4B staining confirmed that expression of PpCESA8 or PpCESA3 rescued the defects in cellulose deposition in the leaf midribs of the double *ppcesa3/8*KO (Fig. 2). Lines from the transformation with *proCESA8::CESA8* were expected to be restored to the wild type phenotype because *ppcesa3*KO, which also expresses *PpCESA8* under control of the *PpCESA8* promoter, showed no defects in cellulose deposition in the leaf midrib. All three *proCESA8::CESA8* lines had significantly stronger S4B fluorescence than *ppcesa8*KO. This demonstrates substantial restoration of the phenotype, although fluorescence was still significantly weaker than the wild type (Fig. 2). Two lines from a transformation with *proCESA3::CESA3* (3R29 and 3R52) were not significantly different from *ppcesa8*KO-5B, which is expected since they both lack *PpCESA8* and express *PpCESA3* under control of the *PpCESA3* promoter. In the third line (3R45) fluorescence was restored to wild type levels (Fig. 2). Y-axis scales differ between experiments due to the use of different exposure time settings.

Secondary cell wall microfibrils are helically oriented and laterally aggregated

A first order retardation plate was used with polarized light microscopy to determine the optical sign, and thus the cellulose microfibril orientation, of wild type and *ppcesa3/8KO* midrib cell walls (Fig. 3). In mature wild type leaves, the larger bundle sheath-like cells that surround the central stereids showed blue addition colors when oriented parallel to the major axis of the plate and yellow subtraction colors when oriented perpendicular to the major axis (Fig. 3), indicating that the net orientation of

positively birefringent cellulose microfibrils is longitudinal. In contrast, the walls of the smaller central stereids were colorless when oriented parallel or perpendicular to the major axis (Fig. 3). However, when oriented at 45^{o} to the retardation plate, these cells showed alternating bands of blue and yellow (Fig. 3), indicating that the microfibrils in their walls are helical with an angle near 45^{o}. The central midrib cells of developing wild type leaves showed a transition from colorless to blue to yellow along the apical to basal developmental gradient when the midrib was oriented parallel to the major axis of the plate (Fig. 3). This indicates that the microfibril orientation changes from transverse to longitudinal and then to helical as the cells mature. In contrast, the central midrib stereids of mature *ppcesa3/8KO* leaves had blue addition colors when oriented parallel to the major axis, yellow subtraction colors when oriented perpendicular to the major axis, and no interference color when oriented at 45^{o} to the retardation plate indicating that microfibrils are longitudinal, rather than helical. Developing *ppcesa3/8KO* leaves had no longitudinal gradient in interference colors (Fig. 3).

The walls of midrib cells were examined by transmission electron microscopy in ultrathin sections of chemically fixed gametophore leaves. Despite the reduced cellulose content detected by other means, the walls of midrib cells were thickened compared to walls of adjacent lamina cells in all *ppcesa*KO*s*, as well as wild type leaves (Fig. 4). When we attempted to prepare specimens by high pressure freezing and freeze-substitution, the leaves fractured in a plane parallel to the midrib. This resulted in a loss of midrib cells and precluded examination of midrib cell walls in these specimens. We were able to examine the lamina and margin cells of freeze-

substituted leaves in wild type and two lines of each mutant. The walls of these cells appeared similar between wild type, and single and double *ppcesa*KOs (Fig. S3). However, measurements revealed that lamina cell external walls, i.e. those facing the external environment, were thinner in *ppcesa*KOs (Fig. S4).

The mesoscale organization of cellulose in the midribs of wild type, *ppcesa3/8*KO, and *ppcesa8*KO leaves was examined using a broadband SFG microscope (Lee et al. 2016). Because it detects only non-centrosymmetric ordering of functional groups, SFG provides a means of analyzing cellulose in intact cell walls with relatively little interference from matrix components (Barnette et al. 2011). For each genotype, full SFG spectra collected from three different locations along the midribs of each of three different leaves were averaged (Fig. 5). The sampling depth of the SFG microscope for cellulosic samples is 20-25 μm (Lee et al. 2016). Given that the thickness of turgid leaves is about 50-60 μm at the midrib and that they likely collapse to less than half their thickness when dried, we conclude that most of the leaf thickness contributes to the SFG signal. In spectra collected from the wild type, a strong peak at 2944 cm^{-1}, which is characteristic of secondary cell walls, was observed in the CH/CH_2 stretch region along with a 3320 cm^{-1} peak in the OH stretch region. In contrast, the spectra collected from *ppcesa3/8*KO and *ppcesa8*KO midribs had weaker peak intensity overall with a broad CH/CH_2 stretch peak centered around 2910 cm^{-1}. Compared to *ppcesa3/8*KO, the spectra from *ppcesa8*KO midribs had a weak signal at 2963 cm^{-1} that was absent in spectra collected from *ppcesa3/8*KO midribs. A scan across a wild type leaf shows that the 2944 cm^{-1} signal is associated with the midrib and was not observed in the cells of the lamina (Fig. 5). Equivalent scans of *ppcesa3/8*KO and

*ppcesa8*KO leaves confirm the absence of a strong 2944 cm^{-1} peak from the midribs of these mutants (Fig. 5).

PpCESA proteins are functionally specialized

Based on the *ppcesa3*KO, *ppcesa8*KO, and *ppcesa3/8*KO phenotypes, PpCESA3 and PpCESA8 appear to be partially redundant. To determine whether the relative strengths of these phenotypes are related to gene expression levels, we used reverse transcription quantitative PCR to measure the expression of *PpCESA3* and *PpCESA8* in the wild type and mutants. In the *ppcesa3*KOs, *PpCESA8* was significantly upregulated compared to wild type (Fig. 6), providing a possible explanation for the lack of a mutant phenotype in these lines. In contrast, *PpCESA3* was not significantly upregulated in the *ppcesa8*KOs compared to wild type, potentially explaining the intermediate phenotype in these mutants.

*ppcesa3*KOs, *ppcesa8*KOs and *pp*cesa*3/8*KOs were tested for changes in rhizoid and caulonema development to determine whether developmental defects were restricted to the gametophores. When cultured on medium containing auxin, all lines produced the expected leafless gametophores with numerous rhizoids (Fig. S5), indicating no defects in rhizoid development in any of the KOs. Caulonema produced by colonies grown in the dark on vertically oriented plates were all negatively gravitropic (Fig. S6). Although appearance of the caulonema varied among experiments, those produced by KOs were always similar to control wild type within the same experiment. Caulonemal length was not significantly different between *ppcesa3/8*KOs and wild type (Table 1).

To determine whether other PpCESAs are functionally interchangeable with PpCESA3 and PpCESA8, we tested for rescue of *ppcesa3/8*KO-86lox by various *PpCESA*s driven by the *PpCESA8* promoter. Polarization microscopy screening of at least 21 and up to 27 stably transformed lines for each vector revealed little or no midrib birefringence for the *proCESA8::CESA4*, *proCESA8::CESA7* and *proCESA8::CESA10* lines and moderate to strong midrib birefringence for 92% and 78% of the *proCESA8::CESA3* and *proCESA8::CESA5* lines, respectively. Quantitative analysis of S4B staining (Fig. 7) confirmed that the *ppcesa3/8*KO phenotype was partially rescued by *proCESA8::CESA3* (3 out of 3 lines) and *proCESA8::CESA5* (2 out of 3 lines) as we observed for *proCESA8::CESA8* (Fig. 2). However, the *proCESA8::CESA4*, *proCESA8::CESA7* and *proCESA8::CESA10* vectors showed no rescue (Fig. 7). Western blot analysis confirmed that PpCESA proteins were expressed in all lines except *proCESA8::CESA4*-11 and *proCESA8::CESA5*-7 (Fig. S7). PpCESA6 differs from PpCESA7 by only 2 amino acids and was not tested. Although expressed with the same promoter, protein accumulation varies among the different transgenic lines (Fig. S7). Similar differences in protein accumulation may also explain variation in the extent of rescue by the *proCESA3::CESA3* and *proCESA8::CESA8* vector (Fig. 2).

Finally, we examined *ppcesa4/10*KOs and *ppcesa6/7*KOs produced for another study to determine whether they phenocopy the *ppcesa3/8*KO phenotype. Genotype verification for these lines is presented in Fig. S8 and Fig. S9. The *ppcesa4/10*KOs showed slight, but significant reduction in midrib S4B fluorescence. However, for *ppcesa6/7*KOs the reduction was substantial and significant (Fig. 7), showing the

PpCESA6/7 and PpCESA3/8 have non-redundant roles in secondary cell wall deposition in leaf midrib cells.

Discussion

PpCESA3 and PpCESA8 function redundantly in cellulose deposition in stereid secondary cell walls.

Targeted knockout of *PpCESA3* and *PpCESA8* blocked deposition of cellulose in the thick walls of stereid cells as indicated by 1) reduction of the strong birefringence associated with the midribs in *ppcesa3/8*KOs, 2) reduction in the midrib fluorescence of *ppcesa3/8*KO leaves stained with S4B, 3) lack of CBM3a labeling of sections from *ppcesa3/8*KO leaf midribs (Fig. 1), and 4) reduction in *ppcesa3/8*KO gametophore cell wall cellulose content as measured by Updegraff assay. Evidence that knockout of *PpCESA3* and *PpCESA8* is responsible for the observed phenotype includes consistency of the phenotype in three independent KOs and restoration of cellulose deposition in the midribs by transformation of *ppcesa3/8*KO with vectors driving expression of PpCESA3 or PpCESA8 (Fig. 2). Whereas we detected no reduction in midrib cellulose in *ppcesa3*KO, the phenotypes of *ppcesa8*KOs were intermediate between wild type and *ppcesa3/8*KO (Fig. 2). This, combined with the observations that only *PpCESA8* is up-regulated to compensate for loss of its paralog (Fig. 6) and expression of PpCESA3 under control of its native promoter only partially restores the wild type phenotype (Fig. 2), are consistent with the hypothesis that the PpCESA3 and PpCESA8 proteins are functionally interchangeable and that a dosage effect is responsible for the *ppcesa8*KO phenotype. The formation of morphologically normal

gametophores in *ppcesa3/8*KOs (Fig. 1) indicates that PpCESA3 and PpCESA8 serve a different role in development than PpCESA5, which supports normal cell division and cell expansion required for gametophore development (Goss et al. 2012). It is possible that PpCESA3 and PpCESA8 contribute to primary cell wall deposition since *ppcesa3/8*KO lamina cells had thinner external walls (Fig. S4) and tended to collapse during embedding (Fig. 1). Alternatively, PpCESA3 and PpCESA8 may contribute to secondary thickening of lamina cell walls after they stop expanding.

CESA evolution in both *P. patens* and Arabidopsis involve sub-functionalization and neo-functionalization.

There are many parallels in the evolution of the *P. patens* and Arabidopsis *CESA* families. In both species, different CESAs are responsible for primary and secondary cell wall deposition. In Arabidopsis, the secondary CESAs are AtCESA4, -7 and -8 (Taylor et al. 2003) and primary CESAs are AtCESA1,-3, and members of the 6-like group (Desprez et al. 2007; Persson et al. 2007). In *P. patens*, midrib secondary cell wall synthesis involves PpCESA3, -6, -7 and -8, whereas gametophore primary cell wall synthesis requires PpCESA5 (Goss et al. 2012). At least some primary CESAs can substitute for secondary CESAs and vice versa in both species. In Arabidopsis, *AtCESA3pro::AtCESA7* partially rescues *atcesa3*, and *AtCESA8pro::AtCESA1* partially rescues *atcesa8* (Carroll et al. 2012). In *P. patens*, *PpCESA8pro::PpCESA5* rescues *ppcesa3/8*KO. This indicates that the *CESA* division of labor for primary and secondary cell wall deposition in vascular plants and mosses is due at least in part to sub-functionalization. However, neo-functionalization has also occurred in both species, resulting in the requirement for two or more non-interchangeable CESA

isoforms for secondary cell wall biosynthesis. In Arabidopsis, *atcesa4*, *atcesa7*, and *atcesa8* null mutants share a phenotype (Taylor et al. 2000) that cannot be complemented by expressing one of the other secondary AtCESAs with the promoter for the missing isoform (Kumar et al. 2016). Likewise in *P. patens*, *ppcesa3/8*KO *and ppcesa6/7*KO share the same phenotype and *ppcesa3/8*KO is not complemented by *PpCESA8pro*::*PpCESA7*. Studies are ongoing to determine whether the secondary PpCESAs physically interact to form a CSC, as has been shown for the secondary AtCESAs (Taylor et al. 2003; Timmers et al. 2009). Finally, the *CESA* families of both species show some redundancy. In Arabidopsis the 6-like *CESA*s (*AtCESA2*, *-5*, *-6* and *-9*) are partially redundant (Persson et al. 2007), as are *PpCESA3* and *-8* in *P. patens*. PpCESA6 and -7 differ by only three amino acids and the genes that encode them appear to be redundant (Wise et al. 2011).

A recent study has shown that secondary cell wall deposition, including CESA expression, is regulated by NAC transcription factors in both *P. patens* and Arabidopsis (Xu et al. 2014). Three *P. patens* NAC genes, *PpVNS1*, *PpVNS6*, and *PpVNS7*, were preferentially expressed in leaf midribs and *ppvns1/ppvns6/ppvns7*KOs were defective in stereid development. Overexpression of *PpVNS7* activated PpCESA3 (Xu et al. 2014). Phylogenetic analyses of NACs place eight *PpVNS* proteins within the clade that has variously been named subfamily NAC-c (Shen et al. 2009), subfamily Ic (Zhu et al. 2012), or the VNS group (Xu et al. 2014), and also includes the Arabidopsis vascular-related NACs VND6 (ANAC101), VND7 (ANA030), NST1 (ANAC043), NST2 (ANAC066) and NST3/SND1 (ANAC012). The three PpVNS proteins that regulate stereid development form a single sister clade

with five other PpVNS proteins implicated also in other processes (Xu et al. 2014). Based on this phylogenetic analysis, the common ancestor of the mosses and seed plants had a single VNS gene, and it also had a single CESA gene (Kumar et al. 2016; Roberts and Bushoven 2007; Yin et al. 2009). Both lineages now include secondary CESA s that are regulated by VNSs and primary CESAs that are not, indicating that CESA subfunctionalization occurred independently in mosses and seed plants.

Secondary cell wall microfibrillar texture is similar in mosses and vascular plants.

In vascular plants, both water conducting tracheary elements and supportive fibers are characterized by helical (Barnett and Bonham 2004) and aggregated (Donaldson 2007; Fernandes et al. 2011; Thomas et al. 2014) cellulose microfibrils. The midribs of *P. patens* leaves include hydroid cells that transport water and stereid cells that provide support, but only the stereids have thick cell walls (Xu et al. 2014). With highly reduced cellulose in their stereid secondary cell walls, *ppcesa3/8*KOs provided a negative control for structural characterization of secondary cell walls in wild type *P. patens*. A sharp SFG CH/CH_2 stretch peak at 2944 cm^{-1} is characteristic of angiosperm secondary cell walls (Park et al. 2013) and extensive empirical testing has shown that this spectral feature is attributable to lateral microfibril aggregation (Lee et al. 2014). The 2944 cm^{-1} peak was also present in SFG spectra of wild type *P. patens* midribs. In contrast, the spectra of *ppcesa3/8*KO leaf midribs lacked the 2944 cm^{-1} peak and instead had a broad peak between 2800 and 3000 cm^{-1}, which is characteristic of primary cell walls and other samples lacking aggregated microfibrils (Lee et al. 2014;

Park et al. 2013). This suggests that lateral aggregation of microfibrils is a common feature of the secondary cell walls of moss stereids and vascular plant tracheary elements and fibers. Polarization microscopy with a first order retardation plate revealed that the microfibrils in the stereid cell walls are deposited in a helical pattern, as observed in secondary cell walls of tracheary elements and fibers (Barnett and Bonham 2004). Although deficient in cellulose, the stereid cell walls of *ppcesa3/8*KOs were thickened, indicating that secondary cell wall synthesis involves deposition of non-cellulosic components, which proceeded in the absence of cellulose deposition. This has also been observed in developing tracheary elements treated with cellulose synthesis inhibitors (Taylor et al. 1992). Thus, stereid cell walls share structural characteristics with the cell walls of tracheary elements and fibers.

Mosses and vascular plants have acquired similar secondary cell walls through convergent evolution.

Thick, cellulose-rich secondary cell walls provide added support for aerial organs of mosses and vascular plants alike. Within these cell walls, the lateral aggregation and helical orientation of the microfibrils contributes to their strength and resiliency. Although cortical microtubules play an important role in cellulose microfibril orientation, oriented cellulose deposition can occur in the absence of cortical microtubules, and it has previously been suggested that aggregation and helical orientation of microfibrils in secondary walls is a consequence of high CSC density during rapid cellulose deposition (Emons and Mulder 2000; Lindeboom et al. 2008). Regulation at the level of CSC secretion was emphasized in this model (Emons and

Mulder 2000), but CSC density can potentially be regulated at the level of transcription.

Rapid cellulose synthesis during secondary cell wall deposition in specific cell types requires precise temporal and spatial regulation of CESA expression that is distinct from the regulatory requirements for primary cell wall synthesis. We suggest that these distinct regulatory needs were met through the evolution of independent regulatory control of primary and secondary CESAs by sub-functionalization in both mosses and seed plants. In seed plants, phylogenetic analysis shows that the first divergence of the *CESA* family separated the genes that encode the primary and secondary CESAs and was followed by independent diversification within each group (Roberts et al. 2012). This, along with evidence that some primary CESAs are interchangeable with secondary CESAs (Carroll et al. 2012), indicates that sub-functionalization was an early event in the evolution of the seed plant CESA family. In *P. patens*, the genes that encode secondary PpCESA3 and PpCESA8 and primary PpCESA5 are also sub-functionalized and therefore specialized, although they encode interchangeable proteins.

Several lines of evidence indicate that the capacity to deposit a secondary cell wall evolved independently in mosses and seed plants. Structural and paleobotanical evidence suggests that the support and water-conducting cells of bryophytes and vascular plants are not homologous (Carafa et al. 2005; Ligrone et al. 2002). Phylogenetic evidence indicates that the primary and secondary CESAs diversified independently in mosses and seed plants (Kumar et al. 2016; Roberts and Bushoven 2007; Yin et al. 2009) and, as explained above, so did the NAC transcription factors

that regulate the secondary CESAs. There are even examples of convergent evolution of secondary cell walls within the angiosperm lineage. Cotton fiber secondary cell walls are synthesized by the same CESAs that are responsible for secondary cell wall deposition in tracheary elements and fibers (Haigler et al. 2012), whereas the secondary cell walls of epidermal trichomes are synthesized by the primary CESAs (Betancur et al. 2011). These observations are consistent with independent evolutionary origins for secondary cell walls in different land plant lineages and different cell types within angiosperm lineages.

Taken together, these data indicate that *CESA* duplication, followed by adoption of regulatory elements within the secondary *CESA* promoters that enable control by NAC transcription factors, occurred independently in mosses and vascular plants. The resulting uncoupling of the secondary CESAs from the regulatory constraints associated with primary cell wall deposition, along with a mechanistic linkage between CESA expression and microfibril texture as well as selection for strength and resiliency, may have contributed to the capacity of different plants to synthesize cellulose-rich secondary cell walls with similar microfibrillar textures.

Materials and methods

Vector construction

All primer pairs are shown in Table S1, along with annealing temperatures used for PCR. Amplification programs for Taq Polymerase (New England Biolabs, Ipswich, MA, USA) consisted of a 3 min denaturation at 94 ℃; 35 cycles of 15 s at 94 ℃, 30 s at the annealing temperature, and 1 min/kbp at 72 ℃. Amplification programs for

Phusion Polymerase (New England Biolabs) consisted of a 30 s denaturation at 98 ℃; 35 cycles of 7 s at 98 ℃, 7 s at the annealing temperature, and 30 s/kbp at 72 ℃.

To construct the CESA8KO vector, a 3' homologous region was amplified from *P. patens* genomic DNA with primers 174JB and 193JB using Taq DNA polymerase, cut with Sal1 and BspD1, and cloned into the SalI/BstBI site of pBHSNR (gift of Didier Schaefer, University of Neuchâtel). The resulting plasmid was cut with KasI and NsiI to accept the KasI/NsiI fragment of a 5' homologous region amplified from *P. patens* genomic DNA with primers 203JB and 185JB (Table S1). The CESA8KO vector was cut with EcoRI and NsiI for transformation into wild type *P. patens*. The CESA3KO, CESA4KO, CESA6/7KO, and CESA10KO vectors were constructed using Gateway Multisite Pro cloning (Invitrogen, Grand Island, NY, USA) as described previously (Roberts et al. 2011). Flanking sequences 5' and 3' of the coding regions were amplified with appropriate primer pairs (Table S1) using Phusion DNA polymerase (New England Biolabs) and cloned into pDONR 221 P1-P4 and pDONR 221 P3-P2, respectively, using BP Clonase II (Invitrogen). Similarly, an *nph* selection cassette was amplified from pMBL6 (gift of Jesse Machuka, University of Leeds) cloned into pDONR 221 P3r-P4r. All entry clones were sequence-verified. For vectors conferring hygromycin resistance, entry clones with flanking sequences in pDONR 221 P1-P4 and pDONR 221 P3-P2 were inserted into BHSNRG (Roberts et al. 2011). For vectors conferring G418 resistance, entry clones with flanking sequences in pDONR 221 P1-P4 and pDONR 221 P3-P2 were linked with the entry clone containing the *nph* selection cassette and inserted into pGEM-gate (Vidali et al. 2009) using LR Clonase

II Plus (Invitrogen). The vectors in BHSNRG or pGEM-gate were cut with BsrGI for transformation into wild type or mutant *P. patens* lines.

Expression vectors for HA-tagged PpCESAs under control of *PpCESA* promoters were constructed using Gateway Multisite Pro cloning (Invitrogen). The *PpCESA4* (DQ902545), *PpCESA5* (DQ902546), *PpCESA7* (DQ160224) and *PpCESA8* (DQ902549) coding sequences were amplified from cDNA clones pdp21409, pdp24095, pdp38142 and pdp39044 (RIKEN BioResource Center, Tsukuba, Ibaraki JP), respectively, using forward primers containing a single hemagglutinin (HA) tag and appropriate reverse primers (Table S1) and cloned into pDONR 221 P5-P2 using BP Clonase II (Invitrogen). The *PpCESA3* (XP_001753310) and *PpCESA10* (XP_001776974) coding sequences were similarly amplified from expression vectors. pDONR 221 P1-P5r entry clones containing approximately 2 kB of sequence upstream of the *PpCESA3* or *PpCESA8* start codon (Tran and Roberts 2016), were linked to the sequence verified entry clones containing the *HA-PpCESA* coding sequences and inserted into pSi3(TH)GW (Tran and Roberts 2016) using LR Clonase II Plus (Invitrogen). These vectors target the expression cassettes to the intergenic 108 locus, which can be disrupted with no effect on phenotype (Schaefer and Zryd 1997). Rescue vectors were cut with SwaI for transformation into a *P. patens ppcesa3/8*KO line from which the *hph* resistance cassette had been removed (see below).

Culture and transformation of *P. patens*

Wild type *P. patens* lines (haploid) derived from the sequenced Gransden strain (Rensing et al. 2008) by selfing and propagation from a single spore in 2006 (GD06) or 2011 (GD11) were gifts of Pierre-Francois Perroud, Washington University. Wild

type and transformed *P. patens* lines were cultured on basal medium supplemented with ammonium tartrate (BCDAT) as described previously (Roberts et al. 2011). Protoplasts were prepared and transformed as described previously (Roberts et al. 2011). Stable transformants were selected with 50 μg mL^{-1} G418 (CESA3KO vector) or 15 μg mL^{-1} hygromycin (CESA8KO and complementation vectors). The *hph* selection cassette was removed from *ppces3*/*ppcesa8*KO by transforming protoplasts with NLS-Cre-Zeo (Vidali et al. 2010) selecting for 7 d on BCDAT plates containing 50 μg mL^{-1} zeocin, replica plating zeocin resistant colonies on BCDAT with and without 15 μg mL^{-1} hygromycin, and recovering hygromycin-sensitive colonies. Protein expression was tested by western blot analysis as described previously (Scavuzzo-Duggan et al. 2015) in selected lines transformed with HA-PpCESA expression vectors.

Genotype analysis

For PCR screening, DNA was extracted as described previously (Roberts et al. 2011) and 2.5 μL samples were subjected to 35 cycles of amplification (45 s at 94°C, 45 s at the annealing temperature shown in Table S1, 1 min/kbp at 72 ℃) with PAQ5000 DNA polymerase (Agilent Technologies, http://www.home.agilent.com/) in 25 μL reactions. Primers used to test for target integration, target-gene disruption, and selection cassette excision are listed in Table S1.

Phenotype analysis

Cell wall birefringence of unfixed leaves mounted in water was examined using an Olympus BHS compound microscope with D Plan-Apo UV 10X/0.4, 20X/0.7, and 40X/0.85 objectives, and polarizer and circular-polarizing analyzer, with and without a

first order retardation plate (Olympus, Center Valley, PA, USA). Images were captured with a Leica DFC310FX digital camera with Leica Application Suite software, version 4.2.0 (Leica Microsystems Inc., Buffalo Grove, IL, USA) with manual exposure under identical conditions.

For direct fluorescent labeling of cellulose, whole gametophores (3 per line) dissected from colonies grown for four weeks on solid BCDAT medium were dipped in 100% acetone for 5 sec to permeabilize the cuticle, rinsed in phosphate buffered saline (PBS), incubated in PBS containing 0.1 mg/ml S4B (Anderson et al. 2010) for 30 min, and rinsed in PBS. All fully expanded leaves (12-20) were cut from each gametophore and mounted in PBS. Fluorescence images of each leaf, centered on the brightest part of the midrib, were captured using a Zeiss Axio Imager M2 with 43HE DsRed filter set, Plan-Neofluar 20X/0.5 objective, AxioCam MR R3 camera, and Zen Blue software, version 1.1.2.0 (Carl Zeiss Microscopy, Jena, Germany) under identical conditions using manual exposure. The midrib in each image was selected manually (Fig. S10) and average pixel intensity was measured using ImageJ, Fiji version (Schindelin et al. 2012). For comparison of KOs to the wild type, three independent lines of each KO genotype (n=3) and two independent wild type lines (GD06 and GD11, n=2) were sampled in triplicate. For analysis of rescue lines, three independent explants were sampled for each genetic line (n=3).

For affinity cytochemistry of cellulose, gametophores dissected from colonies grown for two weeks on BCDAT medium were fixed and embedded in LR White resin (Polysciences, Inc., Warrington, PA, USA) as described previously (Kulkarni et al. 2012). Sections (1 μm) were mounted and labeled with CBM3a as described

previously (Berry et al. 2016). Images were captured with a Zeiss Axio Imager M2 with 38 Green Fluorescent Protein filter set, EC Plan-Neofluar 40X/0.75 objective, AxioCam MR R3 camera, and Zen Blue software, version 1.1.2.0 (Carl Zeiss Microscopy) under identical conditions using manual exposure. Fluorescence and polarization images were not altered after capture. Bright field and differential interference contrast images were captured using automatic exposure and some images used for illustrative purposes were adjusted for uniformity using the color balance and exposure functions in Photoshop, version CS6 (Adobe Systems, San Jose CA, USA). *ppcesa3*KOs, *ppcesa8*KOs, and *ppcesa3/8*KOs were tested for changes in caulonema gravitropism and rhizoid development as described previously (Roberts et al. 2011). Images were captured using a Leica M165FC stereomicroscope with Leica DFC310FX camera and Leica Application Suite software, version 4.2.0 (Leica Microsystems Inc.). Caulonema length for each colony was measured as the distance from the edge of the colony to tip of the longest caulonema filament using Leica Application Suite software.

Cell wall analysis

Alcohol insoluble residue (AIR) was prepared from gametophores dissected from 8-10 4-week-old explants of *P. patens* wild type (three samples from independent cultures) and *ppcesa3/8*KO (samples from three independent lines) cultured on BCDAT medium. Tissue was ground in liquid nitrogen and extracted three times, 30 min each, with 70% (v/v) ethanol and once with 100% ethanol and the residue was dried under vacuum. The AIR (~1 mg) was weighed to 0.001 mg and mixed with 1 mL of acetic acid:water:nitric acid (8:2:1, v/v) in screw-cap vials and the suspension was heated in

a boiling water bath for 30 min (Updegraff 1969). After cooling, the tubes were centrifuged at 16,900 x g for 5 min and the supernatant discarded. The pellet was resuspended in 2 mL of deionized water, centrifuged, and the supernatant was discarded. The washing step was repeated at least 10 more times until the supernatant was neutralized and the pellet was resuspended in 1 mL of water. The amount of cellulose remaining after hydrolysis was quantified by sulfuric acid assay (Albalasmeh et al. 2013) with glucose as the standard. Briefly, 100 µL of hydrolysate (six technical replicates per sample) was diluted to 1 mL with water in a glass tube, 3 mL of concentrated sulfuric acid was added, and samples were vortexed for 30 s and chilled on ice for 2 min. Reactions were measured at 315 nm against a reagent blank.

<u>High pressure freezing-freeze substitution and transmission electron microscopy</u>

Gametophytes of *P. patens* GD06 and PpCESAKOs were high pressure-frozen using a Leica EMPACT2 high pressure freezer (Leica Microsystems, Inc.) followed by freeze-substitution in 0.1% uranyl acetate in acetone for 48 h at -90^{o}C before the temperature was ramped up slowly to -50^{o}C (Wilson and Bacic 2012). The samples were rinsed with acetone twice at -50^{o}C before the acetone was replaced with ethanol and the samples were subsequently infiltrated with LR White resin (ProSciTech Pty. Ltd., Thuringowa Central QLD Australia) in a series of ethanol/resin dilutions. The samples were rinsed three times in 100% resin before polymerization with UV light at -20^{o}C for 48 h. Thin sections (70 nm) were cut using a Leica Ultracut R (Leica Microsystems, Inc.) and post-stained with uranyl acetate and lead citrate (Wilson and Bacic 2012). Images were taken using a Tecnai G2 Spirit transmission electron

microscope (FEI, Hillsboro, OR USA). Cell wall thickness was measured using ImageJ, Fiji version (Schindelin et al. 2012).

Ultrathin sections (70 nm) were also cut from blocks prepared for affinity cytochemistry (see above), mounted on Formvar coated copper grids, and stained with uranyl acetate and lead citrate (Wilson and Bacic 2012). Sections were imaged using a FEI/Phillips CM-200 transmission electron microscope (FEI).

Sum Frequency Generation spectroscopy

Leaves of wild type GD06, 8KO-5B, and 3/8KO-86 lines were mounted abaxial side down in water on glass slides and allowed to air-dry overnight. SFG spectra were collected 5 μm intervals along a 200 μm line scan perpendicular to the midrib at its thickest point using an SFG microscope system described previously (Lee et al. 2016). The SFG spectra were collected with the following polarization combination: SFG signal = s-, 800 nm = s-, and broadband mid-IR = p-polarized with the laser incidence plane and the laser incidence plane aligned along the axis of midrib.

Reverse transcription quantitative PCR

RNA was extracted from gametophores from two independent wild type and three independent lines each of *pp*cesa3KO and *pp*cesa8KO as described previously (Tran and Roberts 2016). cDNA samples were tested in duplicate as described previously using primer pairs for amplification of *PpCESA3* and PpCESA8. The primers have been previously tested for specificity and efficiency (Tran and Roberts 2016). Primers for actin and v-Type H^+translocating pyrophosphatase reference genes were described previously (Le Bail et al. 2013). Target/average reference cross point ratios were

calculated for each sample and standard errors were calculated for independent genetic lines.

Statistical analysis

For statistical analysis, one-way Analysis of Variance (ANOVA) with post-hoc Tukey Honest Significant Difference (HSD) test was performed at astatsa.com/OneWay_Anova_with_TukeyHSD/.

Supplemental Materials

Table S1. Primers used for vector construction and genotype analysis.

Fig. S1. Genotype analysis of *ppcesa8, ppcesa3* and *ppcesa3/8* KO lines.

Fig. S2: Phenotype analysis of a *ppcesa3/*8 double KO line transformed with vectors driving expression of *PpCESA3* or *PpCESA8* with their native promoters.

Fig. S3. Transmission electron microscopy images of leaf cell walls from wild type and *cesa*KO lines of *P. patens.*

Fig. S4. Thickness of outer cell walls measured from transmission electron microscopy images.

Fig. S5: *P. patens* wild type and KO lines cultured on medium containing 1 μM naphthalene acetic acid (auxin) to induce rhizoid initiation and inhibit leaf initiation.

Fig. S6: *P. patens* wild type and KO lines cultured in the dark on vertically oriented plates containing medium supplemented with 35 mM sucrose to test for caulonema gravitropism.

Fig. S7. Western blot analysis of protein expression for *P. patens* lines derived from transformation of *ppcesa3/8*KO-86lox with vectors driving expression of PpCESAs under control of the *PpCESA8* promoter.

Acknowledgements

This work was supported primarily by National Science Foundation Award IOS-1257047. Analysis of mutants by SFG spectroscopy was supported as part of The Center for LignoCellulose Structure and Formation, an Energy Frontier Research Center funded by the U.S. Department of Energy, Office of Science, Office of Basic Energy Sciences under Award Number DE-SC0001090. CBM3a affinity cytochemistry and freeze substitution transmission electron microscopy were supported by the Australian Research Council Centre for Excellence in Plant Cell Walls Grant CE1101007. High-pressure freezing and transmission electron microscopy was conducted at the Melbourne Advanced Microscopy Facility at the Bio21 Institute and the Biosciences Microscopy Unit at The University of Melbourne. DNA sequencing and qPCR were conducted using the Rhode Island Genomics and Sequencing Center, a Rhode Island NSF EPSCoR research facility, supported in part by the National Science Foundation EPSCoR Cooperative Agreement EPS-1004057. Clones pdp39044 and pdp10281 were from RIKEN BRC. We also thank Chessa Goss and Virginia Lai for preliminary work on *ppceas8*KO, Alfred Schupp for assistance with vector construction, Evan Preisser for assistance with statistics, and Sarah Kiemle for conducting Updegraff assays.

Tables

Table 1. Caulonema length for wild type and *ppcesa3/8*KOs grown on vertical plates in the dark. Data are from two independent experiments (n=2). ANOVA analysis showed no significant differences between genetic lines.

Genetic line	Caulonema length (mm)	Standard Error
WT GD06	4.69	0.50
*ppcesaA3/8*KO-43	5.70	0.87
*ppcesaA3/8*KO-57	4.51	1.14
*ppcesaA3/8*KO-86	5.69	0.47

Figures

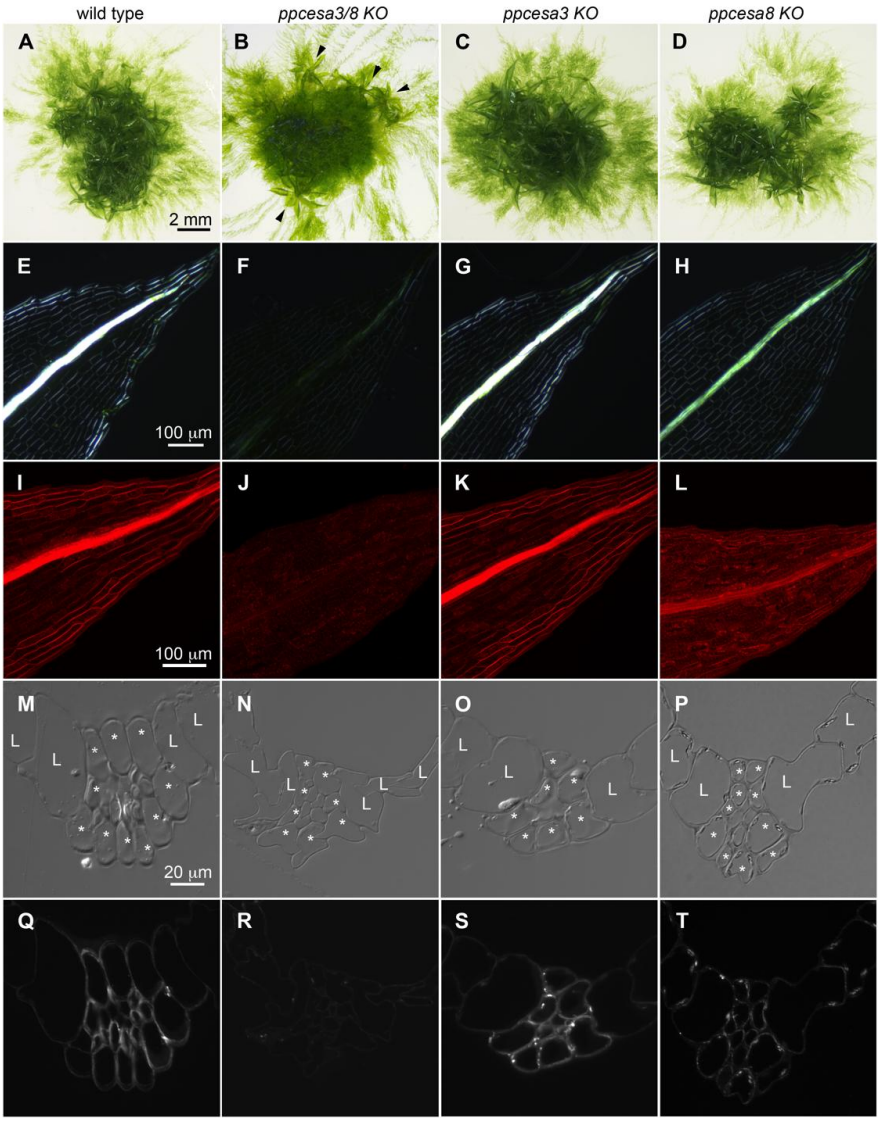

Figure 1: Phenotypes of *ppcesa3/8*KO, *ppcesa3*KO and *ppcesa8*KO compared to wild type *Physcomitrella patens*. (A-D) Colony morphology is similar in wild type, *ppcesa*3KOs and *ppcesa*8KOs; horizontal growth is typical of gametophores produced by *ppcesa*3/8KO (arrowheads). (E-H) Polarized light microscopy of leaves shows that the midribs of wild type and *ppcesa*3KO are highly birefringent. The midribs of *ppcesa*3/8KO leaves have low birefringence and *ppcesa*8KO leaves have moderate birefringence. (I-L) Fluorescence microscopy of leaves stained with S4B shows strong fluorescence in the midribs of wild type and *ppcesa*3KO, low fluorescence in the midribs of *ppcesa*3/8KO leaves and intermediate fluorescence in the midribs of *ppcesa*8KO leaves. (M-P) Differential interference contrast microscopy of sections through the midribs of maturing leaves (L=lamina cell, *=bundle sheath cell). In wild type and *ppcesa*3KO, the walls of bundle sheath cells and the stereid cells they surround show enhanced contrast due to higher refractive index. (Q-T) Fluorescence microscopy of the same sections shown in M-P labeled with CBM3a. The bundle sheath and stereid cells of wild type and *ppcesa*3KO leaves are strongly labeled, whereas labeling is weak in *ppcesa*3/8KO and intermediate in *ppcesa*8KO leaves.

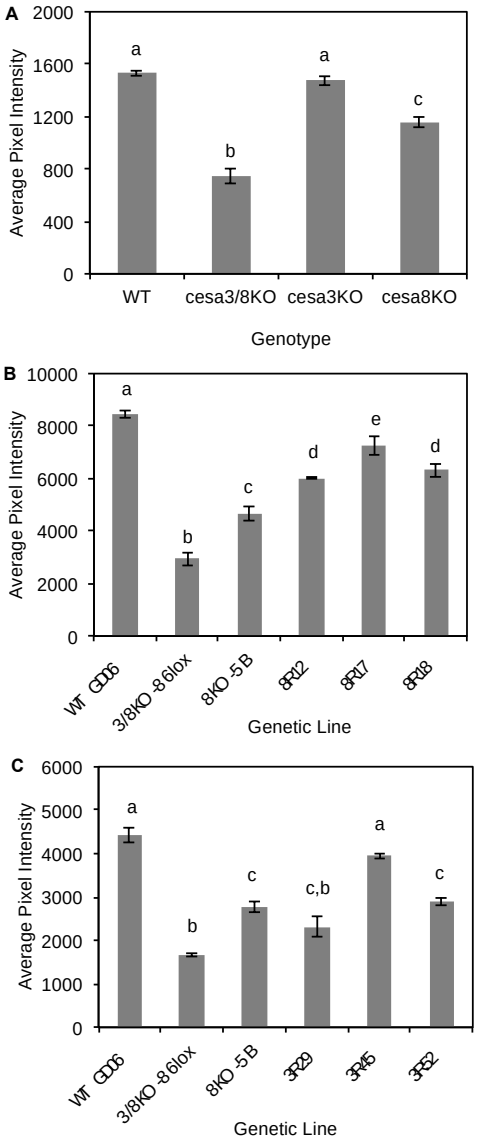

Figure 2: Quantitative analysis of S4B fluorescence intensity in leaf midribs of *P. patens* wild type, *ppcesa*KO, and rescue lines. (A) Fluorescence was significantly weaker in *ppcesa*3/8KOs compared to wild type (WT). *ppcesa*3KOs were not significantly different from wild type, whereas *ppcesa8*KOs were intermediate between the wild type and *ppcesa*3/8KOs and significantly different from both. For each mutant genotype, three independent genetic lines were sampled in triplicate. Two independent wild type lines (GD06 and GD11) were sampled in triplicate. Bars indicate the standard error of the mean for three mutant (n=3) or two wild type (n=2) lines. Genotypes with different letters are significantly different. (B) Lines derived from transformation of *ppcesa*3/8KO-86lox with *proCESA8::CESA8* (8R) had significantly higher fluorescence compared to the parent double KO line and *ppcesa*8KO, but significantly less than WT. (C) Lines derived from transformation of *ppcesa*3/8-86lox with *proCESA3::CESA3* (3R) had significantly higher fluorescence compared to the parent double KO line (except 3R29) and were not significantly different from either *ppcesa*8KO lines (3R29 and 3R52) or WT (3R45). For B and C, three independent explants were sampled for each genetic line. Bars indicate the standard error of the mean for three explants from the same line (n=3 or n=2 (WT, 3/8KO, 8KO in C)).

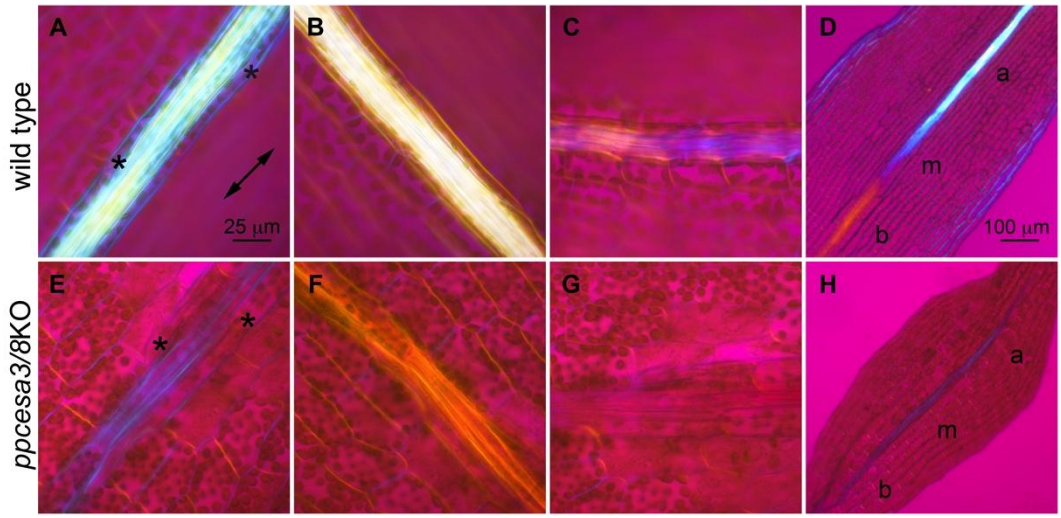

Figure 3: Polarized light microscopy with first order retardation plate. Double pointed arrow indicates the vibration direction of the major axis. (A-C) Midrib of a mature wild type leaf oriented parallel, perpendicular, and at 45^{o} to the major axis of the retardation plate. Bundle sheath cells (*) flank the central midrib. (D) Midrib of a developing wild type leaf oriented parallel to the major axis of the retardation plate showing change in microfibril orientations through the basal (b), medial (m), and apical (a) regions of the midrib. (E-G) Midrib of a mature *ppcesa*3/8KO leaf oriented parallel, perpendicular, and at 45^{o} to the major axis of the retardation plate. (H) Midrib of a developing *ppcesa*3/8KO leaf oriented parallel to the major axis of the retardation plate showing no change in microfibril orientation through the basal, medial, and apical regions of the leaf. Bar in A is also for B-C and E-G and bar in D is also for H.

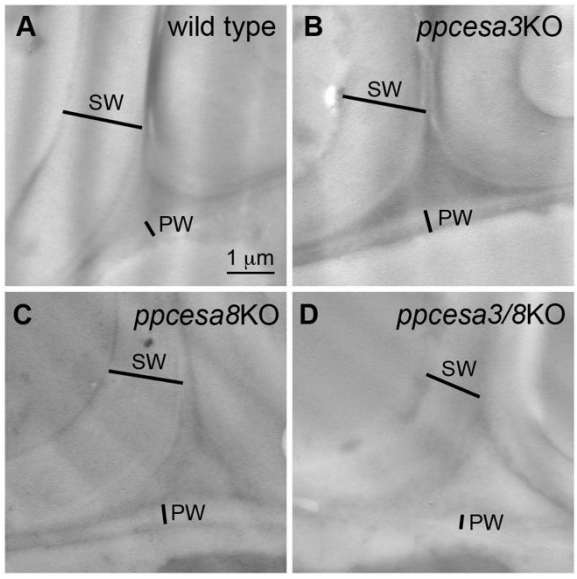

Figure 4: Transmission electron microscopy images of leaf midribs of *P. patens* showing adjacent cells with primary cell walls (PW) and secondary cell walls (SW) in (A) wild type, and (B-D) mutant leaves.

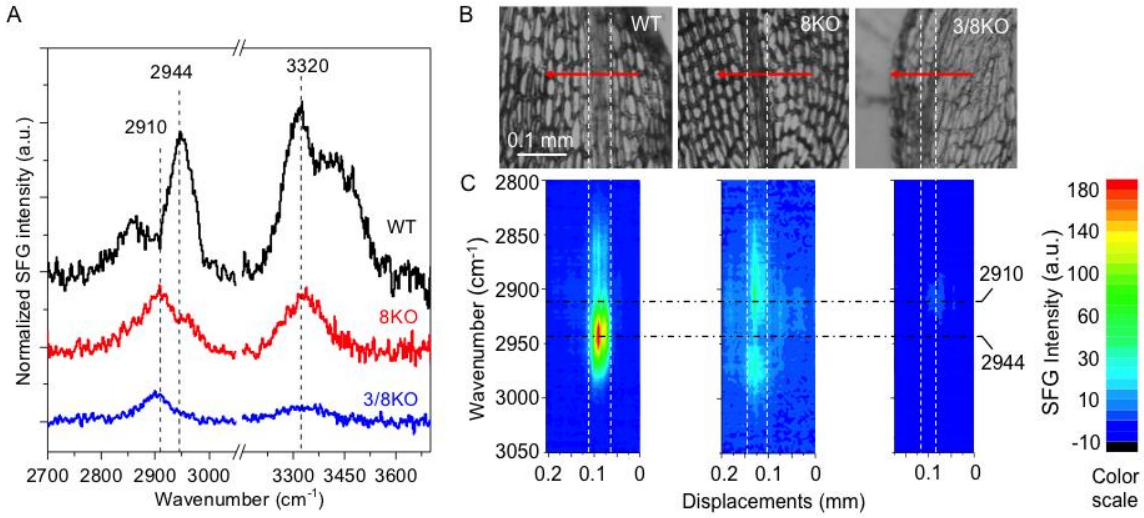

Figure 5: Sum Frequency Generation (SFG) spectroscopy of *P. patens* leaves. (A) Full SFG spectra collected from leaf midribs (each is the average of nine spectra, from three different positions on each of three different leaves). A strong peak in the C-H stretch region (2944 cm^{-1}) is present in spectra from wild type (WT), greatly diminished in spectra from *ppcesa8*KO (8KO), and absent in spectra from *ppcesa3/8*KO (3/8KO). (B) *P. patens* wild type, *ppcesa8*KO, and *ppcesa3/8*KO leaves with SFG scan trajectories traversing the midribs. Step size was 5 µm/step. SFG spectra were collected from 2850 to 3150 cm^{-1}, covering the entire CH region. (C) 2D projection image of SFG spectra collected across the midribs of each leaf shown in B. Each column in each image is an entire spectrum collected from one point plotted against displacement along the scan trajectory. Colors indicate SFG intensity as shown in the legend.

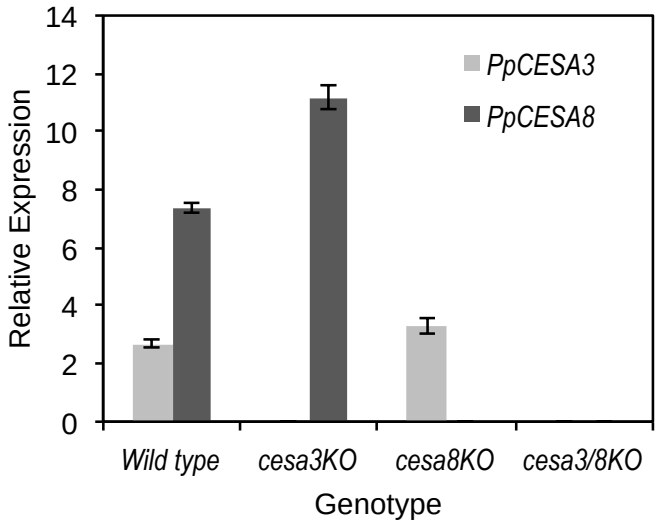

Figure 6: RT-qPCR analysis of *PpCESA3* and *PpCESA8* expression in wild type, *ppcesa3*KOs and *ppcesa8*KOs. Target/average reference cross point ratios (using actin and v-Type H^+translocating pyrophosphatase reference genes) were determined for three independent lines of each mutant (3KO-5, -35, -126; 8KO-5B, -4C, -10C; and 3/8KO-43, -57, -86) and two independent wild type lines (GD06 and GD11) with two technical replicates each. Bars indicate the standard error of the mean for the three mutant (n=3) or two wild type (n=2) lines.

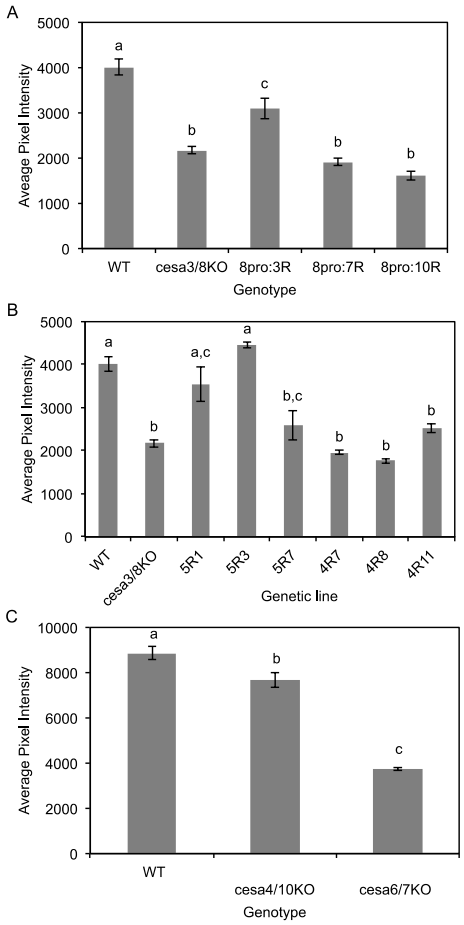

Figure 7: Quantitative analysis of S4B fluorescence intensity in leaf midribs. (A,B) Wild type (WT), *ppcesa*3/8KO-86lox, and *ppcesa*3/8KO-86lox transformed with *proCESA8::CESA* expression vectors. For each rescue genotype, three independent genetic lines were sampled in triplicate and measured with 6 samples of wild type (GD06) and 8 samples of *ppcesa*3/8KO-86lox. (A) For lines derived from transformation of *ppcesa*3/8KO-86lox with *proCESA8::CESA3* (8pro:3R), *proCESA8::CESA7* (pro8:7R), and *proCESA8::CESA10* (pro8:10R) genotypes, the three independent lines did not differ significantly and were combined. *proCESA8::CESA7* and *proCESA8::CESA10* lines did not differ significantly from the parent double KO line ($p > 0.05$), whereas *proCESA8::CESA3* lines had significantly higher fluorescence compared to the parent double KO line, but significantly less than WT ($p < 0.05$). Bars indicate the standard error of the mean for three independent lines. Genotypes with different letters are significantly different. (B) For lines derived from transformation of *ppcesa*3/8KO-86lox with *proCESA8::CESA5* (pro8:5R) and *proCESA8::CESA4* (pro8:4R), the three independent lines were significantly different and were analyzed separately. *proCESA8::CESA5* (5R) lines were not significantly different from the wild type ($p > 0.05$), except for 5R7, which was not significantly different from *ppcesa*3/8KO-86lox ($p > 0.05$). *proCESA8::CESA5* lines did not differ significantly from *ppcesa*3/8KO-86lox ($p > 0.05$). Bars indicate the standard error of the mean for three gametophores from the same line (n=3). Lines with different letters are significantly different ($p < 0.05$. (C) Mid rib fluorescence was slightly, but significantly reduced in *cesa4/10*KO compared to wild type ($p = 0.037$). Reduction in midrib fluorescence in *cesa6/7*KO was substantial and highly significant ($p = 0.0011$). Bars indicate the standard error of the mean for three independent mutant lines or 3 replicates of wild type (n=3).

References cited:

Albalasmeh AA, Berhe AA, Ghezzehei TA (2013) A new method for rapid determination of carbohydrate and total carbon concentrations using UV spectrophotometry. Carbohydr Polym 97: 253-261

Anderson CT, Carroll A, Akhmetova L, Somerville C (2010) Real-time imaging of cellulose reorientation during cell wall expansion in Arabidopsis roots. Plant Physiol 152: 787-796

Barnett JR, Bonham VA (2004) Cellulose microfibril angle in the cell wall of wood fibres. Biol Rev Camb Philos Soc 79: 461-472

Barnette AL, Bradley LC, Veres BD, Schreiner EP, Park YB, Park J, Park S, Kim SH (2011) Selective detection of crystalline cellulose in plant cell walls with sum-frequency-generation (SFG) vibration spectroscopy. Biomacromolecules 12: 2434-2439

Barnette AL, Lee C, Bradley LC, Schreiner EP, Park YB, Shin H, Cosgrove DJ, Park S, Kim SH (2012) Quantification of crystalline cellulose in lignocellulosic biomass using sum frequency generation (SFG) vibration spectroscopy and comparison with other analytical methods. Carbohydr Polym 89: 802-809

Berry EA, Tran ML, Dimos CS, Budziszek MJ, Jr., Scavuzzo-Duggan TR, Roberts AW (2016) Immuno and affinity cytochemical analysis of cell wall composition in the moss *Physcomitrella patens*. Front Plant Sci 7: 248

Betancur L, Singh B, Rapp RA, Wendel JF, Marks MD, Roberts AW, Haigler CH (2011) Phylogenetically distinct cellulose synthase genes support secondary wall thickening in arabidopsis shoot trichomes and cotton fiber. J Integr Plant Biol 52: 205-220

Blake AW, McCartney L, Flint JE, Bolam DN, Boraston AB, Gilbert HJ, Knox JP (2006) Understanding the biological rationale for the diversity of cellulose-directed carbohydrate-binding modules in prokaryotic enzymes. J Biol Chem 281: 29321-29329

Carafa A, Duckett JG, Knox JP, Ligrone R (2005) Distribution of cell-wall xylans in bryophytes and tracheophytes: new insights into basal interrelationships of land plants. New Phytol 168: 231-240

Carpita N, McCann M (2000) The cell wall. In: Buchanan B, Gruissem W, Jones R (eds) Biochemistry and Molecular Biology of Plants. American Society of Plant Physiologists, Rockville, MD, pp 52-108

Carroll A, Mansoori N, Li S, Lei L, Vernhettes S, Visser RG, Somerville C, Gu Y, Trindade LM (2012) Complexes with mixed primary and secondary cellulose synthases are functional in Arabidopsis plants. Plant Physiol 160: 726-737

Delmer DP (1999) Cellulose biosynthesis: Exciting times for a difficult field of study. Annu Rev Plant Physiol Plant Mol Biol 50: 245-276

Desprez T, Juraniec M, Crowell EF, Jouy H, Pochylova Z, Parcy F, Hofte H, Gonneau M, Vernhettes S (2007) Organization of cellulose synthase complexes involved in primary cell wall synthesis in Arabidopsis thaliana. Proc. Natl. Acad. Sci. USA 104: 15572-15577

Donaldson L (2007) Cellulose microfibril aggregates and their size variation with cell wall type. Wood Sci Technol 41: 443-460

Emons AMC, Mulder BM (2000) How the deposition of cellulose microfibrils builds cell wall architecture. Trends Plant Sci 35-40

Fernandes AN, Thomas LH, Altaner CM, Callow P, Forsyth VT, Apperley DC, Kennedy CJ, Jarvis MC (2011) Nanostructure of cellulose microfibrils in spruce wood. Proc Natl Acad Sci U S A 108: E1195-1203

Gonneau M, Desprez T, Guillot A, Vernhettes S, Hofte H (2014) Catalytic subunit stoichiometry within the cellulose synthase complex. Plant Physiol 166: 1709-1712

Goss CA, Brockmann DJ, Bushoven JT, Roberts AW (2012) A *CELLULOSE SYNTHASE* (*CESA*) gene essential for gametophore morphogenesis in the moss *Physcomitrella patens*. Planta 235: 1355-1367

Haigler CH, Betancur L, Stiff MR, Tuttle JR (2012) Cotton fiber: a powerful single-cell model for cell wall and cellulose research. Front Plant Sci 3: 104

Hebant C (1977) The Conducting Tissues of Bryophytes. J. Cramer, Vaduz

Hill JL, Jr., Hammudi MB, Tien M (2014) The Arabidopsis cellulose synthase complex: a proposed hexamer of CESA trimers in an equimolar stoichiometry. Plant Cell 26: 4834-4842

Jarvis MC (2013) Cellulose biosynthesis: counting the chains. Plant Physiol 163: 1485-1486

Kenrick P, Crane PR (1997) The origin and early evolution of plants on land. Nature 389: 33-39

Kimura S, Laosinchai W, Itoh T, Cui X, Linder CR, Brown RM, Jr. (1999) Immunogold labeling of rosette terminal cellulose-synthesizing complexes in the vascular plant *Vigna angularis*. Plant Cell 11: 2075-2085

Kulkarni AR, Peña MJ, Avci U, Mazumder K, Urbanowicz BR, Pattathil S, Yin Y, O'Neill MA, Roberts AW, Hahn MG, Xu Y, Darvill AG, York WS (2012) The ability of land plants to synthesize glucuronoxylans predates the evolution of tracheophytes. Glycobiology 22: 439–451

Kumar M, Atanassov I, Turner S (2016) Functional analysis of cellulose synthase CESA protein class-specificity. Plant Physiol 173: 970-983

Le Bail A, Scholz S, Kost B (2013) Evaluation of reference genes for RT qPCR analyses of structure-specific and hormone regulated gene expression in *Physcomitrella patens* gametophytes. PLoS One 8: e70998

Lee CM, Kafle K, Huang S, Kim SH (2016) Multimodal Broadband Vibrational Sum Frequency Generation (MM-BB-V-SFG) Spectrometer and Microscope. J Phys Chem B 120: 102-116

Lee CM, Kafle K, Park YB, Kim SH (2014) Probing crystal structure and mesoscale assembly of cellulose microfibrils in plant cell walls, tunicate tests, and bacterial films using vibrational sum frequency generation (SFG) spectroscopy. Phys Chem Chem Phys 16: 10844-10853

Ligrone R, Vaughn KC, Renzaglia KS, Knox JP, Duckett JG (2002) Diversity in the distribution of polysaccharide and glycoprotein epitopes in the cell walls of bryophytes: new evidence for the multiple evolution of water-conducting cells. New Phytol 156: 491-508

Lindeboom J, Mulder BM, Vos JW, Ketelaar T, Emons AM (2008) Cellulose microfibril deposition: coordinated activity at the plant plasma membrane. J Microsc 231: 192-200

Newman RH, Hill SJ, Harris PJ (2013) Wide-angle x-ray scattering and solid-state nuclear magnetic resonance data combined to test models for cellulose microfibrils in mung bean cell walls. Plant Physiol 163: 1558-1567

Nixon BT, Mansouri K, Singh A, Du J, Davis JK, Lee JG, Slabaugh E, Vandavasi VG, O'Neill H, Roberts EM, Roberts AW, Yingling YG, Haigler CH (2016)

Comparative structural and computational analysis supports eighteen cellulose synthases in the plant cellulose synthesis complex. Sci Rep 6: 28696

Oehme DP, Downton MT, Doblin MS, Wagner J, Gidley MJ, Bacic A (2015) Unique aspects of the structure and dynamics of elementary Ibeta cellulose microfibrils revealed by computational simulations. Plant Physiol 168: 3-17

Park YB, Lee CM, Koo BW, Park S, Cosgrove DJ, Kim SH (2013) Monitoring meso-scale ordering of cellulose in intact plant cell walls using sum frequency generation spectroscopy. Plant Physiol 163: 907-913

Persson S, Paredez A, Carroll A, Palsdottir H, Doblin M, Poindexter P, Khitrov N, Auer M, Somerville CR (2007) Genetic evidence for three unique components in primary cell-wall cellulose synthase complexes in Arabidopsis. Proc. Natl. Acad. Sci. USA 104: 15566-15571

Rensing SA, Lang D, Zimmer AD, Terry A, Salamov A, Shapiro H, Nishiyama T, Perroud PF, Lindquist EA, Kamisugi Y, Tanahashi T, Sakakibara K, Fujita T, Oishi K, Shin IT, Kuroki Y, Toyoda A, Suzuki Y, Hashimoto S, Yamaguchi K, Sugano S, Kohara Y, Fujiyama A, Anterola A, Aoki S, Ashton N, Barbazuk WB, Barker E, Bennetzen JL, Blankenship R, Cho SH, Dutcher SK, Estelle M, Fawcett JA, Gundlach H, Hanada K, Heyl A, Hicks KA, Hughes J, Lohr M, Mayer K, Melkozernov A, Murata T, Nelson DR, Pils B, Prigge M, Reiss B, Renner T, Rombauts S, Rushton PJ, Sanderfoot A, Schween G, Shiu SH, Stueber K, Theodoulou FL, Tu H, Van de Peer Y, Verrier PJ, Waters E, Wood A, Yang L, Cove D, Cuming AC, Hasebe M, Lucas S, Mishler BD, Reski R, Grigoriev IV, Quatrano RS, Boore JL (2008) The *Physcomitrella* genome reveals evolutionary insights into the conquest of land by plants. Science 319: 64-69

Roberts AW, Bushoven JT (2007) The cellulose synthase (*CESA*) gene superfamily of the moss *Physcomitrella patens*. Plant Mol Biol 63: 207-219

Roberts AW, Dimos C, Budziszek MJ, Goss CA, Lai V (2011) Knocking out the wall: protocols for gene targeting in *Physcomitrella patens*. Methods Mol Biol 715: 273-290

Roberts AW, Roberts EM, Haigler CH (2012) Moss cell walls: structure and biosynthesis. Front Plant Sci 3: 166

Scavuzzo-Duggan TR, Chaves AM, Roberts AW (2015) A complementation assay for in vivo protein structure/function analysis in *Physcomitrella patens* (Funariaceae). App Plant Sci 3: 1500023

Schaefer DG, Zryd JP (1997) Efficient gene targeting in the moss *Physcomitrella patens*. Plant J 11: 1195-1206

Schindelin J, Arganda-Carreras I, Frise E, Kaynig V, Longair M, Pietzsch T, Preibisch S, Rueden C, Saalfeld S, Schmid B, Tinevez JY, White DJ, Hartenstein V, Eliceiri K, Tomancak P, Cardona A (2012) Fiji: an open-source platform for biological-image analysis. Nat Methods 9: 676-682

Schuetz M, Smith R, Ellis B (2013) Xylem tissue specification, patterning, and differentiation mechanisms. J Exp Bot 64: 11-31

Shen H, Yin Y, Chen F, Xu Y, Dixon RA (2009) A bioinformatic analysis of NAC genes for plant cell wall development in relation to lignocellulosic bioenergy production. Bioenerg Res 2: 217-232

Taylor JG, Owen TP, Jr., Koonce LT, Haigler CH (1992) Dispersed lignin in tracheary elements treated with cellulose synthesis inhibitors provides evidence that molecules of the secondary cell wall mediate wall patterning. Plant J 2: 959-970

Taylor NG, Gardiner JC, Whiteman R, Turner SR (2004) Cellulose synthesis in the Arabidopsis secondary cell wall. Cellulose 11: 329-338

Taylor NG, Howells RM, Huttly AK, Vickers K, Turner SR (2003) Interactions among three distinct CesA proteins essential for cellulose synthesis. Proc Natl Acad Sci USA 100: 1450-1455

Taylor NG, Laurie S, Turner SR (2000) Multiple cellulose synthase catalytic subunits are required for cellulose synthesis in Arabidopsis. Plant Cell 12: 2529-2539

Thomas LH, Forsyth VT, Martel A, Grillo I, Altaner CM, Jarvis MC (2014) Structure and spacing of cellulose microfibrils in woody cell walls of dicots. Cellulose 21: 3887-3895

Timmers J, Vernhettes S, Desprez T, Vincken JP, Visser RG, Trindade LM (2009) Interactions between membrane-bound cellulose synthases involved in the synthesis of the secondary cell wall. FEBS Lett. 583: 978-982

Tran ML, Roberts AW (2016) *Cellulose synthase* (*CESA*) gene expression profiling of *Physcomitrella patens*. . Plant Biol 18: 362–368

Updegraff DM (1969) Semimicro determination of cellulose in biological materials. Anal Biochem 32: 420-424

Vandavasi VG, Putnam DK, Zhang Q, Petridis L, Heller WT, Nixon BT, Haigler CH, Kalluri U, Coates L, Langan P, Smith JC, Meiler J, O'Neill H (2016) A structural study of CESA1 catalytic domain of Arabidopsis cellulose synthesis complex: evidence for CESA trimers. Plant Physiol 170: 123-135

Vidali L, Burkart GM, Augustine RC, Kerdavid E, Tuzel E, Bezanilla M (2010) Myosin XI is essential for tip growth in Physcomitrella patens. Plant Cell 22: 1868-1882

Vidali L, van Gisbergen PA, Guerin C, Franco P, Li M, Burkart GM, Augustine RC, Blanchoin L, Bezanilla M (2009) Rapid formin-mediated actin-filament elongation is essential for polarized plant cell growth. Proc Natl Acad Sci U S A 106: 13341-13346

Wilson SM, Bacic A (2012) Preparation of plant cells for transmission electron microscopy to optimize immunogold labeling of carbohydrate and protein epitopes. Nat Protoc 7: 1716-1727

Wise HZ, Saxena IM, Brown RM, Jr. (2011) Isolation and characterization of the cellulose synthase genes *PpCesA6* and *PpCesA7* in *Physcomitrella patens*. Cellulose 18: 371-384

Xu B, Ohtani M, Yamaguchi M, Toyooka K, Wakazaki M, Sato M, Kubo M, Nakano Y, Sano R, Hiwatashi Y, Murata T, Kurata T, Yoneda A, Kato K, Hasebe M, Demura T (2014) Contribution of NAC transcription factors to plant adaptation to land. Science 343: 1505-1508

Yang JH, Wang H (2016) Molecular mechanisms for vascular development and secondary cell wall formation. Front Plant Sci 7: 356

Yin Y, Huang J, Xu Y (2009) The cellulose synthase superfamily in fully sequenced plants and algae. BMC Plant Biol 9: 99

Zhong R, Ye ZH (2015) Secondary cell walls: biosynthesis, patterned deposition and transcriptional regulation. Plant Cell Physiol 56: 195-214

Zhu T, Nevo E, Sun D, Peng J (2012) Phylogenetic analyses unravel the evolutionary history of NAC proteins in plants. Evolution 66: 1833-1848

Supplemental Materials

Table S1. Primers used for vector construction and genotype analysis.

Primer pair	Sequences	Annealing temp.	Amplicon size	Amplified region
174JB 193JB	TACGGCAGGATGTATGAGCA TACTTCCACGGCTTCTTGCT	57°C	2003	5' targeting region *PpCESA8*
203JB 185JB	ATCAACAACAGCAAGGCCAT AGCACTTGGTTCAACCGATC	57°C	1041	3' targeting region *PpCESA8*
3KOattB1 3KOattB4	GGGGACAAGTTTGTACAAAAAAGCAGGC TCTGCAGACAGAGGGAGAAGAA GGGGACAACTTTGTATAGAAAAGTTGGG TGCAAGCTAATTCCCAAGCTG	66°C	894	5' targeting region *PpCESA3*
3KOattB3 3KOattB2	GGGGACAACTTTGTATAATAAAGTTGAA CGAAGCAAACGATTTGTAGAG GGGGACCACTTTGTACAAGAAAGCTGGG TGGAGACGTGGTTATTAGTGTTCG	66°C	898	3' targeting region *PpCESA3*
4KOattB1 4KOattB4	GGGGACAAGTTTGTACAAAAAAGCAGGC TGTCCCAGCCTCATCTACCAA GGGGACAACTTTGTATAGAAAAGTTGGG TTGCGAGCAGCAACCATATAC	68 ℃	1108	5' targeting region *PpCESA4*
4KOattB3 4KOattB2	GGGGACAACTTTGTATAATAAAGTTGGC GATCAGGATACTGCCATT GGGGACCACTTTGTACAAGAAAGCTGGG TGCACGTTTATAAGGTTAAATTTGCT	68 ℃	1148	3' targeting region *PpCESA4*
10KOattB1 10KOattB4	GGGGACAAGTTTGTACAAAAAAGCAGGC TCCTGTCAAGTTGCCAAACCT GGGGACAACTTTGTATAGAAAAGTTGGG TCAACGATCCAATCCCTGTCT	68 ℃	963	5' targeting region *PpCESA10*
10KOattB3 10KOattB2	GGGGACAACTTTGTATAATAAAGTTGCT ACTTTGGGTGCGCATTG GGGGACCACTTTGTACAAGAAAGCTGGG TCCGCACTACTCTAAACTTCAAGC	68 ℃	909	3' targeting region *PpCESA10*
6KOattB1 6KOattB4	GGGGACAAGTTTGTACAAAAAAGCAGGC TGACATTTCACCCAGTGAGCA GGGGACAACTTTGTATAGAAAAGTTGGG TCTTTCTTCCTCGCACCTCAC	60 ℃	1060	5' targeting region *PpCESA6*
7KOattB3 7KOattB2	GGGGACAAGTTTGTACAAAAAAGCAGGC TTACTCTTAACCGCAGCCTTG GGGGACAACTTTGTATAATAAAGTTGGT GATGGAGGAATCGAGGAA	60 ℃	599	3' targeting region *PpCESA7*
pMBL6attB4r pMBL6attB3r	GGGGACAACTTTTCTATACAAAGTTGGC TTATCGATACCGTCGACCT GGGGACAACTTTATTATACAAAGTTGGG CCCGTTATCCTCTTGAGT	68°C	2014	Selection cassette from pMBL6
8KOFlankF VectorR-hph	CTGGACAGACTTTCTCTCCGTTAT TCCGAGGGCAAAGAAATAGA	57°C	1121	5' integration *PpCESA8*
VectorF-hph 8KOFlankR	TGACAGATAGCTGGGCAATG CGTAAGAATATCCTCCGTCACC	57°C	637	3' integration *PpCESA8*
8KOFlankF 8KOFlankR	See above See above	57°C	731	*PpCESA8*KO cassette excision

3KOFlankF VectorR2-npt	GTTTCGTTTGGTTTCGCTGT TGCTTTGAAGACGTGGTTGG	57°C	1362	5' integration PpCESA3
VectorF2-npt 3KOFlankR	AAGTGGACGGAAGGAAGGAG TTGAAGCCGATGTGTAGCAG	57°C	1259	3' integration *PpCESA3*
4KOflankF VectorR-hph	TGTCAAGTGTCTAGCCATCCA TCTATTTCTTTGCCCTCGGA	59 ℃	1520	5' integration *PpCESA4* *hph* cassette
VectorF-hph 4KOflank-R2	TGACAGATAGCTGGGCAATG GCAATGGTGGTGGTGGTATC	58 ℃	1832	3' integration *PpCESA4* *hph* cassette
4KOflankF VectorR-npt	See above CCCGAAATTACCCTTTGTTG	57 ℃	1263	5' integration *PpCESA4* *npt* cassette
VectorF-npt 4KOflank-R2	GCCCTGTGCAAGGTAAGAAG See above	57 ℃	1839	3' integration *PpCESA4* w/ *npt* cassette
6KOF2 VectorR-hph	GCTTCAATGCTGTACCACAAACCAC TCCGAGGGCAAAGAAATAGA	57 ℃	1647	5' integration *PpCESA6*
VectorF-hph CESA7FlankR	TGACAGATAGCTGGGCAATG AAGCCCTAACTTCCAGCACC	57 ℃	833	3' integration *PpCESA7*
10KOflankF VectorR-hph	TTCCGACCTGATGTAAACCTG See above	57 ℃	1461	5' integration *PpCESA10* *hph* cassette
VectorF-hph 10KOflankR2	See above CATCCATTCATTTTCATGATGC	57 ℃	1136	3' integration *PpCESA10* *hph* cassette
10KOflankF VectorR-npt	See above See above	57 ℃	1274	5' integration *PpCESA10 npt* cassette
VectorF-npt 10KOflankR2	See above See above	57 ℃	1132	3' integration *PpCESA10 npt* cassette
CESA8TargetF CESA8TargetR	GTCTTCTTCGATGTACTGACAC TACTTCCACGGCTTCTTGCT	57°C	339	PpCESA8 deletion test
CESA3TargetF5 CESA3TargetR5	CGTGTGTCCAACTTGCAGTG CTTTAATTCGGCGACGCTGG	64°C	1266	*PpCESA3* deletion test
CESA6TargetF CESA6TargetR	GTGAGGTGCGAGGAAGAAAG TTCCCTAACTCCACCACTGC	60 ℃	142	*PpCESA6* deletion test
CESA7TargetF CESA7TargetR	CTTGTGAGGAAGTGCGGGAA ACATTACTCAACGGCCTCGG	60 ℃	1254	*PpCESA7* deletion test
CESA4TargetF CESA4TargetR2	AGGTGAGGTGGAAATGTTGC GCGTTGCAGATAGCATCACT	58 ℃	1731	*PpCESA4* t deletion test
CESA10TargetF CESA10TargetR	TGGGATTGAACATGAGACGA CACGCAGCCAATCATAGAGA	57 ℃	973	*PpCESA10* deletion test
4KOattB1 4KOattB2	See above See above	68 ℃	2321	*PpCESA4*KO cassette excision
HACESA3attB5 CESA8attB2	GGGGACAACTTTGTATACAAAAGTTGCG ATGGAGTACCCATACGATGTTCCAGATT ACGCTATGGAGGCTAATGCGGGCCTGGT GGGGACCACTTTGTACAAGAAAGCTGGG TATTACAAGCAGGTGAGGCCGCACCG	68°C	3370	*PpCESA8* coding sequence
HACESA3attB5 CESA3CDSattB2	See above GGGGACCACTTTGTACAAGAAAGCTGGG	68°C	3373	*PpCESA3* coding

	TATCACAAGCAGGTGAGGCCGCACCG			sequence
HACESA5attB5 CESA5attB2	GGGGACAACTTTGTATACAAAAGTTGCG ATGGCCTACCCCTACGATGTGCCCGATT ACGCTATGGAGGCTAATGCAGGCCTTAT GGGGACCACTTTGTACAAGAAAGCTGGG TACTAACAGCTAAGCCCGCACTCGAC	68°C	3337	*PpCESA5* coding sequence
HACESA4attB5 CESA4CDSattB2	GGGGACAACTTTGTATACAAAAGTTGCG ATGGAGTACCCATACGATGTTCCAGATT ACGCTATGAAGGCGAATGCGGGGCTGTT GGGGACCACTTTGTACAAGAAAGCTGGG TACTATCGACAGTTGATCCCACACTG	68°C	3391	*PpCESA4* coding sequence
HACESA7attB5 CESA6_7attB2	GGGGACAACTTTGTATACAAAAGTTGCG ATGGAGTACCCATACGATGTTCCAGATT ACGCTATGGAGGCGAATGCAGGGCTGCT GGGGACCACTTTGTACAAGAAAGCTGGG TATCAACAGTTTATCCCGCACTGCGA	68°C	3382	*PpCESA7* coding sequence
HACESA10attB5 CESA10CDSattB2	GGGGACAACTTTGTATACAAAAGTTGCG ATGGAGTACCCATACGATGTTCCAGATT ACGCTATGGAGTCGAGTCCAGGGCTTCT GGGGACCACTTTGTACAAGAAAGCTGGG TACTATCAGCAGTTGATCCCGCACTC	68°C	3379	*PpCESA10* coding sequence

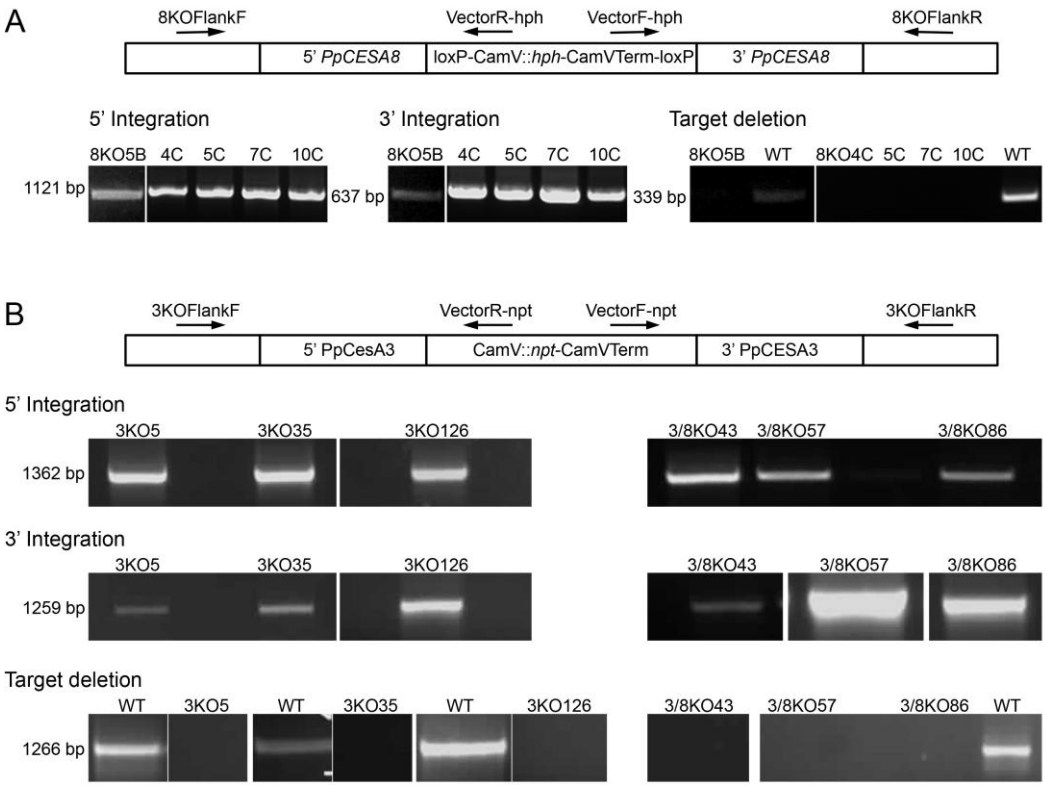

Fig. S1. Genotype analysis of *ppcesa8*, *ppcesa3* and *ppcesa3/8* KO lines. (A) Genotyping strategy and results for *ppcesa8* KO lines. 5' integration tested by PCR with primer pair 8KOFlankF/VectorR-hph produced the expected 1121 bp fragment in lines 8KO5B, 5KO4C, 5KO5C, 5KO7C and 8KO10C. 3' integration tested by PCR with primer pair VectorF-hph/8KOFlankR produced the expected 637 bp fragment in the same 5 lines. Target deletion was verified in the 3 KO lines by the absence of a product from primer pair CESA8TargetF/CESA8TargetR, which anneal within the *PpCESA8* coding sequence and amplify a 339 bp fragment in the wild type. (B) Genotyping strategy and results for *ppcesa3* and *ppcesa3/8* KO lines. 5' integration tested by PCR with primer pair 3KOFlankF/VectorR-npt produced the expected 1362 bp fragment in lines 3KO5, 3KO35, 3KO126, 3/8KO43, 3/8KO57, and 3/8KO86. 3' integration tested by PCR with primer pair VectorF-npt/3KOFlankR produced the expected 1259 bp fragment in the same 6 lines. Target deletion was verified in the 6 KO lines by the absence of a product from primer pair CESA3TargetF5/CESA3TargetR5, which anneal within the *PpCESA3* coding sequence and amplify a 1266 bp fragment in the wild type.

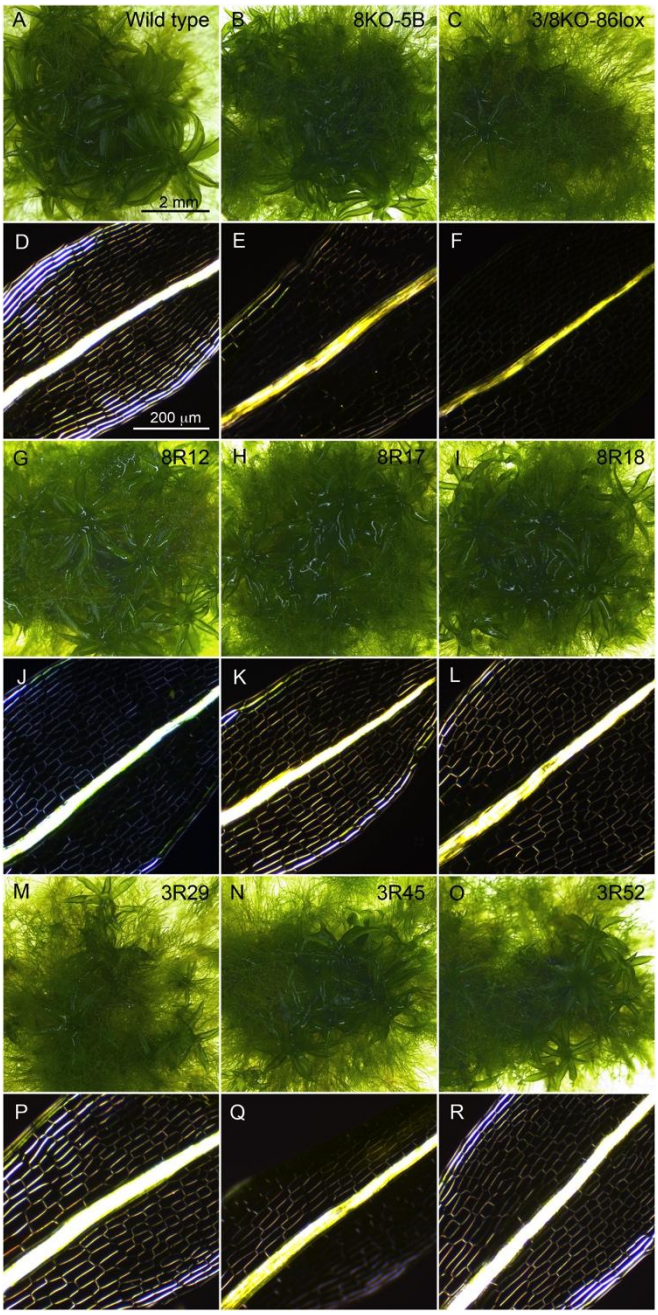

Fig. S2: Phenotype analysis of a *ppcesa3/*8 double KO line transformed with vectors driving expression of *PpCESA3* or *PpCESA8* with their native promoters. Bright field images captured with a stereomicroscope show colony morphology (A-C, G-I, M-O) and polarization images show cell wall birefringence (D-F, J-L, P-R). (A-F) Wild type with erect gametophores (A) and strong cell wall birefringence (D), *ppcesa8* KO with erect gametophores (B) and intermediate cell wall birefringence (E) and *ppces3/8* KO with horizontal gametophores (C) and weak birefringence (F) are shown for comparison to complemented lines. (G-R) Complemented lines have erect gametophores (G-I, M-O) and strong cell wall birefringence (J-L, P-R).

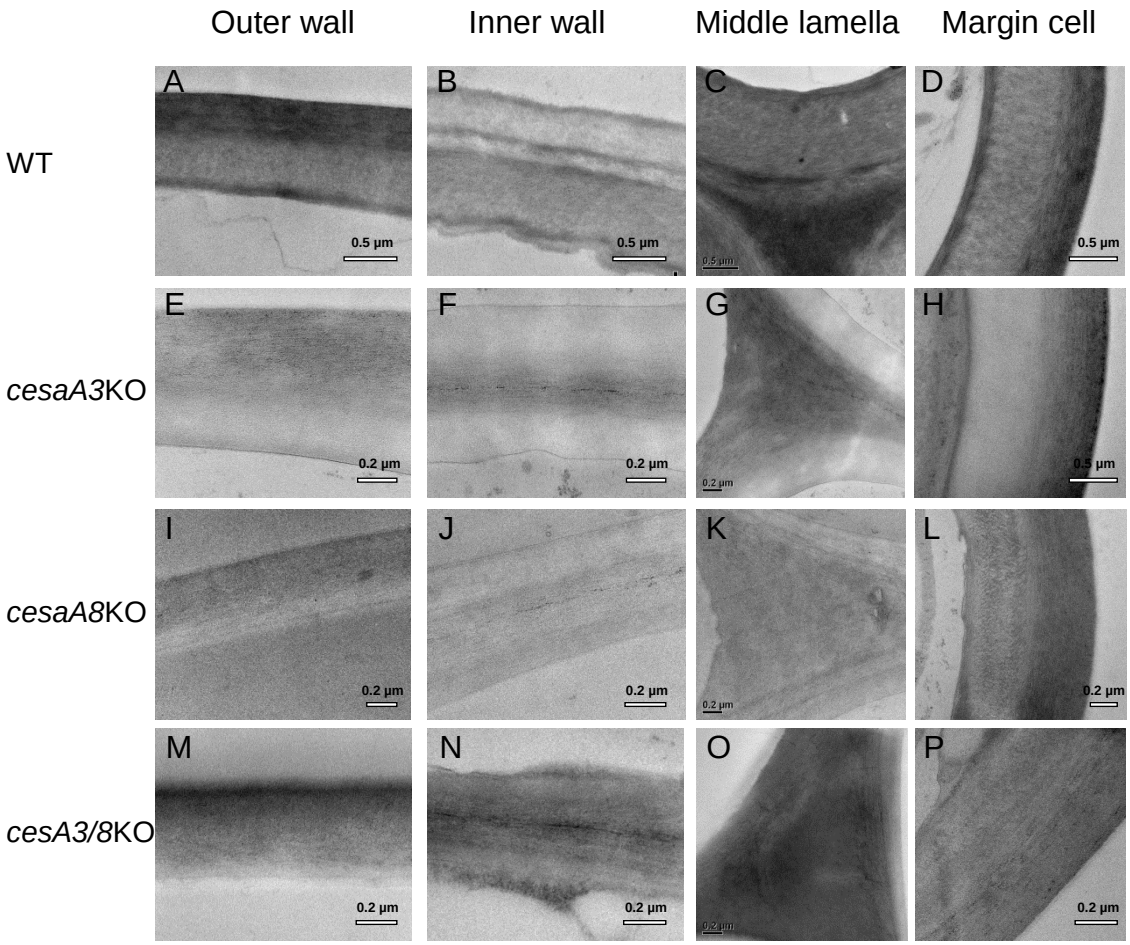

Fig. S3. Transmission electron microscopy images of leaf cell walls from wild type and *cesa*KO lines of *P. patens.* In lamina cells, outer walls face the external environment, inner walls are between cells, and middle lamellae are from cell junctions. Margin cells are from leaf edges.

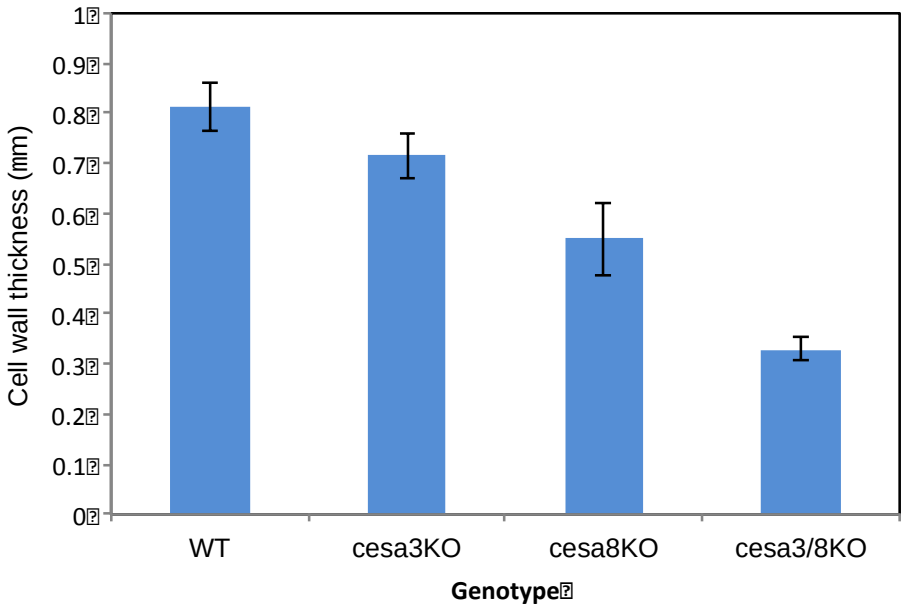

Fig. S4. Thickness of outer cell walls measured from transmission electron microscopy images. Error bars represent standard error of the mean (n=2 lines per genotype).

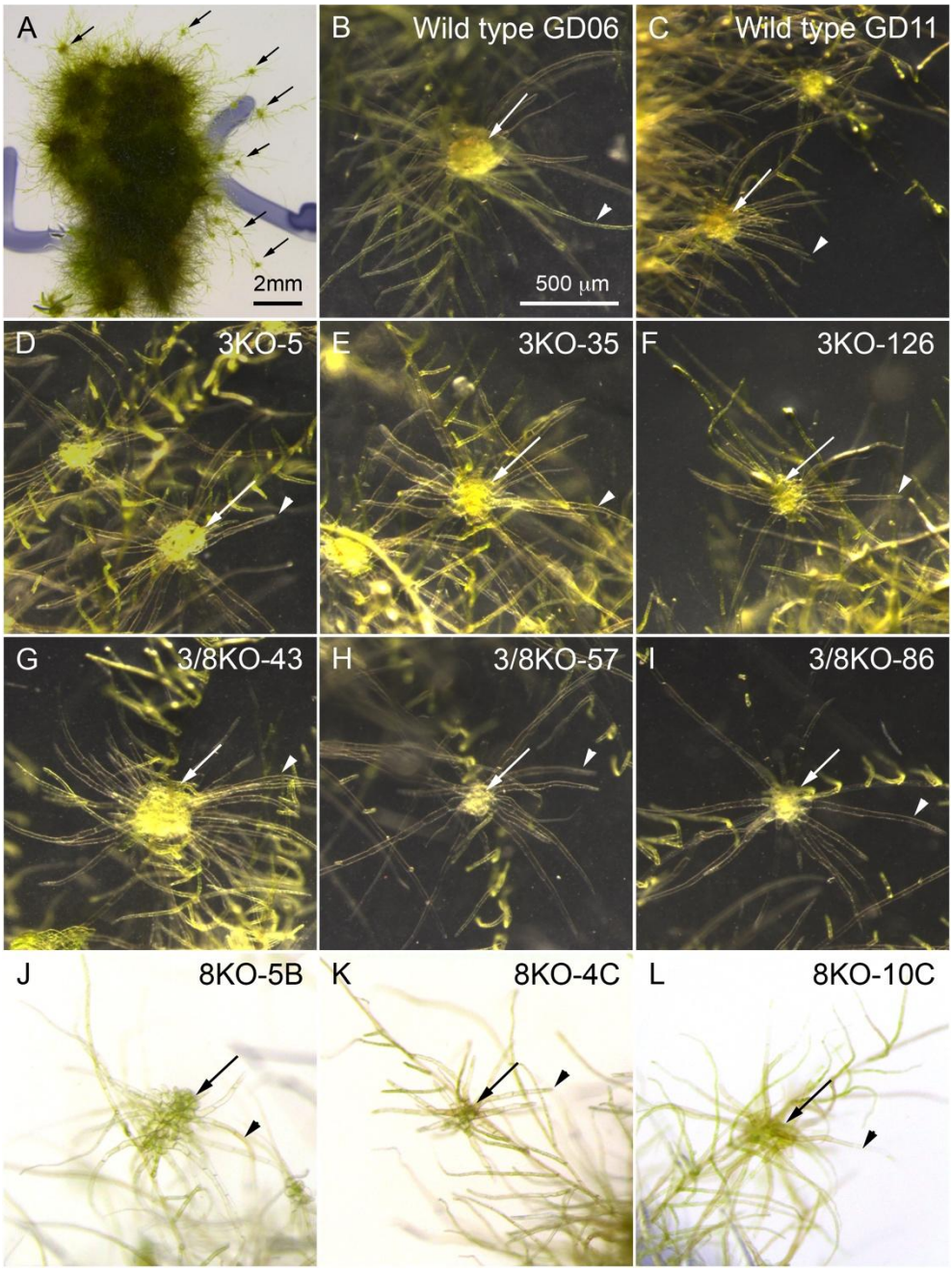

Fig. S5: *P. patens* wild type and KO lines cultured on medium containing 1 μM naphthalene acetic acid (auxin) to induce rhizoid initiation and inhibit leaf initiation. (A) A wild type colony with leafless gametophores (arrows). (B,C) Dark field images of wild type leafless gametophores with multiple rhizoids (arrowheads). (D-I) Dark field images of *ppcesa3* KO and *ppcesa3/8* KO leafless gametophores with multiple rhizoids. (J-L) Bright field images of *ppcesa8* KO leafless gametophores with multiple rhizoids. No defects in rhizoid initiation or growth were noted in any of the KO line

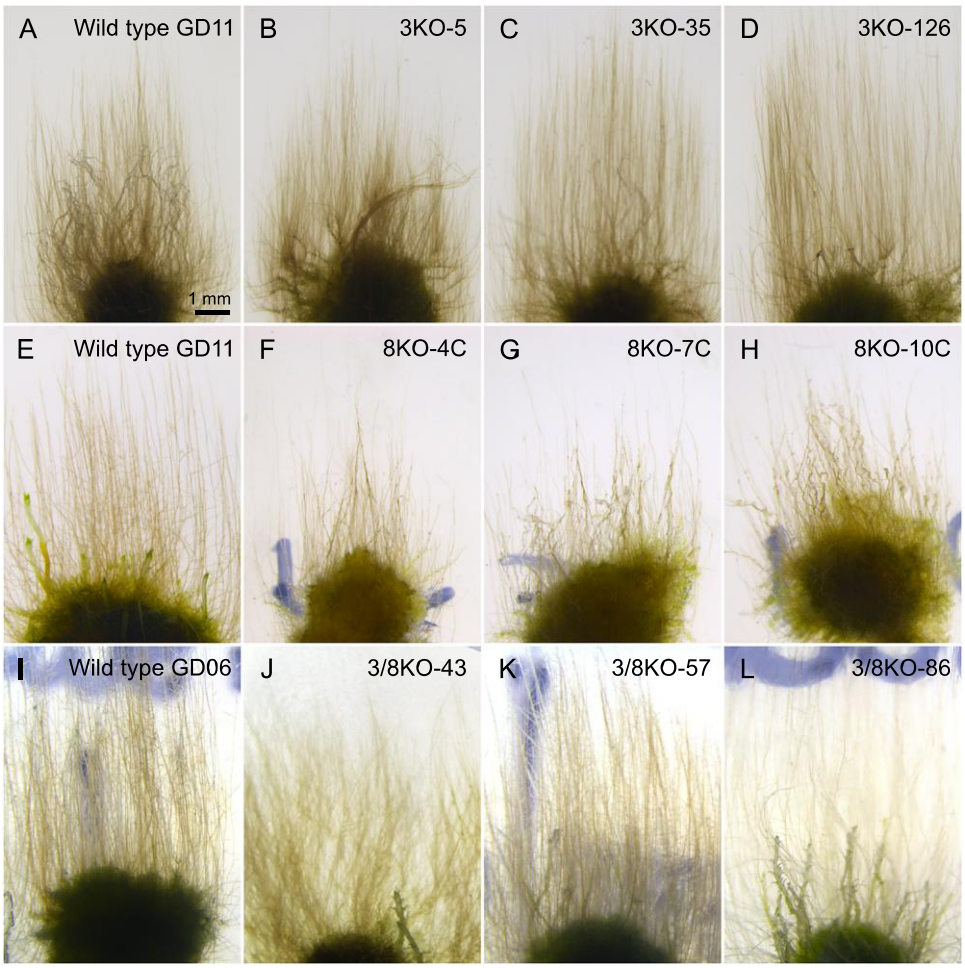

Fig. S6: *P. patens* wild type and KO lines cultured in the dark on vertically oriented plates containing medium supplemented with 35 mM sucrose to test for caulonema gravitropism. KO lines in columns 2-4 of each row are compared to their background wild type line from the same experiment in column 1. No significant differences in caulonema length or gravitropic behavior were detected.

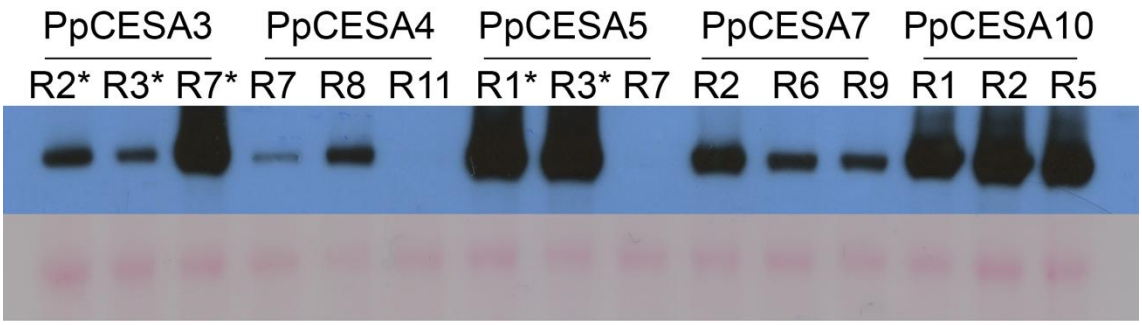

Fig. S7. Western blot analysis of protein expression for *P. patens* lines derived from transformation of *ppcesa3/8*KO-86lox with vectors driving expression of PpCESAs under control of the *PpCESA8* promoter. Western blot probed with anti-HA is shown above the same blot stained with Ponceau S as a loading control. Protein loading per lane was 3.6 μg. Asterisks indicate lines that rescued the mutant phenotype.

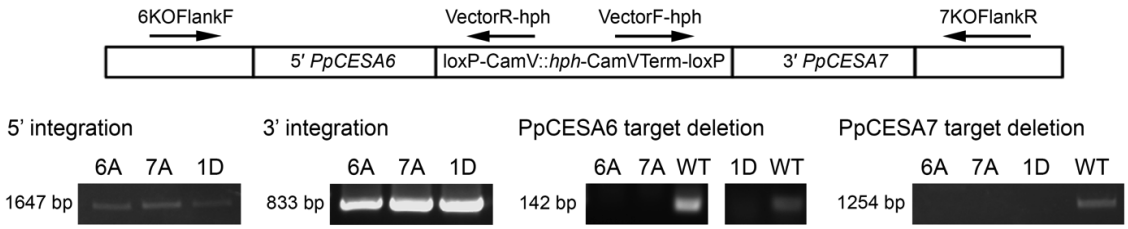

Fig. S8: PCR-based genotyping of *ppcesa6/7* KO lines. Primers used for amplification of 5' and 3' ends are indicated as black arrows on the diagram showing the PpCESA6/7KO vector integrated so as to delete PpCESA6 and PpCESA7, which occur as a tandem repeat. The products confirming 5’ (1647 bp) and 3’ (833 bp) integration amplified in three KO lines (6A, 7A and 1D) selected from two transformations. Products from amplification of the target genes *PpCESA6* (142 bp) and *PpCESA7* (1254 bp) were observed in wild type (WT), but not in KO line.

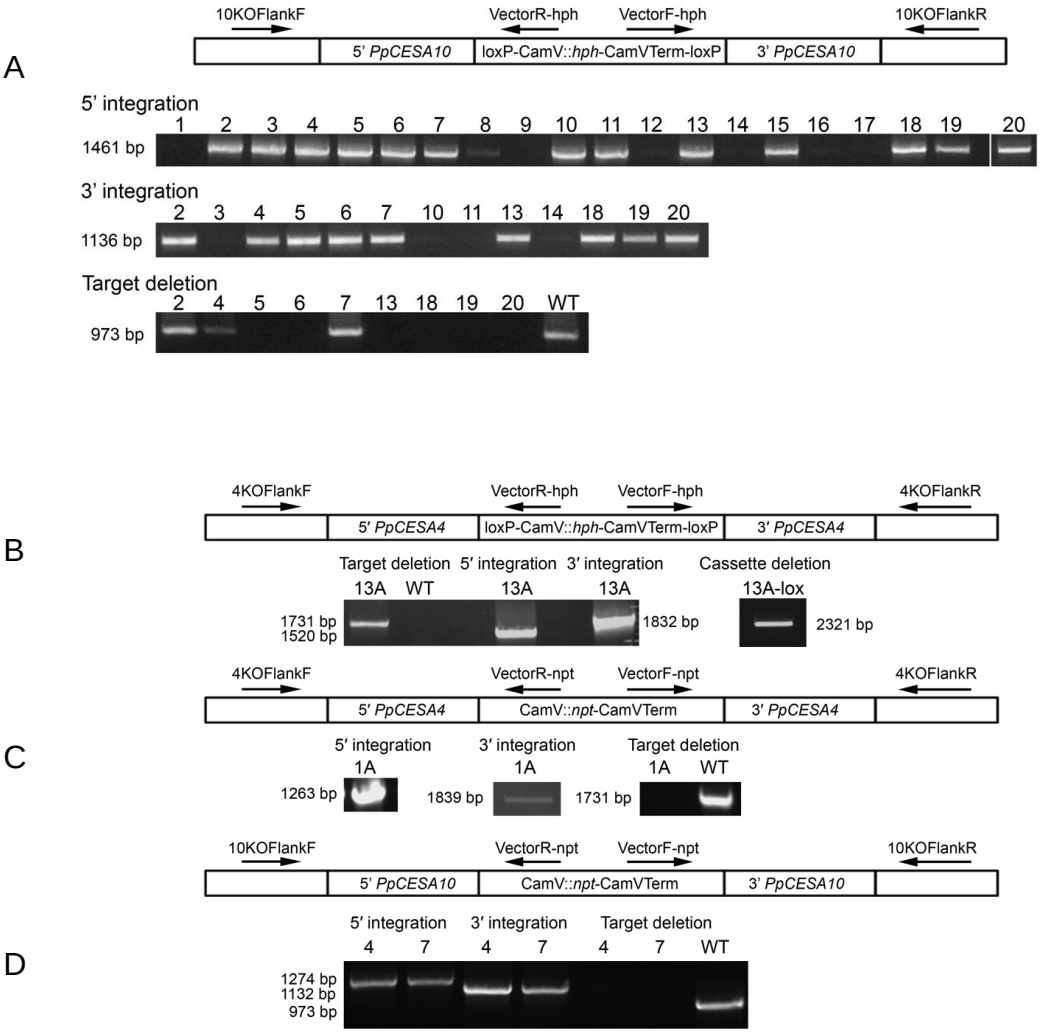

Fig. S9: PCR-based genotyping of *ppcesa4/10* KO lines. (A) Six *ppcesa10*KO lines recovered from one transformation with the PpCESA10KO vector conferring hygromycin resistance were verified by amplification the 5' integration site (1461 bp) and 3' integration site (1136 bp) and lack of amplification of the target gene (973 bp). (B) *ppcesa4*KO-13A recovered from a transformation with the CESA4KO vector conferring hygromycin resistance was verified by amplification the 5' integration site (1521 bp) and 3' integration site (1832 bp) and lack of amplification of the target gene (1731 bp) and *cre*-mediated deletion of the selection cassette was verified by amplification across the deletion site (2321 bp). (C) A double *ppcesa4/10*KO line from transformation of *ppcesa10*KO-5 with the CESA4KO vector conferring G418 resistance was verified by amplification the 5' integration site (1263 bp) and 3' integration site (1839 bp) and lack of amplification of the target gene (1731 bp). (D) Double *ppcesa4/10*KO lines from transformation of *ppcesa4*KO-lox with the CESA10KO vector conferring G418 resistance was verified by amplification the 5' integration site (1274 bp) and 3' integration site (1132 bp) and lack of amplification of the target gene (973 bp).

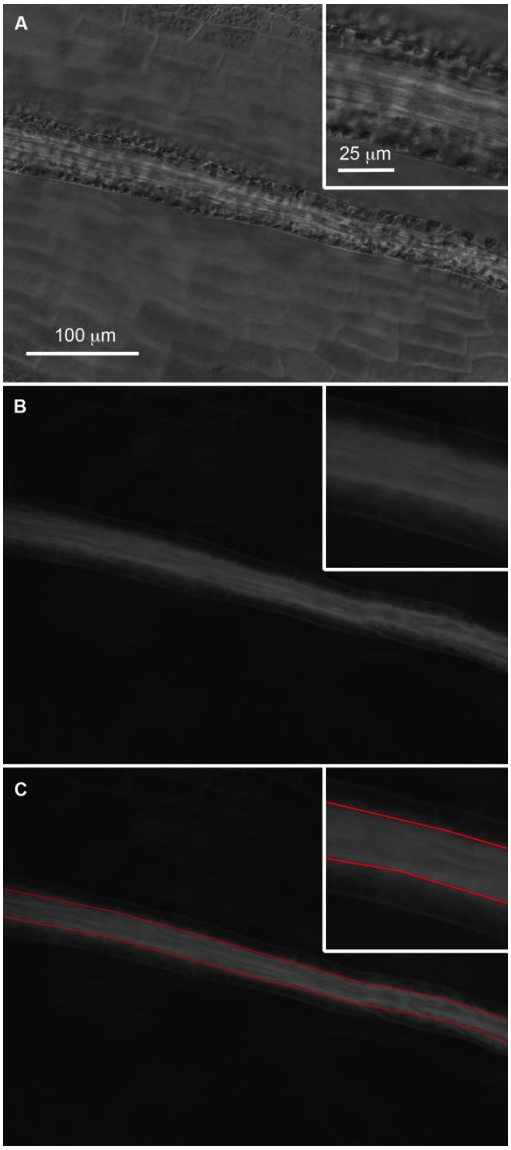

Fig. S10: Quantification method for S4B fluorescence. Representative paired DIC (A) and fluorescence (B,C) micrographs of a *P. patens* leaf stained with S4B. Insets show the central midrib and surrounding bundle sheath at higher magnification. The central midrib was selected manually using the polygon selection tool in ImageJ (Fiji version) as shown by the red lines in C.

Manuscript 2

Manuscript formatted for the publication in *Planta*

Short title: Identify functions of CESAs in *Physcomitrella*

Title: Morphological analysis of cellulose synthase (CESA) mutants in *Physcomitrella patens*

Xingxing Li[a], Mai L. Tran[a], Joanna H. Norris[a] , Alison W. Roberts[a]

[a]Department of Biological Sciences, University of Rhode Island, Kingston RI 02881, USA

One sentence summary: The P*hyscomitrella* clade-B PpCESAs (PpCESA4, PpCESA6, PpCESA7, and PpCESA10) are not required for leafy gametophore morphogenesis, indicating PpCESA5 forms homo-oligomeric cellulose synthesis complexes; meanwhile PpCESA4 and PpCESA10 are involved in the tip growth of protonema cells.

List of author contributions: A.W.R. conceived the project, and supervised experiments; X.L. designed and performed experiments, and analyzed the data; M.L.T and J.H.N performed experiments; X.L. and A.W.R. wrote the manuscript. All authors read and approved the manuscript.

Funding information: This work was supported by National Science Foundation Award IOS-1257047. DNA sequencing and qPCR were conducted using the Rhode Island Genomics and Sequencing Center, a Rhode Island NSF EPSCoR research facility, supported in part by the National Science Foundation EPSCoR Cooperative Agreement EPS-1004057. We also thank Bowen Jiang for assistance with statistics.

Abstract

Cellulose produced by plasma membrane rosette Cellulose Synthesis Complexes (CSCs) is an essential component of plant cell walls, providing vital mechanical strength. The catalytic subunits of CSCs, called cellulose synthase (CESA) proteins, are encoded by gene families that vary in size among different plant species. *Arabidopsis* has 10 functionally non-redundant *CESA* genes, and assembly of its CSCs requires the participation of at least three members from this gene family, which means these CSCs are obligate hetero-oligomeric. The moss *Physcomitrella patens* has rosette CSCs and seven CESA genes that have not been fully characterized functionally. According to phylogenetic studies, the PpCESAs are not members of the clades comprising the different subunits of the hetero-oligomeric seed plant CSCs. Hence, it is unknown whether *P. patens* CSCs are also hetero-oligomeric. Previous functional analyses showed that *ppcesa5* knockout (KO) mutants are unable to produce gametophores. Double *ppcesa3/8*KOs were shown to be defective in secondary cell wall deposition in gametophore leaf midribs. Here, we continue investigating functions of *PpCESAs* through morphological analysis of *ppcesa* KO mutants to gain clues about the composition of *P. patens* CSCs. Our results show that B-clade PpCESAs (PpCESA4, 6, 7, and 10) are not required for gametophore morphogenesis. However, PpCESA4 and 10 are found to serve a function in the tip growth of protonema filaments, indicating the potential roles of cellulose in the cells undergoing tip growth.

Introduction

Cellulose is a key component in plant cell walls. In the primary cell wall (deposited during cell expansion), the oriented deposition of cellulose microfibrils serves the vital load-bearing role important in determining the orientation of cell expansion and thus overall plant morphology (Taylor, 2008). After cell expansion has stopped, certain cells, such as collenchyma cells, sclerenchyma cells, and xylem cells, can deposit thickened secondary cell walls (inside the primary wall) that mechanically support plants to stand upright and efficiently conduct water and minerals (Mauseth, 2012). Cellulose is highly abundant in the secondary walls (Taylor, 2008). Cellulose microfibrils, in higher plants, are synthesized by rosette cellulose synthesis complexes (CSCs) embedded in the plasma membrane. The catalytic core of these complexes is assembled from cellulose synthase (CESA) subunits (Delmer, 1999; Kimura et al., 1999; McFarlane et al., 2014). In seed plants, the CSCs for cellulose deposition in both primary and secondary cell wall requires three types of functional distinct CESAs for function (McFarlane et al., 2014). In Arabidopsis, mutants for *CESA1*, *CESA3*, and *CESA6* have cellulose defects in primary cells wall causing developmental retardation and phenotypic changes in hypocotyls and roots (Arioli et al., 1998; Fagard et al., 2000; Williamson et al., 2001; Burn, et al., 2002; Robert et al., 2004). Mutations in any of the three secondary cell wall CESAs (CESA4, 7, and 8) result in severe defects in secondary cell wall cellulose deposition leading to collapsed xylem cells in *Arabidopsis* (Turner & Somerville, 1997; Taylor et al., 1999; Taylor et al., 2000; Taylor et al., 2003). The moss *Physcomitrella patens* is an intriguing model bryophyte that is commonly used in genetics studies and mutational analysis because of its ability

to be genetically manipulated due to the naturally occurring high rate of homologous recombination. Gene knockin and knockout transformations can be accomplished within one month and phenotyped in a few weeks in *P. patens* (Kamisugi, Cuming, & Cove, 2005). This is rapid compared to transformation and phenotypic analysis in *Arabidopsis*, which takes about three months (Clough & Bent, 1998). Rapidly elongating protonema cells in *P. patens* can be used as an alternative model to examine tip-growth related mechanisms (Rounds & Bezanilla, 2013). Leafy gametophores consist of several distinguishable cell types including support cells (stereids) and water-conducting cells (hydroids), but they develop from single-celled shoot apical meristems, making *P. patens* a less complicated model to study plant organ morphogenesis (Harrison et al., 2009). *Physcomitrella patens* has seven CESA genes which can be divided into two sub-clades (A-clade: *PpCESA3*, *5*, and *8*; B-clade: *PpCESA4*, *6*, *7*, and *10*), but are not orthologs of seed plants CESAs (Goss et al., 2012; Roberts & Bushoven, 2007).

We carried out morphological analysis of *CESA* knockout (KO) mutants in order to investigate functions of CESAs in *P. patens*. So far, PpCESA5 is known to be required in gametophore development based on the "no leafy gametophore" phenotype of *ppcesa5*KO mutant (Goss et al., 2012). Both of double *ppcesa3/8*KO and *ppcesa6/7*KO mutants show significantly reduced cellulose deposition in secondary cell walls in midribs of gametophore leaves, indicating PpCESA3, 8, 6, and 7 are involved in secondary cell wall thickening of stereids (Norris et al., 2017). Here, we show that the quadruple *ppcesa4/6/7/10*KO*s* are able to produce morphologically normal leafy gametophores, indicating that the B-clade PpCESAs are not required in

gametophore morphogenesis. Since ppcesa3/8KO also produces morphologically normal gametophores (Norris et al., 2017), together the current results suggest that PpCESA5 might be able to form homo-oligomeric CSCs, solely functioning in gametophore development. In addition, knocking out *PpCESA4* and *PpCESA10* causes morphological changes in protonemal colonies, suggesting the importance of cellulose in the tip-growing *P. patens* protonema cells.

Results

Genotyping and morphological analysis (rhizoid, caulonema, and gametophore) of *ppcesa4/6/7/10*KO

Three verified quadruple *ppcesa4/6/7/10*KO lines were recovered from three different transformations of *ppcesa4/10*KO-4B with the CESA6/7KO vector (Norris et al., 2017) and tested for 5' and 3' integration of the vector and deletion of the target gene (**Figure 1**). All of the quadruple KO lines were able to produce leafy gametophores that were morphologically similar to wild type (**Figure 2 A-H**) indicating that the B-clade PpCESAs are not required for gametophore morphogenesis. The quadruple KOs were also tested for developmental defects in rhizoid and caulonema development. All of the three quadruple KOs produced leafless gametophores with several rhizoids similar to wild-type after growing on medium supplied with auxin for two weeks (**Figure S1)**, indicating that PpCESA4, PpCESA6, PpCESA7, and PpCESA10 are not required for normal rhizoid development. When explants of quadruple KOs were cultured vertically in the dark, caulonemal filaments produced by the resulting colonies grew upright against gravity and were similar in appearance to wild-type

controls (**Figure S2 A-F**). Caulonemal length was also not significantly different between the mutant lines and wild-type lines (**Figure S2 G**).

Cellulose deposition of the secondary cell wall in *ppcesa4/6/7/10*KO

By polarization microscopy and S4B staining, Norris et al. (2017) showed a large and significant reduction in cellulose deposition in the midribs of *ppcesa6/7*KO gametophore leaves, whereas the gametophore leaves of *ppcesa4/10*KOs showed a small, but significant reduction compared to wild-type. To clarify the roles of the clade B PpCESAs in secondary cell wall deposition, we used polarization microscopy to examine midrib birefringence in *ppcesa4/6/7/10*KO compared to wild-type (Gd11). We found that gametophore leaves of three *ppcesa4/6/7/10*KO lines all had substantially reduced midrib birefringence (**Figure 2 J-L**), similar to the phenotypes of previously described *ppcesa6/7*KOs and *ppcesa3/8*KOs, and more dramatic than *ppcesa4/10*KOs (Norris et al., 2017). To quantify the defect in secondary cell wall deposition relative to *ppcesa4/10*KOs and *ppcesa6/7*KOs, we stained mutant gametophore leaves with cellulose-specific fluorescent dye S4B and used fluorescence microscopy to measure the cellulose content in midribs of the mutant leaves. All mutants showed a significant reduction in brightness compared with the midribs of wild-type gametophore leaves (**Figure 3**), consistent with previous results. The quadruple KO midribs had significantly reduced brightness compared to *ppcesa*4/10KOs but were not significantly different from *ppcesa*6/7KOs (**Figure 3**). The phenotype similarity of *ppcesa4/6/7/10*KO compared to *ppcesa6/7*KO, but not *ppcesa*4/10KO (Norris et al., 2017) indicates a major role for PpCESA6 and

PpCESA7 and a minor role for PpCESA4 and PpCESA10 in secondary cell wall deposition in gametophore leaf midribs.

Morphological analysis of protonema colonies

Protonemal filaments of *P. patens* extend by apical cell division and tip growth, branching to form colonies (Cove, 2005). To test whether clade B PpCESAs are required for protonemal tip growth, Chlorophyll autofluorescence images of colonies were analyzed for area, solidity, and circularity. **Figure 4** summarizes the results of this assay for ppcesa4/6/7/10KOs, ppcesa6/7KOs, and ppcesa4/10KOs. Circularity is the ratio of colony area to colony perimeter and indicates the degree of polarized extension. A score of 1 represents a perfect circle, while scores approaching 0 represent a more linear shape. Solidity quantifies the presence of concavities in the colony and reflects the degree of polarization and branching of the protonema filaments. The lowest solidity with the highest branching of the filaments was scored 0 and the highest solidity possible with less branching of filaments was scored 1 (Vidali et al., 2007). Graphs in **Figure 5** show that when compared with wild-type control, colonies of *ppcesa4/6/7/10*KO showed increased solidity and circularity. *pcesa6/7*KOs showed no difference in area, solidity or circularity compared to wild-type ($P>0.05$, ANOVA). All *ppcesa4/10*KOs showed significantly increased solidity and circularity compared to wild-type similar to *ppcesa4/6/7/10*KO, consistent with defects in protonemal tip growth. We further analyzed single *ppcesa4*KOs and *ppcesa10*KOs. Only two of the three *ppcesa4*KO lines, *ppcesa4*KO-13A and *ppcesa4*KO-14B, had significantly increased solidity and circularity compared to wild-type. There was no significant difference observed among the three ppcesa10KOs. We also tested

*ppcesa5*KO and *ppcesa3/8*KO to test the roles of the clade A PpCESAs in protonema tip growth. One of the three *ppcesa5*KOs, *ppcesa5*KO-20, showed the significantly increased solidity and circularity compared to both wild-type and the other two ppcesa5KOs. None of *ppcesa3/8*KOs showed any significant difference compared with wild-type in the three parameters.

Discussion

Mutation analysis for the B-clade *PpCESA*s revealed that they are not required for gametophore morphogenesis. This is evident from the fact that quadruple *ppcesa4/6/7/10*KOs are still able to produce normal leafy gametophores (**Figure 2**), unlike *ppcesa5*KO. Gametophore buds of *ppcesa5*KOs are defective in cell expansion, cytokinesis, and leaf initiation, resulting in failure of leafy shoot formation (Goss et al., 2012). None of these phenomena were observed in *ppcesa4/6/7/10*KOs. The *ppcesa3/8*KOs also produce morphologically normal gametophores (Norris et al., 2017). Thus *ppcesa5*KOs are the only mutants that are defective in gametophore morphogenesis. It has also been shown that constitutively expressing PpCESA3 and PpCESA8 can rescue *ppcesa5*KO indicating A-clade PpCESAs are functionally interchangeable (Norris et al., 2017). Thus, the unique mutant phenotype of *ppcesa5*KOs might be attributable to PpCESA5 having non-overlapping expression with PpCESA3 and PpCESA8 and the non-interchangeable functions with the B-clade PpCESAs (Scavuzzo-Duggan et al., unpublished). According to this, PpCESA5 might be able to form homo-oligomeric CSCs in order to properly deposit cellulose microfibrils into the cell walls of newly emerged gametophore buds. The

interchangeable functions of different CESA members are seen only in limited cases in seed plants. Promoter-swap assays in *Arabidopsis* showed that the defective phenotype of *atcesa3* mutants can be partially rescued by driving expression of *AtCESA7* using the *AtCESA3* promoter and *atcesa8* mutants can be partially rescued by driving expression of *AtCESA1* using the *AtCESA8* promoter (Carroll et al., 2012).

Results of S4B staining (**Figure 3**) showed that: 1) there is no significant difference between *ppcesa4/6/7/10*KO*s* and *ppcesa6/7*KO in cellulose content in the midrib secondary cell walls of the mutant leaves; 2) there is a slight but significant reduction in *ppcesa4/10KO* compared to the wild-type. These results suggest that compared with PpCESA6 and PpCESA7, PpCESA4 and PpCESA10 only have a minor role in secondary cell wall deposition. This is consistent with previous gene expression data showing that *PpCESA4* and *PpCESA10* have lower expression in gametophores than in protonema (Hiss et al., 2014; Tran & Roberts, 2016). The fact that *ppcesa3/8*KOs and *ppcesa6/7*KOs are similar in phenotype showing cellulose defects in secondary cell walls provides a clue that CSCs involved in cellulose deposition in *P. patens* secondary cell walls might be hetero-oligomeric consisting of PpCESA3, PpCESA8, PpCESA6, and PpCESA7 (Norris et al., 2017).

Tip growth in certain types of cells, such as root hairs and pollen tubes, is regulated by highly coordinated mechanisms which guide deposition of new cell wall materials strictly proceeding in a limited area of the cell surface (Carol & Dolan, 2002; Cosgrove, 2005; Cheung & Wu, 2008; Lee & Yang, 2008; Nielsen, 2009; Gu & Nielsen, 2013). Several studies pointed out that cellulose is an essential cell wall component in cells undergoing tip growth (Newcomb & Bonnett, 1965; Emons &

Wolters-Arts, 1983; Emons, 1994; Galway et al., 2011; Park et al., 2011). Mutational analyses in *Arabidopsis* showed that some *atcesa* mutants are severely defective in germinating pollen and elongating pollen tube, indicating important roles of cellulose in the tip-growing cells (Persson et al., 2007). Elongating *P. patens* protonemal filaments are another ideal model to investigate the role of cell wall deposition in tip-growth related mechanisms (Roberts et al., 2012). Crystalline cellulose has been detected by affinity cytochemistry with Cellulose Binding Module 3A (CBM3A) in primary cell walls of subapical cells and the very tip region of the apical cells in expanding *P. patens* protonema filaments (Berry et al., 2016), indicating the potential roles of cellulose during tip growth of protonema. Here, our study shows that *P. patens* CESAs (PpCESA4 and 10) have roles in tip growing protonema, supporting the point of view that cellulose is significant for cell tip growth. This is evident from the abnormal protonema colony morphology of *ppcesa4/10*KOs, which show significantly increased circularity and solidity (**Figure 5**). Increased circularity and solidity are caused by slower elongation and less branches of the protonema filaments (Vidali et al., 2007). Quantitative affinity cytochemistry of cellulose content using S4B or CBM3A will be needed to prove that the mutant phenotypes were caused by the decreased cellulose in cell walls of tip-growing protonema cells. Based on available evidence, PpCESA6, PpCESA7, and the A-clade PpCESAs do not seem to contribute to protonemal tip growth, since no obvious phenotypic changes were observed in corresponding KO mutants. Although colony circularity and solidity of *ppcesa5*KO-20 was shown to be significantly increased in our analysis, this is likely due to other genetic effects since the other *ppcesa5*KO lines were not different from

wild-type. It remains possible that PpCESA5, PpCESA3 and PpCESA8 function redundantly in tip growth. This can be tested by producing and analyzing a ppcesa3/5/8 triple KO mutant. Tip growth in our *ppcesa4/10*KO and *ppcesa4/6/7/10*KO was not abolished, suggesting the deposition of cellulose in cell walls of tip-growing protonema involves proteins other than the PpCESAs. Several members from one of the Cellulose Synthase-like (CSL) gene family, CSLD, were shown to be required for tip growth of root hairs and pollen tubes in *Arabidopsis* (Favery et al., 2001; Wang et al., 2001; Bernal et al., 2008; Park et al., 2011). *P. patens* also has the CSLD gene family, and expression of these genes have enhanced expression in cultures containing only protonema (Roberts & Bushoven, 2007). Thus, it will be interesting to carry out mutational analysis to investigate functions of CSLD genes in *P. patens* protonema.

Materials and methods

Transformation and genotyping

Except *ppcesa4/6/7/10*KOs, the *ppcesa*KO lines used in this study were created previously and described in Norris et al. (2017).

To create the quadruple *ppcesa4/6/7/10*KO lines, the hygromycin sensitive *ppcesa4/10*KO-4B line (Norris et al., 2017) was transformed with the *CESA6/7KO* vector conferring hygromycin resistance and stably transformed colonies were genotyped as described for primary *ppcesa6/7*KO lines in Norris et al. (2017). Primers used for genotyping are listed in supplemental table 1.

Polarization microscopy of cell wall birefringence

Cell wall birefringence of leaf midribs was analyzed as described in Norris et al., (2017). Three independent lines of each knockout mutant and three biological replicates of wild-type were cultured for 15 days on BCDAT medium. The first fully expanded leaf of each gametophore was cut off with a pair of micro-dissecting scissors (Electron Microscopy Sciences, Hatfield, PA, USA) and mounted in the water on a glass slide. An Olympus BHS compound microscope equipped with a polarizer and circular-polarizing analyzer (Olympus Corp., Shinjuku, Tokyo, Japan) was used to visualize the gametophore leaves. Images were captured with a Leica M165FC digital camera (Leica Microsystems Inc., Buffalo Grove, IL, USA) using identical settings for the knockouts and the wild-type control.

Pontamine fast scarlet 4B (S4B) fluorescence histochemistry

S4B staining of leaf midribs was performed as describe (Norris et al., 2017). Three independent lines of each knockout along with three biological replicates of wild-type were cultivated on BCDAT medium for 15 days. For each genotype, three gametophores with 10-12 leaves were collected, permeabilized in acetone for 5 seconds, rinsed in PBS, and stained for 30 min in PBS containing 0.01% S4B. All leaves were rinsed in PBS after staining, cut off with a sharp razor blade, and mounted in PBS on a glass slide. Images were taken using the same microscope and conditions described previously in Norris et al (2017). For data analysis, the midrib of each leaf was outlined by hand and intensity was quantified using ImageJ as described previously (Norris et al., 2017).

Analysis of caulonema and rhizoid development

Caulonema and rhizoid assays were carried out as previously described (Roberts et al., 2011) to test *ppcesa4/10*KO, *ppcesa6/7*KO, *ppcesa4/6/7/10* KO lines for phenotypic changes. For the caulonema and rhizoid assays, samples were analyzed using a Leica M165FC stereomicroscope, and images were recorded using a Leica DFC310FX camera (Leica). The length of caulonema was measured as described in Norris et al. (2017). Three independent experiments (n=3) were done. For each experiment, caulonema colonies were cultured on seven replicate plates containing solid BCDAT? medium. Four explants were placed along the equator of each plate, with each explant representing a unique genotype.

Protonema colony morphology assay

Colony morphology was analyzed as described previously (Bibeau & Vidali, 2014). Protoplasts were isolated from three independent lines for each genotype along with three biological replicates of wild-type using the method described previously (Roberts et al., 2011). However, it was necessary to add 21 units/mL of cellulase from *Trichoderma reesei* (Worthington Biochemical Corporation, Lakewood, NJ, USA) to the digestion mixture when using driselase lot # SLBP0654V (Sigma-Aldrich, St. Louis, MO, USA) for effective digestion. Five thousand protoplasts suspended in 1 mL of PRML were spread on each of three plates containing PRMB medium overlain with cellophane. The plates were incubated at 25^{o}C with constant illumination at 50-80 μmol/m^{2}/s for 4 d and cellophane membranes were then transferred to BCDAT plates for an additional 2 d. Colony morphology was documented by capturing chlorophyll autofluorescence images of approximately 50 regenerated protoplasts per

plate at 63X magnification using an M165FC stereo microscope with 10447407 GFP filter and DFC310FX camera (Leica). Images were analyzed for area, solidity, and circularity with ImageJ (National Institutes of Health, USA) using a macro developed by Vidali et al. (2007).

Statistical analysis

One-way Analysis of Variance (ANOVA) followed by post-hoc Tukey Honest Significant Difference (HSD) test was performed using "R" programming (Vienna, Austria; http://www.R-project.org/) to identify the potential significant difference in caulonema assay and tip growth assay.

Supplemental Materials

Table. S1. Primers designed for knockout vector construction and genotyping.

Table. S2. Data of morphological analysis of protonema colonies.

Fig. S1: B clade PpCESAs are not required for rhizoid development.

Fig. S2. B-clade PpCESAs are not required for caulonema development and gravitropism.

Acknowledgments

This work was supported by National Science Foundation Award IOS-1257047. DNA sequencing and qPCR were conducted using the Rhode Island Genomics and Sequencing Center, a Rhode Island NSF EPSCoR research facility, supported in part by the National Science Foundation EPSCoR Cooperative Agreement EPS-1004057. We also thank Bowen Jiang for assistance with statistics.

Figures

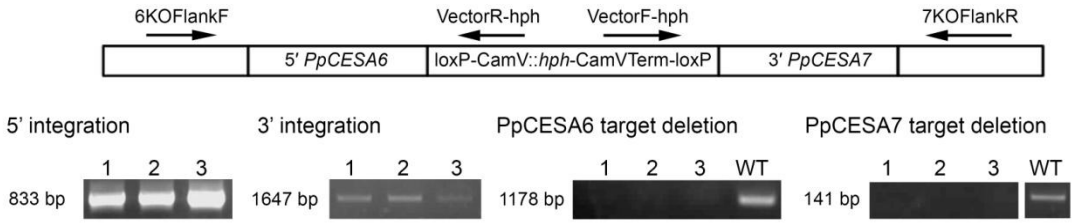

Figure 1: PCR-based genotyping of *ppcesa4/6/7/10*KO lines. Genomic DNA from wild-type *P. patens* (WT) was used as positive control. The expected band for the target gene of 1178 bp (*PpCESA6*) and 141 bp (*PpCESA7*) was observed in WT, but not in KO lines. The expected 5' integration band of 833 bp was present in the KO lines created with PpCESA6/7 KO vector but was not seen in WT. The expected 3' integration band of 1647 bp was observed in the same KO lines above but was also not present in WT. Primer sets used for 5' and 3' ends amplification are indicated as black arrows on the graph showing each gene's locus.

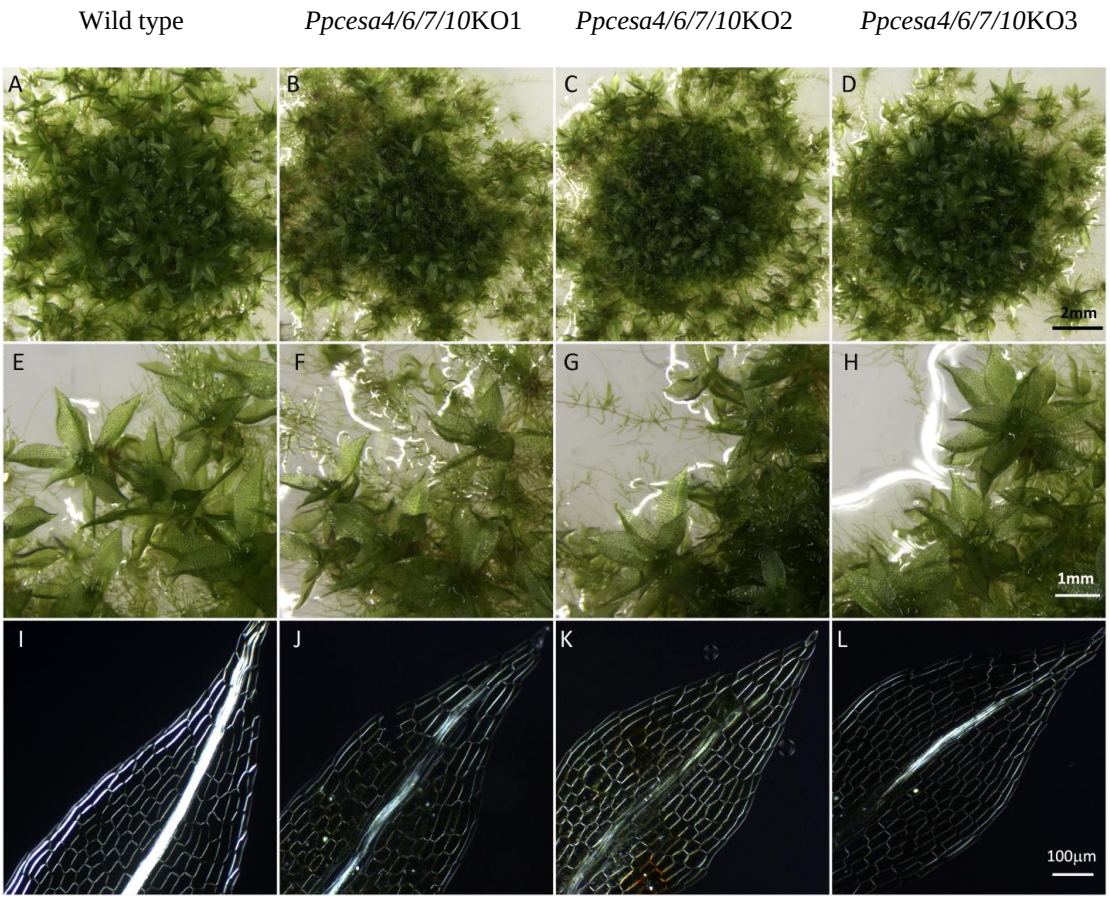

Figure 2: B clade PpCESAs are not required for gametophore development. (A-D) Colony morphology is similar in wild-type (A) and three *ppcesa4/6/7/10*KO lines (B-D). (E-H) Normal looking leafy stalks were observed in all of the lines above. (I-L) Polarized light microscopy of detached leaves from gametophores cultured for 15 days on BCDAT medium for wild-type (I) and three *ppcesa4/6/7/10*KO lines (J-L). The leaf midribs of three knock out lines (J-L) were shown to have lower birefringence compared with wild-type (I) leaf midribs.

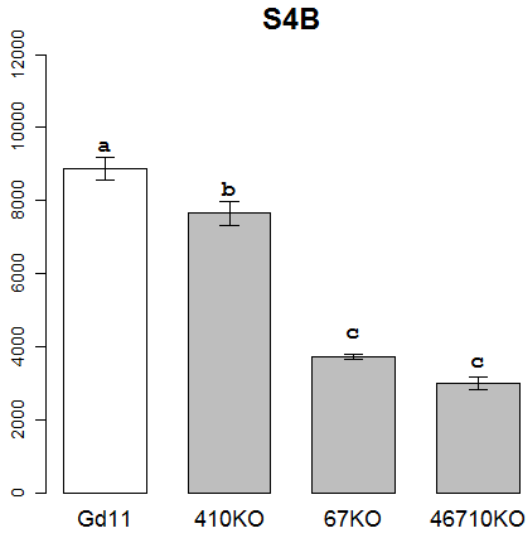

Figure 3: Quantitative analysis of S4B fluorescence intensity in leaf midribs of wild-type *P. patens* and B clade *PpCESA* knockout (KO) mutants. *Ppcesa4/10*KO leaf midribs have a moderate yet significant reduction in fluorescence intensity compared to wild-type. Fluorescence is significantly weaker in *ppcesa6/7*KO than it is wild-type and *ppcesa4/10*KO. *Ppcesa4/6/7/10*KO lines also have significantly decreased fluorescence intensity in leaf midribs compared to wild-type and *ppcesa4/10*KO, but there is no significant difference between *ppcesa6/7*KO and *ppcesa4/6/7/10*KO lines. Three independent genetic lines were tested in triplicate for each mutant genotype. The Gd11 line was used as the wild-type control and sampled in triplicate. Error bars indicate standard error of the mean (*ppcesa4/10*KO, n=3; *ppcesa6/7*KO, n=3; *ppcesa4/6/7/10*KO, n=3; wild-type, n=3).

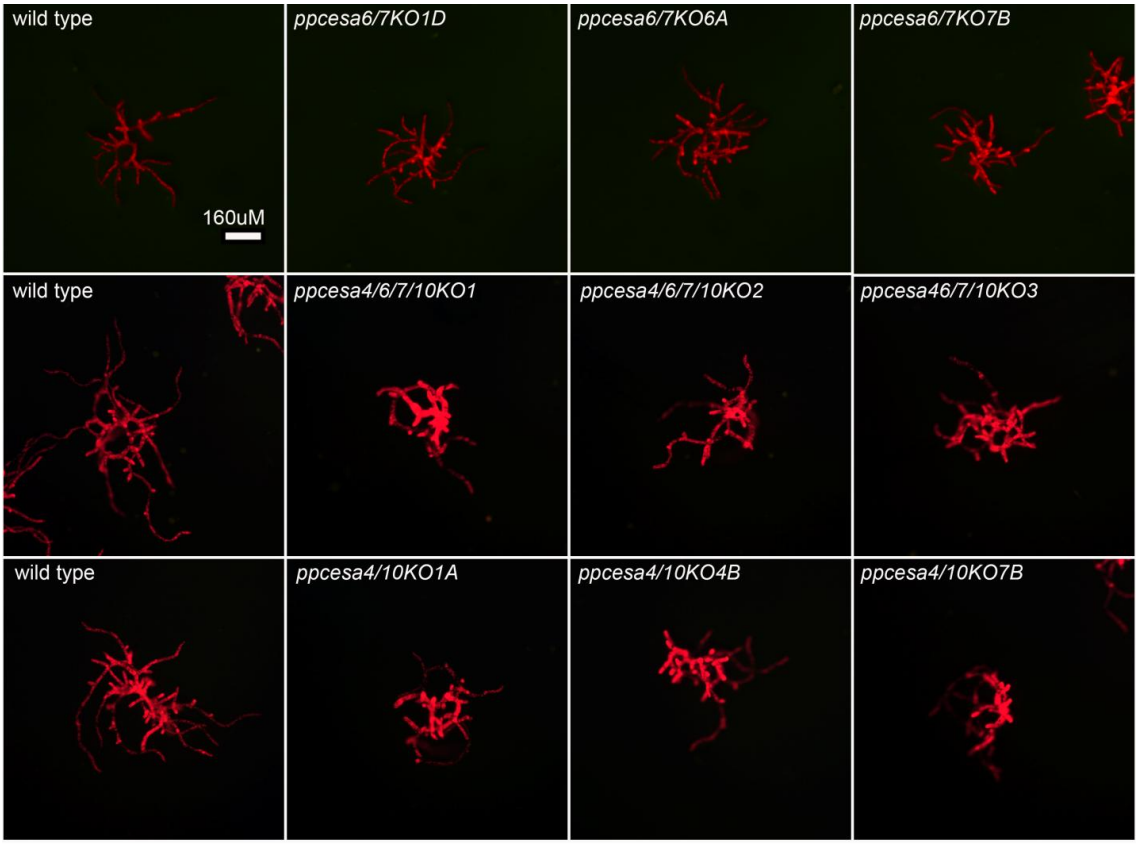

Figure 4: Representative micrographs showing morphologies of B clade PpCESA knockout (KO) mutants protonemal colonies undergoing tip growth. Micrograph show the morphology of colonies with median (add parameter that you used to select the median) as determined by imaging chlorophyll autofluorescence.

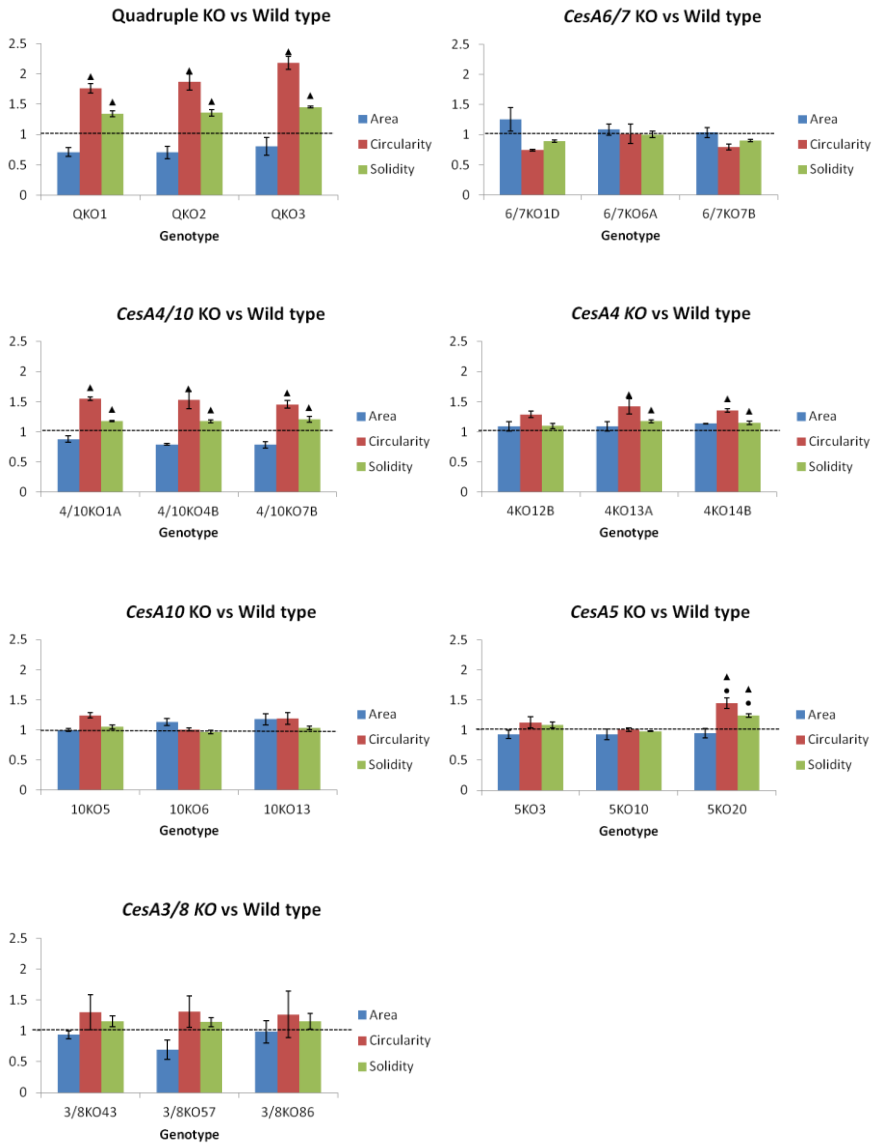

Figure 5: Protonemal colonies of knockout (KO) mutant lines and wild-type *P. patens* line were analyzed for area, circularity, and solidity. Protonemal colonies of *P. patens* KO mutant lines and wild-type line were analyzed for three parameters, area, circularity, and solidity. For circularity, plants with values approaching one are more circular. Solidity scale of 1 represents the highest solidity with 0 as the lowest solidity with the highest branching. Here, the bar graphs show changes of the three parameters in KO mutants. The height of the bar represents the ratio (KO mutant/wild-type). A ratio larger than 1 (indicated by a dotted line on each graph) indicates an increase of that parameter in KO lines compared to wild type and a ratio less than 1 indicates a decrease for KO lines. Error bars display standard error of the mean between each data set (n=3 for each data set). Statistical significant difference between KO mutant and wild-type is indicated by the "▲"sign. The statistically significant difference among KO mutants is indicated by the "●" sign. Raw measurements are reported in **Table S4**.

References cited:

Arioli, T., Peng, L., Betzner, A. S., Burn, J., Wittke, W., Herth, W., … Williamson, R. E. (1998). Molecular analysis of cellulose biosynthesis in Arabidopsis. *Science (New York, N.Y.)*, *279*(5351), 717–720.

Bernal, A. J., Yoo, C.-M., Mutwil, M., Jensen, J. K., Hou, G., Blaukopf, C., … Willats, W. G. T. (2008). Functional Analysis of the Cellulose Synthase-Like Genes CSLD1, CSLD2, and CSLD4 in Tip-Growing Arabidopsis Cells. *Plant Physiology*, *148*(3), 1238–1253. https://doi.org/10.1104/pp.108.121939

Berry, E. A., Tran, M. L., Dimos, C. S., Budziszek, M. J. J., Scavuzzo-Duggan, T. R., & Roberts, A. W. (2016). Immuno and Affinity Cytochemical Analysis of Cell Wall Composition in the Moss Physcomitrella patens. *Frontiers in Plant Science*, *7*. https://doi.org/10.3389/fpls.2016.00248

Burn, J. E., Hocart, C. H., Birch, R. J., Cork, A. C., & Williamson, R. E. (2002). Functional Analysis of the Cellulose Synthase GenesCesA1, CesA2, and CesA3 in Arabidopsis. *Plant Physiology*, *129*(2), 797–807. https://doi.org/10.1104/pp.010931

Carol, R. J., & Dolan, L. (2002). Building a hair: tip growth in Arabidopsis thaliana root hairs. *Philosophical Transactions of the Royal Society B: Biological Sciences*, *357*(1422), 815–821. https://doi.org/10.1098/rstb.2002.1092

Carroll, A., Mansoori, N., Li, S., Lei, L., Vernhettes, S., Visser, R. G. F., … Trindade, L. M. (2012). Complexes with Mixed Primary and Secondary Cellulose Synthases Are Functional in Arabidopsis Plants. *Plant Physiology*, *160*(2), 726–737. https://doi.org/10.1104/pp.112.199208

Cheung, A. Y., & Wu, H.-M. (2008). Structural and signaling networks for the polar cell growth machinery in pollen tubes. *Annual Review of Plant Biology*, *59*, 547–572. https://doi.org/10.1146/annurev.arplant.59.032607.092921

Cosgrove, D. J. (2005). Growth of the plant cell wall. *Nature Reviews. Molecular Cell Biology*, *6*(11), 850–861. https://doi.org/10.1038/nrm1746

Delmer, D. P. (1999). CELLULOSE BIOSYNTHESIS: Exciting Times for A Difficult Field of Study. *Annual Review of Plant Physiology and Plant Molecular Biology*, *50*, 245–276. https://doi.org/10.1146/annurev.arplant.50.1.245

Emons, A. M. C. (1994). Winding threads around plant cells: a geometrical model for microfibril deposition. *Plant, Cell & Environment*, *17*(1), 3–14. https://doi.org/10.1111/j.1365-3040.1994.tb00261.x

Emons, Anne Mie C., & Wolters-Arts, A. M. C. (1983). Cortical microtubules and microfibril deposition in the cell wall of root hairs ofEquisetum hyemale. *Protoplasma*, *117*(1), 68–81. https://doi.org/10.1007/BF01281786

Fagard, M., Desnos, T., Desprez, T., Goubet, F., Refregier, G., Mouille, G., … Höfte, H. (2000). PROCUSTE1 Encodes a Cellulose Synthase Required for Normal Cell Elongation Specifically in Roots and Dark-Grown Hypocotyls of Arabidopsis. *The Plant Cell*, *12*(12), 2409–2423.

Favery, B., Ryan, E., Foreman, J., Linstead, P., Boudonck, K., Steer, M., … Dolan, L. (2001). KOJAK encodes a cellulose synthase-like protein required for root hair cell morphogenesis in Arabidopsis. *Genes & Development*, *15*(1), 79–89.

Galway, M. E., Eng, R. C., Schiefelbein, J. W., & Wasteneys, G. O. (2011). Root hair-specific disruption of cellulose and xyloglucan in AtCSLD3 mutants, and factors affecting the post-rupture resumption of mutant root hair growth. *Planta*, *233*(5), 985–999. https://doi.org/10.1007/s00425-011-1355-6

Goss, C. A., Brockmann, D. J., Bushoven, J. T., & Roberts, A. W. (2012). A CELLULOSE SYNTHASE (CESA) gene essential for gametophore morphogenesis in the moss Physcomitrella patens. *Planta*, *235*(6), 1355–1367. https://doi.org/10.1007/s00425-011-1579-5

Gu, F., & Nielsen, E. (2013). Targeting and regulation of cell wall synthesis during tip growth in plants. *Journal of Integrative Plant Biology*, *55*(9), 835–846. https://doi.org/10.1111/jipb.12077

Harrison, C. J., Roeder, A. H. K., Meyerowitz, E. M., & Langdale, J. A. (2009). Local cues and asymmetric cell divisions underpin body plan transitions in the moss Physcomitrella patens. *Current Biology: CB*, *19*(6), 461–471. https://doi.org/10.1016/j.cub.2009.02.050

Hiss, M., Laule, O., Meskauskiene, R. M., Arif, M. A., Decker, E. L., Erxleben, A., … Rensing, S. A. (2014). Large-scale gene expression profiling data for the model moss Physcomitrella patens aid understanding of developmental progression, culture and stress conditions. *The Plant Journal*, *79*(3), 530–539. https://doi.org/10.1111/tpj.12572

Kimura, S., Laosinchai, W., Itoh, T., Cui, X., Linder, C. R., & Brown, R. M. (1999). Immunogold Labeling of Rosette Terminal Cellulose-Synthesizing Complexes in the Vascular Plant Vigna angularis. *The Plant Cell*, *11*(11), 2075–2085. https://doi.org/10.1105/tpc.11.11.2075

Lee, Y. J., & Yang, Z. (2008). Tip growth: signaling in the apical dome. *Current Opinion in Plant Biology*, *11*(6), 662–671. https://doi.org/10.1016/j.pbi.2008.10.002

Mauseth, J. D. (2012). *Botany: An Introduction to Plant Biology* (5 edition). Burlington, MA: Jones & Bartlett Learning.

McFarlane, H. E., Döring, A., & Persson, S. (2014). The cell biology of cellulose synthesis. *Annual Review of Plant Biology*, *65*, 69–94. https://doi.org/10.1146/annurev-arplant-050213-040240

Newcomb, E. H., & Bonnett, H. T. (1965). CYTOPLASMIC MICROTUBULE AND WALL MICROFIBRIL ORIENTATION IN ROOT HAIRS OF RADISH. *The Journal of Cell Biology*, *27*(3), 575–589.

Nielsen, E. (2009). Plant Cell Wall Biogenesis During Tip Growth in Root Hair Cells. In *Root Hairs* (pp. 85–102). Springer, Berlin, Heidelberg. https://doi.org/10.1007/978-3-540-79405-9_11

Norris, J. H., Li, X., Huang, S., van de Meene, A., Tran, M. L., Killeavy, E., … Roberts, A. W. (2017). Functional specialization of cellulose synthase isoforms in a moss shows parallels with seed plants. *Plant Physiology*. https://doi.org/10.1104/pp.17.00885

Park, S., Szumlanski, A. L., Gu, F., Guo, F., & Nielsen, E. (2011). A role for CSLD3 during cell-wall synthesis in apical plasma membranes of tip-growing root-hair cells. *Nature Cell Biology*, *13*(8), 973–980. https://doi.org/10.1038/ncb2294

Persson, S., Paredez, A., Carroll, A., Palsdottir, H., Doblin, M., Poindexter, P., … Somerville, C. R. (2007). Genetic evidence for three unique components in primary cell-wall cellulose synthase complexes in Arabidopsis. *Proceedings of the National Academy of Sciences*, *104*(39), 15566–15571. https://doi.org/10.1073/pnas.0706592104

Robert, S., Mouille, G., & Höfte, H. (2004). The mechanism and regulation of cellulose synthesis in primary walls: lessons from cellulose-deficient Arabidopsis mutants. *Cellulose*, *11*(3–4), 351–364. https://doi.org/10.1023/B:CELL.0000046415.45774.80

Roberts, A. W., & Bushoven, J. T. (2006). The cellulose synthase (CESA) gene superfamily of the moss Physcomitrella patens. *Plant Molecular Biology*, *63*(2), 207–219. https://doi.org/10.1007/s11103-006-9083-1

Roberts, A. W., Roberts, E. M., & Haigler, C. H. (2012). Moss cell walls: structure and biosynthesis. *Plant Physiology*, *3*, 166. https://doi.org/10.3389/fpls.2012.00166

Rounds, C. M., & Bezanilla, M. (2013). Growth mechanisms in tip-growing plant cells. *Annual Review of Plant Biology*, *64*, 243–265. https://doi.org/10.1146/annurev-arplant-050312-120150

Taylor, N. G. (2008). Cellulose biosynthesis and deposition in higher plants. *New Phytologist*, *178*(2), 239–252. https://doi.org/10.1111/j.1469-8137.2008.02385.x

Taylor, N. G., Scheible, W.-R., Cutler, S., Somerville, C. R., & Turner, S. R. (1999). The irregular xylem3 Locus of Arabidopsis Encodes a Cellulose Synthase Required for Secondary Cell Wall Synthesis. *The Plant Cell*, *11*(5), 769–779. https://doi.org/10.1105/tpc.11.5.769

Tran, M. L., & Roberts, A. W. (2016). Cellulose synthase gene expression profiling of Physcomitrella patens. *Plant Biology*, *18*(3), 362–368. https://doi.org/10.1111/plb.12416

Turner, S. R., & Somerville, C. R. (1997). Collapsed xylem phenotype of Arabidopsis identifies mutants deficient in cellulose deposition in the secondary cell wall. *The Plant Cell*, *9*(5), 689–701. https://doi.org/10.1105/tpc.9.5.689

Vidali, L., Augustine, R. C., Kleinman, K. P., & Bezanilla, M. (2007). Profilin Is Essential for Tip Growth in the Moss Physcomitrella patens. *The Plant Cell*, *19*(11), 3705–3722. https://doi.org/10.1105/tpc.107.053413

Wang, X., Cnops, G., Vanderhaeghen, R., De Block, S., Van Montagu, M., & Van Lijsebettens, M. (2001). AtCSLD3, a cellulose synthase-like gene important for root hair growth in arabidopsis. *Plant Physiology*, *126*(2), 575–586.

Williamson, R. E., Burn, J. E., Birch, R., Baskin, T. I., Arioli, T., Betzner, A. S., & Cork, A. (2001). Morphology of rsw1, a cellulose-deficient mutant of Arabidopsis thaliana. *Protoplasma*, *215*(1–4), 116–127.

Supplemental Materials

Table S2. Primers designed for knockout vector construction and genotyping.

Name	Sequence	Tm (℃)	Amplicon Size (bp)	Description
6KOF2 VectorR-hph	GCTTCAATGCTGTACCACAAACCAC TCCGAGGGCAAAGAAATAGA	57℃	1647	5’ integration test*PpCESA6* with *hph* cassette
VectorF-hph CESA7FlankR	TGACAGATAGCTGGGCAATG AAGCCCTAACTTCCAGCACC	57℃	833	3’ integration test*PpCESA7* with *hph* cassette
CESA6TargetF CESA6TargetR	GTGAGGTGCGAGGAAGAAAG TTCCCTAACTCCACCACTGC	60℃	141	*PpCESA6* deletion
CESA7TargetF CESA7TargetR	GCGAATGCAGGGCTGCTG ACATTACTCAACGGCCTCGG	60℃	1178	*PpCESA7* deletion

Table S2. Data of morphological analysis of protonema colonies. For each knockout mutant analyzed, three independent lines of each genotype were used. Three biological replicates of wild-type control (Gd11) were included in each assay.

		Area			Circularity			Solidity		
*Ppcesa4/6/7/10*KO	Gd11	40399	34210.58	33551.25	0.045009	0.040628	0.041729	0.320442	0.331745	0.310333
	*Ppcesa4/6/7/10*KO1	20285.58	28965.29	27640.76	0.0742	0.069754	0.081085	0.450404	0.401704	0.440667
	*Ppcesa4/6/7/10*KO2	18547.23	30581.31	26905.79	0.089938	0.072162	0.075592	0.469619	0.42	0.418587
	*Ppcesa4/6/7/10*KO3	18319.33	33573.75	35148.9	0.09851	0.083788	0.095483	0.476058	0.459823	0.464363
*Ppcesa6/7*KO	Gd11	17151.1	15971.6	18077.3	0.120936	0.162888	0.12687	0.467615	0.534388	0.459073
	*Ppcesa6/7*KO1D	18683.8	17356.78	27964.1	0.098267	0.101136	0.105921	0.421678	0.426604	0.450877
	*Ppcesa6/7*KO6A	21736.69	17140.63	16779	0.112492	0.12051	0.182764	0.460126	0.466053	0.538861
	*Ppcesa6/7*KO7B	19764.43	15159.16	18061.73	0.111088	0.118288	0.096092	0.453604	0.44251	0.418254
*Ppcesa4/10*KO	Gd11	21327.32	23356.35	23087.82	0.04925	0.050858	0.048978	0.337085	0.337519	0.34933
	*Ppcesa4/10*KO1A	18132.08	19258.27	22136.12	0.073998	0.079321	0.077629	0.397736	0.403546	0.408596
	*Ppcesa4/10*KO4B	18396.81	17776.9	17604.19	0.061352	0.083104	0.083344	0.387321	0.416313	0.401563
	*Ppcesa4/10*KO7B	15770.39	17700.15	19820.19	0.070704	0.078364	0.067808	0.400284	0.442849	0.395275
*Ppcesa10*KO	Gd11	32858.31	29972.58	31806.77	0.03546	0.035046	0.032823	0.308194	0.312196	0.274087
	*Ppcesa10*KO5	33235.38	34680.96	39200.35	0.042865	0.045738	0.039996	0.333037	0.310521	0.29706
	*Ppcesa10*KO6	33246.81	43001.81	35311.71	0.036337	0.033525	0.034508	0.305477	0.28189	0.275992
	*Ppcesa10*KO13	36475.96	42200.94	40752.31	0.04724	0.036285	0.039633	0.324415	0.305329	0.295342
*Ppcesa4*KO	Gd11	24418.73	18226.81	20659.81	0.044644	0.045471	0.046415	0.32436	0.316835	0.344604
	*Ppcesa4*KO12B	24471.96	19759.33	24988.6	0.057773	0.063496	0.055065	0.38431	0.363319	0.335479
	*Ppcesa4*KO13A	25267.94	19759.06	23972.96	0.053075	0.069252	0.072038	0.372088	0.391337	0.395762
	*Ppcesa4*KO14B	24204.48	23930.38	23849.98	0.059488	0.063644	0.062	0.374863	0.364402	0.396656
*Ppcesa5*KO	Gd11	22012.52	24818.33	25844.67	0.043333	0.037596	0.039262	0.314323	0.282108	0.297563
	*Ppcesa5*KO	19099.73	24562.65	23829.94	0.052558	0.042433	0.040492	0.352242	0.319467	0.3025
	*Ppcesa5*KO	18242.9	24602.5	24648.79	0.041725	0.03816	0.041506	0.291517	0.294865	0.292694
	*Ppcesa5*KO	19725.52	26649.79	22635.94	0.064873	0.054306	0.054329	0.388779	0.355002	0.367185

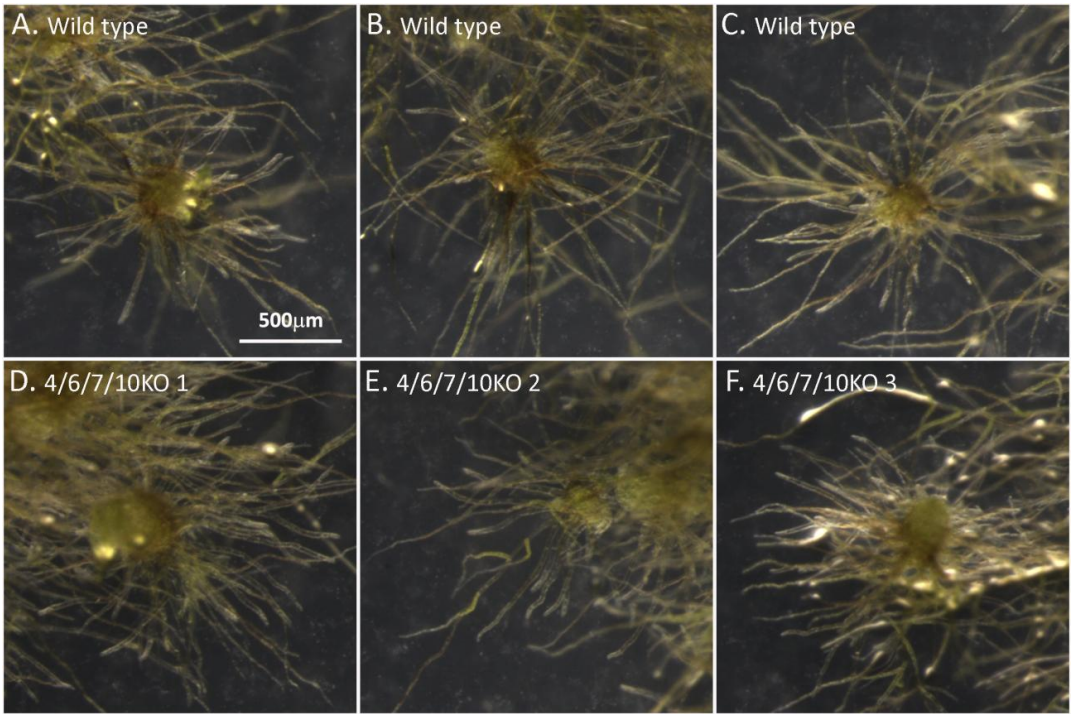

Figure S1: B clade PpCESAs are not required for rhizoid development. *P. patens* wild-type (Gd11) and three independent *ppcesa4/6/7/10*KO lines were cultured on medium supplemented with1 μM naphthalene acetic acid (auxin) to stimulate rhizoid initiation, and inhibit leaf initiation. (A-C) Dark field images of wild-type leafless gametophores with numerous rhizoids. (D-F) Dark field images of *ppcesa4/6/7/10*KO1, *ppcesa4/6/7/10*KO2, and *ppcesa4/6/7/10*KO3 leafless gametophores with numerous rhizoids. None of the three *ppcesa4/6/7/10*KO lines showed defects in rhizoid initiation or growth.

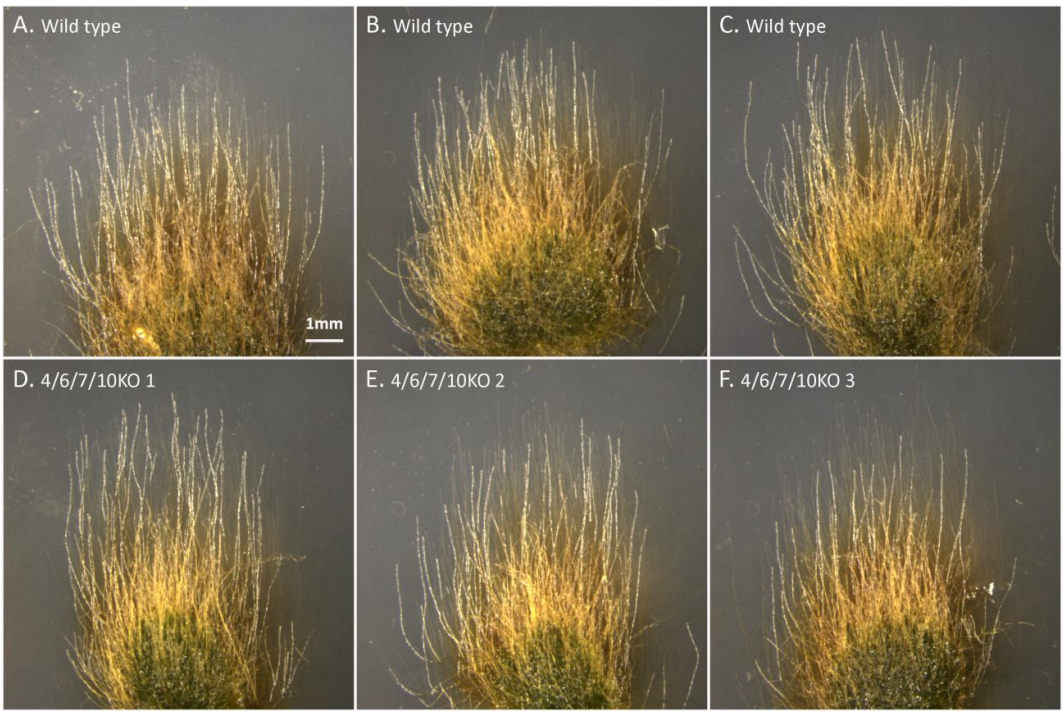

G.

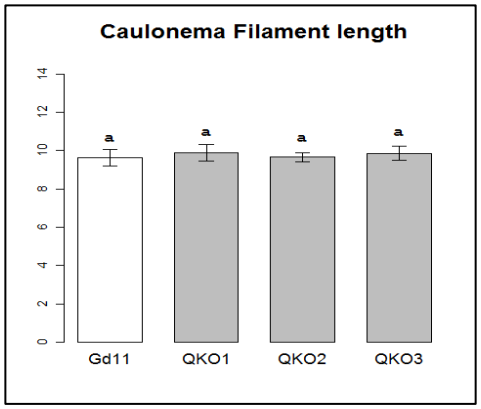

Figure S2: B-clade PpCESAs are not required for caulonema development and gravitropism. *P. patens* wild-type (Gd11) and three independent *ppcesa4/6/7/10*KO lines were cultured on medium containing sucrose to test for caulonema gravitropism. The plates were vertically oriented and kept in the dark. (A-C) Dark field images of wild-type (Gd11) colonies with upright growing caulonema filaments. (D-F) Dark field images of *ppcesa4/6/7/10*KO1, *ppcesa4/6/7/10*KO2, and *ppcesa4/6/7/10*KO3 colonies with upright growing caulonema filaments. Wild-type line and knockout lines were from the same experiment. (G) None of the three *ppcesa4/6/7/10*KO lines showed significant differences in caulonema length (ANOVA, n=3, $P>0.05$) or gravitropic behavior.

Manuscript 3

Manuscript formatted for the publication in *New Phytologist*

Short title: *Physcomitrella* has hetero-oligomeric Cellulose Synthesis Complexes

Title: A hetero-oligomeric Cellulose Synthesis Complex (CSC) involved in the secondary cell wall deposition in *Physcomitrella patens*

Xingxing Li[a], John McManus[b], Alison W. Roberts[a]

[a]Department of Biological Sciences, University of Rhode Island, Kingston RI 02881, USA

[b]Department of Biochemistry and Molecular Biology, The Pennsylvania State University, University Park, PA 16802, USA

One sentence summary: Similar to seed plants, the moss *Physcomitrella patens* contains obligate hetero-oligomeric Cellulose Synthesis Complexes (CSCs) involved in cellulose synthesis in secondary cell walls, indicating that the structure and function of the cellulose production machinery in moss and seed plants are undergoing convergent evolution.

List of author contributions: A.W.R. conceived the project, and supervised experiments; X.L. designed and performed experiments, and analyzed the data; J. M. performed experiments; X.L. wrote the manuscript.

Funding information: This work was supported by National Science Foundation Award IOS-1257047. Production of monoclonal antibodies for PpCESAs was supported as part of The Center for LignoCellulose Structure and Formation, an Energy Frontier Research Center funded by the U.S. Department of Energy, Office of Science, Office of Basic Energy Sciences under Award Number DE-SC0001090.

DNA sequencing and qPCR were conducted using the Rhode Island Genomics and Sequencing Center, a Rhode Island NSF EPSCoR research facility, supported in part by the National Science Foundation EPSCoR Cooperative Agreement EPS-1004057. We also thank Bowen Jiang for assistance with statistics.

Abstract

Cellulose synthesis is catalyzed by plasma membrane Cellulose Synthesis Complexes (CSCs) that have been visualized by freeze-fracture electron microscopy as rosette structures with 6-fold symmetry. In seed plants, CSCs are obligate hetero-oligomeric, consisting of three functionally distinct and non-interchangeable cellulose synthase (CESA) isoforms. *Physcomitrella patens* has rosette CSCs, but its seven CESAs are not members of the clades that comprise the functionally distinct subunits of the hetero-oligomeric seed plant CSCs. Double *ppcesa3/8*KOs and *ppcesa6/7*KOs have defects in secondary cell wall deposition in gametophore leaf midribs, which suggests that PpCESA3, PpCESA8, PpCESA6, and PpCESA7 are required for forming hetero-oligomeric CSCs in gametophores. PpCESA5 is required for primary cell wall deposition in gametophore buds, but it is not known whether other PpCESAs are required for this processes. Here, Real-Time quantitative PCR (RT-qPCR) analysis shows that expression of *PpCESA3, PpCESA8*, and *PpCESA7* are co-regulated. Based on western blot analysis of isolated proteins, PpCESA3, PpCESA8, and PpCESA7 are all highly expressed in gametophores. Co-immunoprecipitation (Co-IP) shows that PpCESA3 and PpCESA8 can both interact with PpCESA6/7 *in planta*. These results support the hypothesis that cellulose microfibrils in the secondary cell walls of *P. patens* leaf midribs are synthesized by obligate hetero-oligomeric CSCs.

Introduction

Cellulose is a biopolymer of β-(1,4)-glucose that forms microfibrils essential in land plant cell walls. It is synthesized by cellulose synthase complexes (CSCs) located on the plasma membrane (Delmer et al., 1999; Somerville et al., 2006; McFarlane et al., 2014). The CSCs of vascular plants were first observed to have a "rosette" structure and associate with the ends of microfibrils in freeze-fracture electron microscopy studies (Mueller & Brown, 1980). Within the CSC, cellulose synthase catalytic subunits (CESAs) catalyze the synthesis of individual glucan chains and are currently the only verified functional subunits (Delmer, 1999; Somerville, 2006; McFarlane et al., 2014; Purushotham et al., 2016).

CESA genes are members of multigene families in vascular plants. *Arabidopsis* has 10 *CESA* genes (McFarlane et al., 2014). *AtCESA4*, *AtCESA7*, and *AtCESA8* were first identified to be specifically involved in secondary cell wall deposition (Turner & Somerville, 1997; Taylor et al., 1999; Scheible et al., 2001; Taylor et al., 2000; Taylor et al., 2003). Proteins encoded by these three genes physically interact and are exclusively required for assembly of CSCs in cells having thickened secondary walls (Taylor et al., 2000; Taylor et al., 2003). Mutations in *AtCESA1*, *AtCESA3*, and *AtCESA6* cause primary cell wall defects (Arioli et al. 1998; Fagard et al., 2000; Burn et al., 2002; Robert et al., 2004). AtCESA3 and AtCESA6 interact with each other according to results of in vitro pull-down assays, and BiFC experiments show that AtCESA1, AtCESA3, and AtCESA6 can interact in vivo (Desprez et al., 2007). *AtCESA2* and *AtCESA5* are shown to be closely related and partially functionally redundant with *AtCESA6* (Desprez et al. 2007; Timmers et al. 2009; Carroll et al.

2012; Li et al., 2013). In *Arabidopsis*, therefore, a primary wall CSC likely consists of AtCESA1, AtCESA3, and one of the AtCESA6 like AtCESAs (McFarlane et al., 2014). The stoichiometry of *Arabidopsis* CSCs has been recently been determined to be a 1:1:1 molecular ratio (Gonneau et al., 2014; Hill et al., 2014). CSCs have also been characterized in other vascular plant models, such as *Populus trichocarpa*. Two types of CSCs (one type contains PdxtCESA7A and PdxtCESA8B; the other one contains PdxtCESA1A and PdxtCESA3) were identified in the xylem of *Populus* by coimmunoprecipitation (Co-IP, Song et al., 2010a). Altogether, current evidence suggests that vascular plant CSCs are hetero-oligomeric and can assembly only when three specific functionally distinct CESA isoforms are present.

Rosette-type CSCs have also been observed in the moss *Physcomitrella patens*, a model nonvascular plant, by freeze-fracture electron microscopy (Roberts et al., 2012; Nixon et al., 2016). The *PpCESA* gene family has seven members clustered in two clades, A-clade (*PpCESA3*, *PpCESA5*, and *PpCESA8*) and B-clade (*PpCESA4*, *PpCESA6*, *PpCESA7*, and *PpCESA10*). Mosses and seed plants are derived from a common ancestor that had a single *CESA*, and *PpCESAs* are not orthologs of vascular plant *CESAs* according to phylogenetic analyses (Roberts & Bushoven, 2007). It is not yet known if the CSCs of *P. patens* are homo-oligomeric or if they have evolved a hetero-oligomeric state independently from seed plants.

In addition to *PpCESA* knockout (KO) and phenotypic analysis, examination of co-expression and protein-protein interaction can provide insight into the composition of the *P. patens* CSCs. Previous mutational analyses showed that *ppcesa5*KO is required for the development of the gametophore (Goss et al., 2012). *Ppcesa3/8*KOs were

recently shown to have substantially reduced cellulose levels in midrib secondary cell walls of the gametophore leaf (Norris et al., 2017). A double B-clade *PpCESAs* KO, *ppcesa6/7*KO, phenocopies the *ppcesa3/8*KO midrib phenotype (Norris et al., 2017). These results are consistent with the hypothesis that cellulose in the secondary cell walls is produced by hetero-oligomeric CSCs consisting of PpCESA3, PpCESA6, PpCESA7 and PpCESA8. Other double B-clade PpCESAs KOs, *ppcesa4/10*KOs, were shown to have morphological changes in colonies formed by tip growing protonema filaments (unpublished data).This result indicates PpCESA4 and PpCESA10 are involved in synthesis of cellulose in primary cell walls. Here, our RT-qPCR analysis revealed a co-regulated expression of three *PpCESA* genes (*PpCESA3*, 7, and *8*), which is similar to the gene expression pattern of *Arabidopsis CESAs* that reside in the same hetero-oligomeric CSCs. Moreover, coordinated accumulation of the corresponding PpCESAs proteins and physical interactions identified among them further support the hypothesis that a type of obligate hetero-oligomeric CSC consisting of PpCESA3, PpCESA8, and PpCESA6/7 is involved in the secondary cell wall deposition of *P. patens* gametophore leaves.

Results

Expression levels of *PpCESAs* in the knockout mutants by RT-qPCR

Correlated expression is expected for PpCESAs that reside in the same CSC. To test this, we performed RT-qPCR on RNA extracted from leafy gametophores collected from Gd11, *ppcesa3*KO, *ppcesa8*KO, *ppcesa3/8*KO, *ppcesa4/10*KO, *ppcesa6/7*KO, and *ppcesa4/6/7/10*KO plants. *PpCESA8* was significantly upregulated in *ppcesa3*KO

(**Figure 1**) consistent with the results of the previous RT-qPCR analysis (Norris et al., 2017). Both *PpCESA3* and *PpCESA8* were significantly downregulated in *ppcesa6/7*KO and *ppcesa4/6/7/10*KO when compared with their expression in the wild-type controls. In reciprocal experiments, *PpCESA7* was significantly downregulated in *ppcesa3/8*KO. Expression of *PpCESA4* and *PpCESA10* were not significantly downregulated in *ppcesa3/8*KO. In addition, no significant change in expression of *PpCESA4* or *PpCESA10* was detected in *ppcesa6/7*KO. Expression of *PpCESA7* was also not changed in *ppcesa4/10*KO. No significant change of *PpCESA5* expression was seen in any of the KO mutants. Expression of the other *PpCESAs* in the gametophores of *ppcesa5*KO *could not be* examined since *ppcesa5*KOs do not produce normal leafy gametophores (Goss et al., 2012). The results here are consistent with the correlated expression of *PpCESA3, PpCESA8, PpCESA6,* and *PpCESA7*.

Characterization of the PpCESA antibodies

Monoclonal antibodies were generated for detection of PpCESA3, PpCESA8, and PpCESA6/7, and specificity was tested by western blot against microsomal protein fractions. For each antibody, a corresponding PpCESA overexpression line was used as a positive control, and the KO line was used as a negative control. **Figure 2** (**left panel**) shows that anti-PpCESA3 recognizes a band that has the predicted size for a PpCESA (120 kD) in both *Act1pro::3xHA-PpCESA3* and wild-type. The band was not detected in *ppcesa3*KO. We were unable to design an antibody that distinguishes PpCESA6 and PpCESA7, which differ by three amino acids. Thus, we made an antibody that can recognize both. Anti-PpCESA6/7 detected a 120 kD band in *Act1pro::3xHA-PpCESA7* and wild-type, but not in *ppcesa6/7*KO (**Figure 2, middle**

panel). The anti-PpCESA8 detected a 120 kD band in *Act1pro::3xHA-PpCESA8* and Gd11. However, it also weakly detected band around 120KD in *ppcesa8*KO (**Figure 2, right panel**). When *ppcesa3/8*KO is used as a negative control, no band was detected. This indicates that anti-PpCESA8 has weak cross-reactivity with PpCESA3 in addition to detecting PpCESA8.

Protein expression profiling of the PpCESAs

We used western blotting to examine the protein expression patterns for PpCESA3, PpCESA8, and PpCESA6/7 at different developmental stages. **Figure 3** shows that none of these proteins were detectable in the Day-6 wild-type cultures consisting of pure protonema. PpCESA3, PpCESA8, and PpCESA6/7 were detected in Day-10 cultures, which contain protonema, emerging gametophore buds, and young gametophores. Finally, much larger amounts of these three PpCESAs were detected in Day-21 cultures, which contain numerous fully developed leafy gametophores. This shows that PpCESA3, PpCESA8, and PpCESA6/7 exhibit similar expression profiles, with highest expression in the gametophores, consistent with roles in gametophore development.

Interactions between the PpCESAs

Based on the similarity of their mutant phenotypes, correlated gene expression, and protein expression profiles, we hypothesized that PpCESA3, PpCESA6, PpCESA7, and PpCESA8 physically interact with each other to form hetero-oligomeric complexes. To address this question, we carried out Co-IP experiments on detergent-solubilized protein extracts from the 15-day-old leafy gametophores of transgenic *P. patens lines* that expressed HA-tagged PpCESAs under the control of their native

promoters in their cognate mutant backgrounds. Complementation of the mutant phenotype was verified for *PpCESA8pro*::*HA-PpCESA8* (*ppcesa6/7*KO, **Figure S2 and S3**). However we could not verify complementation for *PpCESA3pro*::*HA-PpCESA3*, since we have not detected a phenotype for *ppcesa3*KO. For the *PpCESA3pro*::*HA-PpCESA3* line (**Figure 4A**), blotting with anti-PpCESA3 showed that the IP antibody (anti-HA) successfully precipitated HA-PpCESA3 from the lysate of *PpCESA3pro*::*HA-PpCESA3*. When blotted with anti-PpCESA6/7, the target proteins were found in the IP eluate indicating that PpCESA6 and/or PpCESA7 were co-precipitated with HA-PpCESA3. Likewise, PpCESA8 was also detected in the IP eluate by anti-PpCESA8, suggesting a co-precipitation with HA-PpCESA3. In the Co-IP assay for *PpCESA8pro*::*HA-PpCESA8* (**Figure 4B**), blotting with anti-PpCESA8 verified that anti-HA pulled down the HA-PpCESA8. PpCESA6 and PpCESA7 were also detected in the IP eluate indicating co-precipitation with the primary target. Interestingly, anti-PpCESA3 also detected a band in the eluate. Similar results were observed with the reciprocal experiment in which anti-HA was used to pull down HA-tagged PpCESA7 from the protein extracts of the *PpCESA7pro*::*HA-PpCESA7* transgenic line (**Figure 4C**). Again, HA-tagged PpCESA7 was precipitated, and PpCESA3 and PpCESA8 were co-precipitated as expected. For the control experiment, Co-IP was carried out for wild-type *P. patens* (Gd11), which does not produce HA-tagged proteins (**Figure 4D**). As a result, none of the PpCESAs were immuno-detected indicating the IP antibody is specific.

Discussion

Our results are consistent with the hypothesis that the *P. patens* CSCs that synthesize the midrib secondary cell wall are obligate hetero-oligomeric, with members from both clade A and clade B. This hypothesis was suggested by the similar mutant phenotypes of *ppcesa3/8*KO and *ppcesa6/7*KO showing decreased cellulose deposition in the midribs of the gametophore leaves (Norris et al., 2017). Here, it is further supported by 1) co-reguation of *PpCESA3*, *PpCESA8*, and *PpCESA7* gene expression (**Figure 1**), 2) coordinated accumulation of PpCESA3, PpCESA8, and PpCESA6/7 proteins in leafy gametophores (**Figure 3**), and 3) detection of physical interactions between PpCESA3, PpCESA8, and PpCESA6/7 by Co-IP (**Figure 4**). *Arabidopsis* has 10 *CESA* genes that are specialized for primary and secondary cell wall synthesis (Taylor et al., 1999; Fagard et al., 2000; Scheible et al., 2001; McFarlane et al., 2014). Phylogenetic studies show that the *CESA* families in *P. patens* and *Arabidopsis* are similar in size (Yin et al., 2010; Carroll & Specht, 2011; Harholt et al., 2012) Thus, it is imaginable that the *P. patens* CSCs are also hetero-oligomeric (Roberts et al., 2012). However, because *P. patens* CESAs diversified and specialized independently from seed plant CESAs (Roberts & Bushoven, 2007), this hypothesis must be tested independently.

In *Arabidopsis*, the genes that encode CESA isoforms that function within the same CSCs are co-expressed (Persson et al., 2005; Brown et al., 2005; Manfield et al., 2006). Here we show that, similar to the *Arabidopsis CESAs*, the expressions of the *PpCESA3*, *PpCESA8*, and *PpCESA6/7* genes are also co-regulated (both *PpCESA3* and *PpCESA8* have down-regulated expression when *PpCESA6* and *PpCESA7* are

knocked out, and vice versa). One exception is up-regulation of *PpCESA8* to compensate for the loss of *PpCESA3* (Norris et al., 2017). Taking results of phenotype analysis into consideration, it was suggested that PpCESA3 and PpCESA8 have interchangeable functions and may compete for the same positions in the CSCs (Norris et al., 2017). In addition, our Co-IP results show that PpCESA3 is co-immunoprecipitated with PpCESA8 and vice versa (**Figure 4A**). PpCESA8 appears to be dominant over PpCESA3 (in the amount of protein) in wild-type *P. patens*. This is based on the observation that *ppcesa8*KO has an obvious reduction in the leaf midrib cellulose deposition, which is not shown in *ppcesa3*KO (Norris et al., 2017).

In *Arabidopsis*, loss of a single CESA usually is enough to cause either obvious morphological defects or even lethal developmental defects (Taylor et al., 2003; Persson et al., 2007), which means *Arabidopsis* CESAs are functionally distinct. In contrast, the PpCESAs show less functional differentiation. With the exception of *PpCESA5* (Goss et al., 2012), we have to knock out at least two *PpCESAs* from the same clade to observe a strong phenotype. In *P. patens*, CESAs within the same sub-clade (A-clade or B-clade) appear to be functionally interchangeable. The major functional differences might only exist between PpCESAs from different sub-clades. For instance, the mutant phenotype of *ppcesa3/8*KOs can be rescued by expressing *PpCESA8, PpCESA3* or *PpCESA5* under control of the *PpCESA8* promoter, but cannot be rescued by expressing any of the clade-B *PpCESAs* using the same *PpCESA8* promoter (Norris et al., 2017). The "no gametophore" phenotype of *ppcesa5*KOs can be rescued by the expression of *PpCESA3* or *PpCESA8* driven by the *PpCESA5* promoter, but again, it cannot be rescued by expression of any of the clade-

B *PpCESAs* driven by the *PpCESA5* promoter (Scavuzzo-Duggan et al., in revision). In contrast, the AtCESAs have very limited interchangeability, with partial rescue only of *atcesa3 by AtCESA3pro::AtCESA7* and *atcesa8* with *AtCESA8pro:: AtCESA1* (Carroll et al., 2012).

Taken together, including this study, the current evidence indicates that secondary cell wall in the moss *P. patens* are synthesized by an obligate hetero-oligomeric CSC assembled from PpCESAs from both clade A and clade B. Our findings combined with phylogenetic analysis (Roberts & Bushoven, 2006) suggest that hetero-oligomeric CSCs arose in both mosses and seed plants through independent evolution. Norris et al. (2017) showed that diversification of the CESAs happened independently through both subfunctionalization and neofunctionalization in mosses and vascular plants, and these events are associated with convergent evolution of secondary wall structure. This indicates that selection pressure favored cellulose-rich secondary cell walls for better mechanical support to colonize land in both lineages. Here, our results indicate that selection for secondary cell walls with specialized cellulose microfibril textures might have favored emergence of hetero-oligomeric CSCs through convergent evolution in different land plants. Alternatively, the independent evolution of hetero-oligomeric CSCs in the seed plant and moss lineages could be explained by constructive neutral evolution.

Characterization of the PpCESAs shows some consistency with the theory of constructive neutral evolution which can be used to explain the evolution of the hetero-oilgomeric CSCs. According to the hypothesis, after ancestral gene duplication, simple and high-probability mutations are considered to be a sufficient cause leading

to the increased complexity of a multi-protein complex (Doolittle, 2012; Finnigan et al., 2012). Most of these mutations are thought to be insufficient to cause changes in protein biochemical output. However, mutations occuring at the protein-protein binding interface can cause the mutant proteins to lose the ability to interact with the others members in the complex. In that case, a hetero-oligomeric complex eventually might evolve by complementary loss of asymmetric interactions of certain protein subunits in the original homo-oligomeric complex (Doolittle, 2012; Finnigan et al., 2012). We have shown that *ppces6/7*KOs phenocopy *ppcesa3/8*KOs; both show defects in secondary cell walls (Norris et al., 2017). This suggests that clade-A PpCESAs and clade-B PpCESAs carry out non-overlapping functions after neo-functionalization of the common ancestral PpCESA. The distinct functions of these PpCESAs might be caused by mutations at the binding sites, according to the theory above. This assumption is further supported by the Co-IP results here together with results of yeast two hybrid assay showing PpCESA8 cannot interact with itself (unpublished data). In addition, the promoter-swap assays mentioned above suggest there is no major functional difference among the paralogues from the same PpCESA clade, which is also consistent with constructive neutral evolution. To continue to test this theory, more precise characterization of PpCESAs need to be carried out to identify the binding sites of these PpCESAs.

Our study also indicate a possibility that PpCESA5 can form homo-oligomeric CSCs (Li et al., unpublished). We propose this hypothesis based on the distinct isoform function (Goss et al., 2012), unique gene expression pattern as well as the fact that mosses and seed plants derived from the common ancestor which had a single CESA

and consequently homo-oligomeric CSCs (Roberts & Bushoven, 2007). If this hypothesis is proved to be true, it will be another evidence supporting the constructive neutral evolution. But, no matter what the answers will be, implications provided by these studies will be helpful for understanding the roles of the different CESAs composing seed plant CSCs.

Materials and methods

Culture conditions

Wild-type and all transgenic *P.patens* lines used in this study were maintained on BCDAT plates and propagated by subculturing weekly as described (Roberts et al., 2011). To produce growing leafy gametophores, explants of 7-day-old protonemal tissue was transferred onto BCD plates and cultured for 15 days before being harvested for experiments.

Vector construction and transformation

All the PpCESA KO lines used in this study were created previously. Construction of knockout vectors and transformations for making those lines were described in Norris et al. (2017). Transformation for making quadruple *ppcesa4/6/7/10*KOs was described in an unpublished manuscript (Li et al., unpublished).

PpCESA overexpression lines used as positive controls for testing antibody specificity were selected from transformations of *ppcesa5*KO-2 with vectors driving expression of 3X-HA-tagged PpCESA3, PpCESA7 or PpCESA8 under control of the rice Actin1 promoter (Scavuzzo-Duggan et al., in revision).

Expression vectors for HA-tagged *PpCESAs* under control of their native promoters were created using Multi Site Gateway Pro (Invitrogen, Grand Island, NY, USA). The *HA-PpCESA5, HA-PpCESA7,* and *HA-PpCESA8* coding sequences were amplified from cDNA clones pdp24095, pdp38142, and pdp39044 (RIKEN BRC), respectively, using forward primers containing a single HA tag coding sequence flanked by an attB5 site and a reverse primer flanked by an attB2 site (Supplemental Table 2). *HA-PpCESA3* was amplified from a cDNA clone describe previously (Scavuzzo-Duggan et al, in revision) using appropriate primers (Supplemental Table 2). PCR amplification was catalyzed by Phusion High-Fidelity PCR Master Mix (New England Biolab) in 50 L reactions with an initial denaturation (98°C, 30 sec.); 35 cycles of denaturation (98 ℃, 7 sec), annealing (68 ℃, 15 sec), and extension (72 ℃, 40 sec); and a final extension (72 ℃, 5 min) and the products were cloned into pDONR p5-p2 vector (Invitrogen) to create entry clones. To create the *PpCESA*promoter::*HA-PpCESA* vectors, the HA-CESA entry clones along with an entry clone containing the corresponding native promoter (Tran & Roberts, 2016) were inserted into the Si3-pTH-GW destination vector (Tran & Roberts, 2016) using LR Clonase II Plus (Invitrogen). *PpCESA3*pro::*HA-PpCESA3* and *PpCESA5pro*::*HA-PpCESA5* were linearized with SwaI. *PpCESA8pro*::*HA-PpCESA8* was linearized with PciI.

RNA extraction and Real-time quantitative PCR (RT-qPCR)

Total RNA extraction from gametophore leaves followed by cDNA conversion was carried out as described (Tran & Roberts, 2016). RT-qPCR analysis was performed using the ΔΔCt method (Livak & Schmittgen, 2001) of relative quantification with a Roche Lightcycler 480, using SYBR Green I Master Mix (Roche) to monitor doubled

strand DNA synthesis. Primers for *PpCESA* detection were as used in Tran & Roberts (2016), and primers for reference genes, *actin* and *v-Type h+ translocating pyrophosphatase*, were as used in Bail et al. (2013).

Generation of monoclonal anti-PpCESAs

Peptide antigens, designed to regions of each PpCESA for the purpose of raising antibodies specific for each isoform (Table S2), were synthesized chemically and injected into New Zealand white rabbits (Covance Inc., Princeton NJ USA). For PpCESA6 and PpCESA7, it was not possible to generate two unique peptides in order to raise antibodies to differentiate these isoforms. The peptides were conjugated, via the cysteine residue, to Sulfolink Immobilization resin (Thermo Fisher Scientific) according to the manufacturer's instructions. The purification of PpCESA antibodies from total serum was carried out by affinity chromatography. Briefly, 10 mL of serum, buffered with WB (20 mM $NaHPO_4$, pH7.2, 50 mM NaCl) was incubated with the resin-linked peptides for 18h at 4 ℃. The resin was loaded into a column and the flow through was passed over the resin twice. The resin was washed with 20 mL of WB followed by 10 mL of WB containing an additional 250 mM NaCl. Antibodies were eluted from the resin using 5 mL of EB (100 mM glycine, pH 2.5). Fractions of 250 μL containing NB (50 μL 1 M Tris-Cl, pH 8.0) were collected and mixed immediately to neutralize pH. Fractions containing PpCESA antibodies were identified by absorbance at 280 nm and combined. Glycerol was added to 30% and CESA antibodies were stored at -80 ℃. The specificity of each antibody was tested by western blotting against *P. patens* protein extracts.

Protein expression profiling of the PpCESAs

The wild type *P. patens* were used in this assay. The 6-day-old protonema growing on BCD plates were collected for protein extraction of the first time point. The "spot plates" were set up by transferring additional protonema at the day 7 onto BCD media to growing for gametophores. The tissues on the "spot plates" were collected at the day 10 for protein extraction of the second time point. Later, the "spot plate" tissues were collected again at the day 21 and used for protein extraction of the last time point. Microsomal protein isolation and western blot analysis were proceeded as described in the Scavuzzo-Duggan et al. (2015).

Co-immunoprecipitation

Co-immunoprecipitation (Co-IP) experiments were performed according to the method from previous studies with some modifications (Desprez et al., 2007; Song, Shen, & Li, 2010b). Squeeze-dried 15-day-old moss tissue (0.5 g) containing mostly leafy gametophores was ground in liquid nitrogen, and the powder was transferred to a 2 mL centrifuge tube with 1 mL of ice-cold IP buffer [20mM Tris.HCl, pH7.5; 150mM NaCl; 5mM $MgCl_{2;}$ 10% sucrose; 1% glycerol; 1mM EDTA; 1.5% CHAPS (Sigma, St. Louis, MO, USA); 1% protease inhibitor cocktail (Sigma, P9599); 1% phosphatase inhibitor mixture 2 (Sigma, P5726), and 3 (Sigma, P0044); and 1% polyvinylpyrrolidone]. The tube was incubated on ice for 30 min and centrifuged at 20,000 x g for 30 min to pellet insoluble debris. The supernatant was transferred to a new 1.5 mL centrifuge tube with 25 μL of Pierce Anti-HA Magnetic Beads (Thermo Fisher Scientific, Waltham MA USA) and rotated (8 RPM) for 50 min on an end-over-end rotator (Thermo Fisher Scientific). Beads were then collected with a magnetic

stand (Thermo Fisher Scientific), and the unbound sample was removed. 400 μL of TBS-T buffer (Scavuzzo-Duggan et al., 2015) was added to the tube and gently mixed. Beads were collected again by magnetic stand, and the supernatant was discarded. This step was repeated twice. For the last wash, 400 μL of ultrapure water was added to the tube and gently mixed. Beads were collected on a magnetic stand, and the supernatant was removed. For elution, 50 μL of 2X SDS-PAGE sample buffer (Scavuzzo-Duggan et al., 2015) and 50 μL of ultrapure water were added to the tube, and gently mixed. The tube was incubated at 95 ℃-100 ℃ for 10 min. Finally, beads were magnetically separated, and initial input (total protein), unbound fraction, wash, and IP eluate were stored at -20^{o}C for up to three months and used for western blot analysis. Gel electrophoresis and western blot using anti-PpCESA3, anti-PpCESA6/7, and anti-PpCESA8 antibodies were carried out as described in Scavuzzo-Duggan et al. (2015).

Statistical analysis

One-way Analysis of Variance (ANOVA) followed by post-hoc Tukey Honest Significant Difference (HSD) test was performed using "R" programming (Vienna, Austria; http://www.R-project.org/) to identify the potential significant difference in each assay.

Supplemental Materials

Table. S1. Primers for amplification of HA-tagged *PpCESAs.*

Table. S2. Peptide antigens, designed to regions of each PpCESA, used to raise specific antibodies for each PpCESA isoform.

Fig. S1: RT-qPCR analysis of *PpCESA* expression in the KO mutants.

Fig. S2. Quantitative analysis of S4B fluorescence intensity in leaf midribs of *P. patens* wild-type (Gd11), *ppcesa8*KO-lox16 (*cesa8*KO), and *PpCESA8pro::HA-PpCESA8* (HA-CESA8).

Fig. S3. Quantitative analysis of S4B fluorescence intensity in leaf midribs of *P. patens* wild-type (Gd11), *ppcesa6/7*KO-lox23 (6/7KO), and *PpCESA7pro::HA-PpCES7* (HA-CESA7).

Acknowledgments

This work was supported by National Science Foundation Award IOS-1257047. Production of monoclonal antibodies for PpCESAs was supported as part of The Center for LignoCellulose Structure and Formation, an Energy Frontier Research Center funded by the U.S. Department of Energy, Office of Science, Office of Basic Energy Sciences under Award Number DE-SC0001090. DNA sequencing and qPCR were conducted using the Rhode Island Genomics and Sequencing Center, a Rhode Island NSF EPSCoR research facility, supported in part by the National Science Foundation EPSCoR Cooperative Agreement EPS-1004057. We also thank Bowen Jiang for assistance with statistics.

Figures

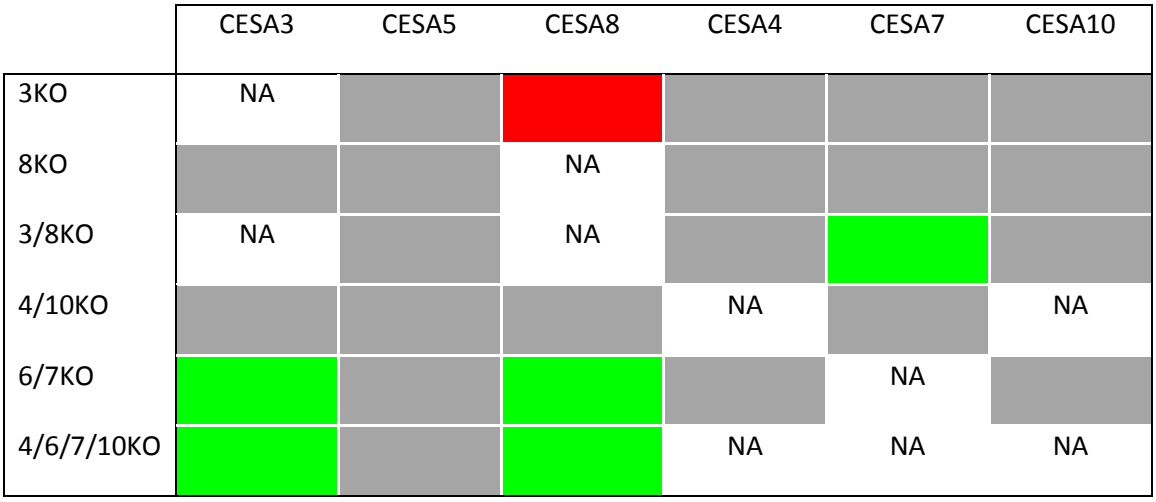

Figure 1: Heat map of *PpCESA* expression in *PpCESA* knockout (KO) mutants. Summary of results from RT-qPCR analysis of RNA isolated from 21-day old cultures of PpCESA KO lines normalized to PpACT and PpVHP refernce genes. Three independent lines of each genotype were tested with two technical replicates. Green=significant down-regulation, $p<0.05$; gray=non-significant differences, $p>0.05$; red=significant up-regulation, $p<0.05$; NA: no expression). Graphs are shown in **supplementary figure 1.**

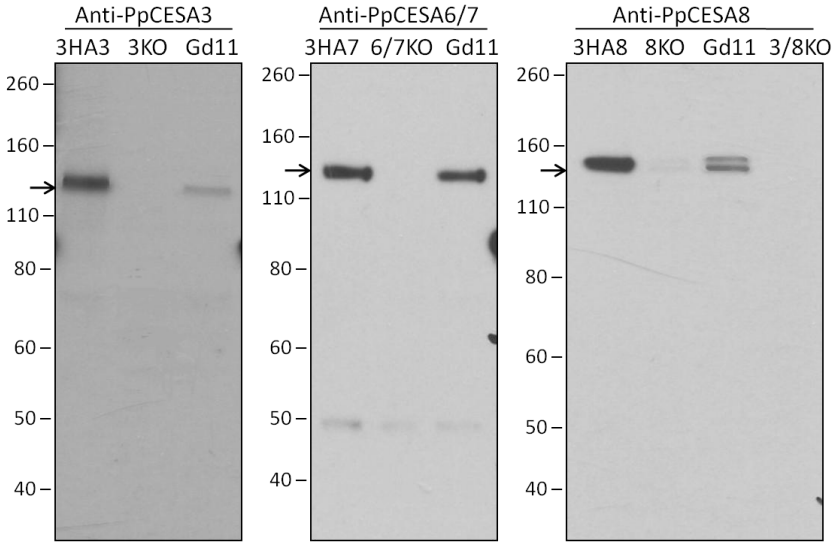

Figure 2: Antibody specificity test. Western blots of microsomal protein extracts from HA-tagged PpCESA overexpression lines (positive control), PpCESA knock out (KO) lines (negative control), and wild-type probed with anti-PpCESA3, anti-PpCESA6/7, and anti-PpCESA8 respectively. Molecular mass markers are given at left in kilodaltons. Black arrows indicate expected position of target bands (~120KD) detected by antibodies. Faint band in 8KO lane, but not 3/8KO line, indicates weak cross reactivity of anti-PpCESA8 with PpCESA3.

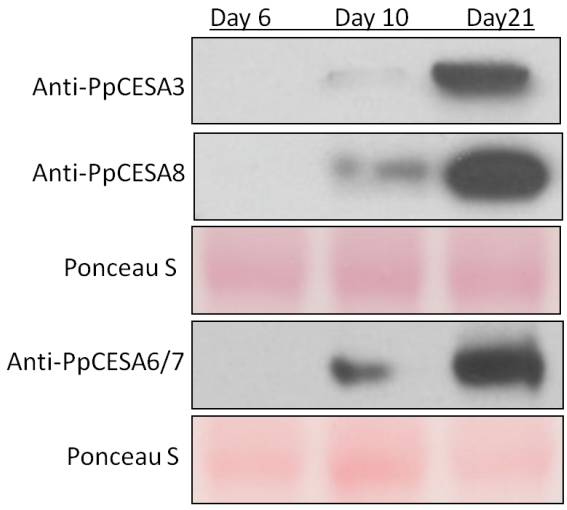

Figure 3: PpCESA protein expression in wild-type *P. patens.* Western blots of microsomal proteins isolated from wild-type *P. patens* cultures and probed with anti-PpCESA3, anti-PpCESA8, and anti-PpCESA6/7. Explants from protonema cultured on solid medium overlaid with cellophane for 6 days were cultured on solid medium without cellophane and harvested after 6 days (protonema only), 10 days (protonema and young gametophores) and 21 days (gametophores). Equal loading of protein (XXX g per lane) was verified by Ponceau S Staining.

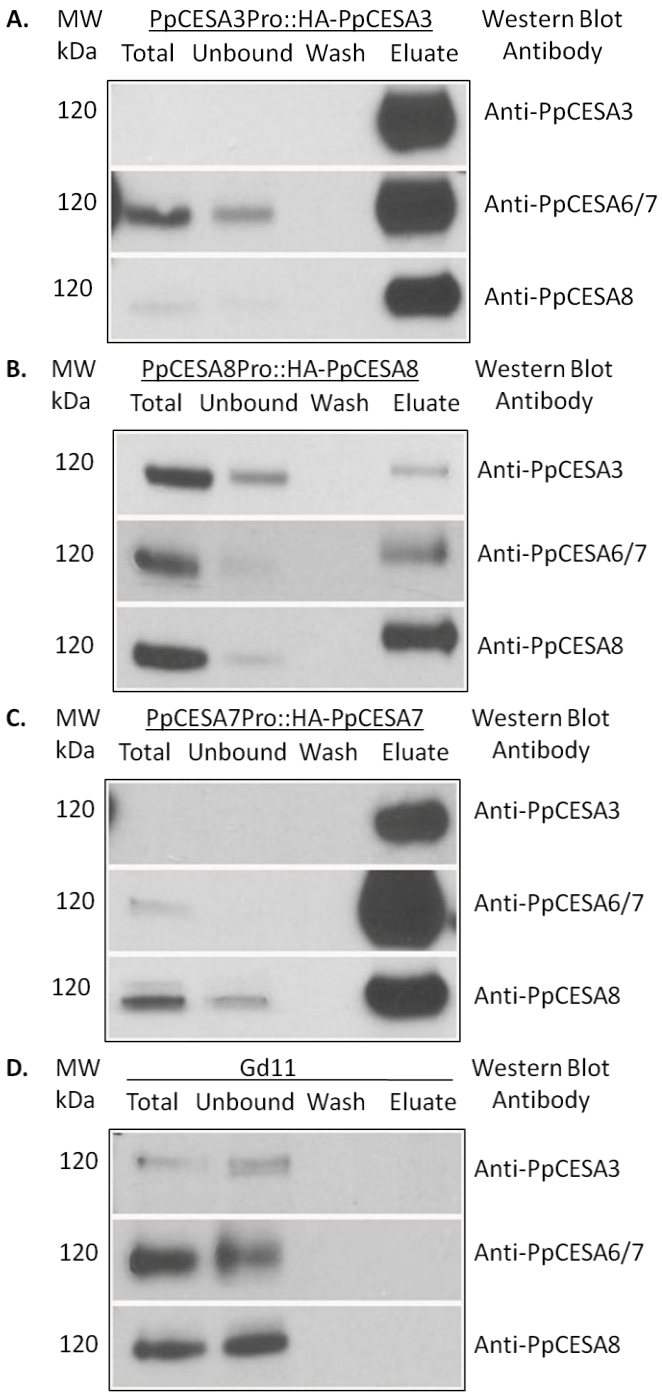

Figure 4: Co-immunoprecipitation (Co-IP) of PpCESAs. Western blots of total protein lysates from lines expressing HA-PpCESAs under control of their native promoters (A-C) and wild-type (D) with unbound, wash and eluate from immunoprecipitation with anti-HA. Blots were probed with antibodies listed on the right of each graph.

References cited:

Arioli, T., Peng, L., Betzner, A. S., Burn, J., Wittke, W., Herth, W., … Williamson, R. E. (1998). Molecular Analysis of Cellulose Biosynthesis in Arabidopsis. *Science*, *279*(5351), 717–720. https://doi.org/10.1126/science.279.5351.717

Bail, A. L., Scholz, S., & Kost, B. (2013). Evaluation of Reference Genes for RT qPCR Analyses of Structure-Specific and Hormone Regulated Gene Expression in Physcomitrella patens Gametophytes. *PLOS ONE*, *8*(8), e70998. https://doi.org/10.1371/journal.pone.0070998

Brown, D. M., Zeef, L. A. H., Ellis, J., Goodacre, R., & Turner, S. R. (2005). Identification of Novel Genes in Arabidopsis Involved in Secondary Cell Wall Formation Using Expression Profiling and Reverse Genetics. *The Plant Cell*, *17*(8), 2281–2295. https://doi.org/10.1105/tpc.105.031542

Burn, J. E., Hocart, C. H., Birch, R. J., Cork, A. C., & Williamson, R. E. (2002). Functional Analysis of the Cellulose Synthase GenesCesA1, CesA2, and CesA3 in Arabidopsis. *Plant Physiology*, *129*(2), 797–807. https://doi.org/10.1104/pp.010931

Carroll, A., Mansoori, N., Li, S., Lei, L., Vernhettes, S., Visser, R. G. F., … Trindade, L. M. (2012). Complexes with Mixed Primary and Secondary Cellulose Synthases Are Functional in Arabidopsis Plants. *Plant Physiology*, *160*(2), 726–737. https://doi.org/10.1104/pp.112.199208

Carroll, A., & Specht, C. D. (2011). Understanding Plant Cellulose Synthases through a Comprehensive Investigation of the Cellulose Synthase Family Sequences. *Frontiers in Plant Science*, *2*. https://doi.org/10.3389/fpls.2011.00005

Delmer, D. P. (1999). CELLULOSE BIOSYNTHESIS: Exciting Times for A Difficult Field of Study. *Annual Review of Plant Physiology and Plant Molecular Biology*, *50*(1), 245–276. https://doi.org/10.1146/annurev.arplant.50.1.245

Desprez, T., Juraniec, M., Crowell, E. F., Jouy, H., Pochylova, Z., Parcy, F., … Vernhettes, S. (2007). Organization of cellulose synthase complexes involved in primary cell wall synthesis in Arabidopsis thaliana. *Proceedings of the National Academy of Sciences*, *104*(39), 15572–15577. https://doi.org/10.1073/pnas.0706569104

Doolittle, W. F. (2012). Evolutionary biology: A ratchet for protein complexity. *Nature*, *481*(7381), 270–271. https://doi.org/10.1038/nature10816

Fagard, M., Desnos, T., Desprez, T., Goubet, F., Refregier, G., Mouille, G., … Höfte, H. (2000). PROCUSTE1 Encodes a Cellulose Synthase Required for Normal Cell Elongation Specifically in Roots and Dark-Grown Hypocotyls of Arabidopsis. *The Plant Cell*, *12*(12), 2409–2423.

Finnigan, G. C., Hanson-Smith, V., Stevens, T. H., & Thornton, J. W. (2012). Evolution of increased complexity in a molecular machine. *Nature*, *481*(7381), 360–364. https://doi.org/10.1038/nature10724

Gonneau, M., Desprez, T., Guillot, A., Vernhettes, S., & Höfte, H. (2014). Catalytic Subunit Stoichiometry within the Cellulose Synthase Complex. *Plant Physiology*, *166*(4), 1709–1712. https://doi.org/10.1104/pp.114.250159

Goss, C. A., Brockmann, D. J., Bushoven, J. T., & Roberts, A. W. (2012). A CELLULOSE SYNTHASE (CESA) gene essential for gametophore morphogenesis in the moss Physcomitrella patens. *Planta*, *235*(6), 1355–1367. https://doi.org/10.1007/s00425-011-1579-5

Harholt, J., Sørensen, I., Fangel, J., Roberts, A., Willats, W. G. T., Scheller, H. V., … Ulvskov, P. (2012). The glycosyltransferase repertoire of the spikemoss Selaginella moellendorffii and a comparative study of its cell wall. *PloS One*, *7*(5), e35846. https://doi.org/10.1371/journal.pone.0035846

Hill, J. L., Hammudi, M. B., & Tien, M. (2014). The Arabidopsis Cellulose Synthase Complex: A Proposed Hexamer of CESA Trimers in an Equimolar Stoichiometry. *The Plant Cell*, *26*(12), 4834–4842. https://doi.org/10.1105/tpc.114.131193

Li, S., Lei, L., & Gu, Y. (2013). Functional analysis of complexes with mixed primary and secondary cellulose synthases. *Plant Signaling & Behavior*, *8*(3), e23179. https://doi.org/10.4161/psb.23179

Livak, K. J., & Schmittgen, T. D. (2001). Analysis of Relative Gene Expression Data Using Real-Time Quantitative PCR and the 2−ΔΔCT Method. *Methods*, *25*(4), 402–408. https://doi.org/10.1006/meth.2001.1262

Manfield, I. W., Jen, C.-H., Pinney, J. W., Michalopoulos, I., Bradford, J. R., Gilmartin, P. M., & Westhead, D. R. (2006). Arabidopsis Co-expression Tool (ACT): web server tools for microarray-based gene expression analysis. *Nucleic Acids Research*, *34*(suppl_2), W504–W509. https://doi.org/10.1093/nar/gkl204

McFarlane, H. E., Döring, A., & Persson, S. (2014). The Cell Biology of Cellulose Synthesis. *Annual Review of Plant Biology*, *65*(1), 69–94. https://doi.org/10.1146/annurev-arplant-050213-040240

Mueller, S. C., & Brown, R. M. (1980). Evidence for an intramembrane component associated with a cellulose microfibril-synthesizing complex in higher plants. *The Journal of Cell Biology*, *84*(2), 315–326.

Nixon, B. T., Mansouri, K., Singh, A., Du, J., Davis, J. K., Lee, J.-G., … Haigler, C. H. (2016). Comparative Structural and Computational Analysis Supports Eighteen Cellulose Synthases in the Plant Cellulose Synthesis Complex. *Scientific Reports*, *6*, 28696. https://doi.org/10.1038/srep28696

Norris, J. H., Li, X., Huang, S., van de Meene, A., Tran, M. L., Killeavy, E., … Roberts, A. W. (2017). Functional specialization of cellulose synthase isoforms in a moss shows parallels with seed plants. *Plant Physiology*. https://doi.org/10.1104/pp.17.00885

Persson, S., Paredez, A., Carroll, A., Palsdottir, H., Doblin, M., Poindexter, P., … Somerville, C. R. (2007). Genetic evidence for three unique components in primary cell-wall cellulose synthase complexes in Arabidopsis. *Proceedings of the National Academy of Sciences*, *104*(39), 15566–15571. https://doi.org/10.1073/pnas.0706592104

Persson, S., Wei, H., Milne, J., Page, G. P., & Somerville, C. R. (2005). Identification of genes required for cellulose synthesis by regression analysis of public microarray data sets. *Proceedings of the National Academy of Sciences of the United States of America*, *102*(24), 8633–8638. https://doi.org/10.1073/pnas.0503392102

Purushotham, P., Cho, S. H., Díaz-Moreno, S. M., Kumar, M., Nixon, B. T., Bulone, V., & Zimmer, J. (2016). A single heterologously expressed plant cellulose synthase isoform is sufficient for cellulose microfibril formation in vitro. *Proceedings of the National Academy of Sciences*, *113*(40), 11360–11365. https://doi.org/10.1073/pnas.1606210113

Robert, S., Mouille, G., & Höfte, H. (2004). The mechanism and regulation of cellulose synthesis in primary walls: lessons from cellulose-deficient Arabidopsis mutants. *Cellulose*, *11*(3–4), 351–364. https://doi.org/10.1023/B:CELL.0000046415.45774.80

Roberts, A., Dimos, C., Budziszek, M., Jr., Goss, C., & Lai, V. (2011). Knocking Out the Wall: Protocols for Gene Targeting in Physcomitrella patens. In Z. A. Popper (Ed.), *The Plant Cell Wall* (pp. 273–290). Humana Press. https://doi.org/10.1007/978-1-61779-008-9_19

Roberts, A. W., & Bushoven, J. T. (2006). The cellulose synthase (CESA) gene superfamily of the moss Physcomitrella patens. *Plant Molecular Biology*, *63*(2), 207–219. https://doi.org/10.1007/s11103-006-9083-1

Roberts, A. W., Roberts, E. M., & Haigler, C. H. (2012). Moss cell walls: structure and biosynthesis. *Plant Physiology*, *3*, 166. https://doi.org/10.3389/fpls.2012.00166

Scavuzzo-Duggan, T. R., Chaves, A. M., & Roberts, A. W. (2015). A Complementation Assay for in Vivo Protein Structure/Function Analysis in Physcomitrella patens (Funariaceae). *Applications in Plant Sciences*, *3*(7), 1500023. https://doi.org/10.3732/apps.1500023

Scheible, W.-R., Eshed, R., Richmond, T., Delmer, D., & Somerville, C. (2001). Modifications of cellulose synthase confer resistance to isoxaben and thiazolidinone herbicides in Arabidopsis Ixr1 mutants. *Proceedings of the National Academy of Sciences*, *98*(18), 10079–10084. https://doi.org/10.1073/pnas.191361598

Somerville, C. (2006). Cellulose Synthesis in Higher Plants. *Annual Review of Cell and Developmental Biology*, *22*(1), 53–78. https://doi.org/10.1146/annurev.cellbio.22.022206.160206

Song, D., Shen, J., & Li, L. (2010a). Characterization of cellulose synthase complexes in Populus xylem differentiation. *New Phytologist*, *187*(3), 777–790. https://doi.org/10.1111/j.1469-8137.2010.03315.x

Song, D., Shen, J., & Li, L. (2010b). Characterization of cellulose synthase complexes in Populus xylem differentiation. *New Phytologist*, *187*(3), 777–790. https://doi.org/10.1111/j.1469-8137.2010.03315.x

Taylor, N. G., Howells, R. M., Huttly, A. K., Vickers, K., & Turner, S. R. (2003). Interactions among three distinct CesA proteins essential for cellulose synthesis. *Proceedings of the National Academy of Sciences of the United States of America*, *100*(3), 1450–1455. https://doi.org/10.1073/pnas.0337628100

Taylor, N. G., Laurie, S., & Turner, S. R. (2000). Multiple Cellulose Synthase Catalytic Subunits Are Required for Cellulose Synthesis in Arabidopsis. *The Plant Cell*, *12*(12), 2529–2539. https://doi.org/10.1105/tpc.12.12.2529

Taylor, N. G., Scheible, W.-R., Cutler, S., Somerville, C. R., & Turner, S. R. (1999). The irregular xylem3 Locus of Arabidopsis Encodes a Cellulose Synthase Required for Secondary Cell Wall Synthesis. *The Plant Cell*, *11*(5), 769–779. https://doi.org/10.1105/tpc.11.5.769

Timmers, J., Vernhettes, S., Desprez, T., Vincken, J.-P., Visser, R. G. F., & Trindade, L. M. (2009). Interactions between membrane-bound cellulose synthases involved in the synthesis of the secondary cell wall. *FEBS Letters*, *583*(6), 978–982. https://doi.org/10.1016/j.febslet.2009.02.035

Tran, M. L., & Roberts, A. W. (2016). Cellulose synthase gene expression profiling of Physcomitrella patens. *Plant Biology*, *18*(3), 362–368. https://doi.org/10.1111/plb.12416

Turner, S. R., & Somerville, C. R. (1997). Collapsed xylem phenotype of Arabidopsis identifies mutants deficient in cellulose deposition in the secondary cell wall. *The Plant Cell*, *9*(5), 689–701. https://doi.org/10.1105/tpc.9.5.689

Yin, Y., Chen, H., Hahn, M. G., Mohnen, D., & Xu, Y. (2010). Evolution and function of the plant cell wall synthesis-related glycosyltransferase family 8. *Plant Physiology*, *153*(4), 1729–1746. https://doi.org/10.1104/pp.110.154229

Supplemental Materials

Table S1. Primers for amplification of HA-tagged *PpCESAs.*

Name	Sequence	Tm (℃)	Amplicon Size (bp)	Description
*HAPpCESA8*attB5	GGGGACAACTTTGTATACAAAAGTTGCGATGGAGTACCCATACGATGTTCCAGATTACGCTATGGAGGCTAATGCGGGCCTGGT	76 ℃	3373	*HA-PpCESA3*
*PpCESA3*attB2	GGGGACCACTTTGTACAAGAAAGCTGGGTGGAGACGTGGTTATTAGTGTTCG			
*HAPpCESA7*attB5	GGGGACAACTTTGTATACAAAAGTTGCGATGGAGTACCCATACGATGTTCCAGATTACGCTATGGAGGCGAATGCAGGGCTGCT	79 ℃	3378	*HA-PpCESA7*
*PpCESA7*attB2	GGGGACCACTTTGTACAAGAAAGCTGGGTATCAACAGTTTATCCCGCACTGCGA			
*HAPpCESA8*attB5	See above	77 ℃	3370	*HA-PpCESA8*
*PpCESA8*attB2	GGGGACCACTTTGTACAAGAAAGCTGGGTATTACAAGCAGGTGAGGCCGCACCG			

Table S2. Peptide antigens, designed to regions of each PpCESA, used to raise specific antibodies for each PpCESA isoform.

Peptide Antigen	Sequence
PpCESA3	CPDHDQEKSSSILSTKDIEKR
PpCESA8	CLDHDYEKSSPIMSTKDIEKR
PpCESA6/7	CVIRQESDGPRPLSN

A

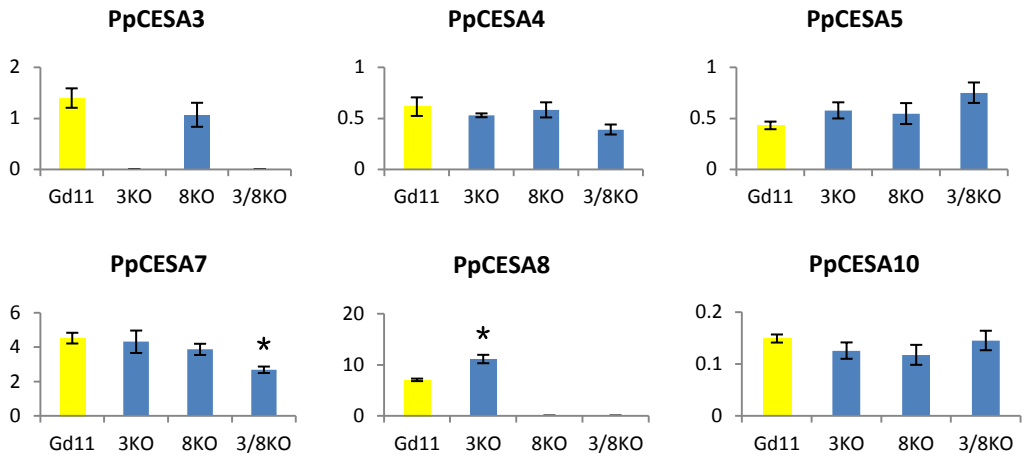

B

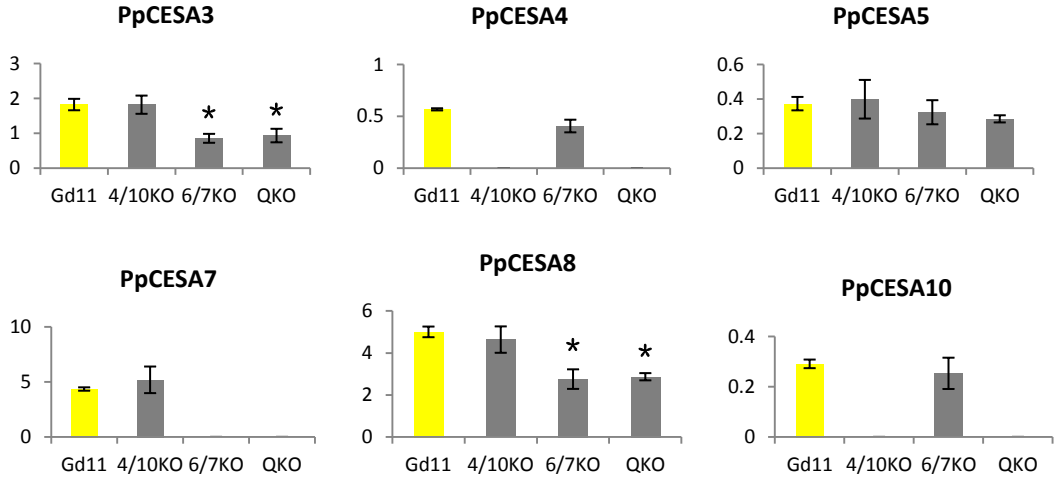

Figure S1: RT-qPCR analysis of *PpCESA* expression in the KO mutants. (A) *PpCESA* expression levels relative to two reference genes (PpACT and PpVHP) in gametophore leaves of three clade-A *PpCESA* KO mutants, *ppcesa3*KO, *ppcesa8*KO, and *ppcesa3/8*KO. (B) The relative expression of *PpCESAs* in the 21-day-old gametophore leaves from the three clade-B *PpCESA* KO mutants, *ppcesa4/10*KO, *ppcesa6/7*KO, and quadruple *ppcesa4/6/7/10*KO (QKO). Numbers on the y-axis represent relative transcript level. *P. patens* lines used as a source of RNA are labeled along the x-axis. Error bars indicate standard error of the mean (n=3). "*": $p<0.05$. Gd11 (wild type): Yellow bar; Clade-A *PpCESA* KO: Blue bar; Clade-B *PpCESA* KO: Gray bar.

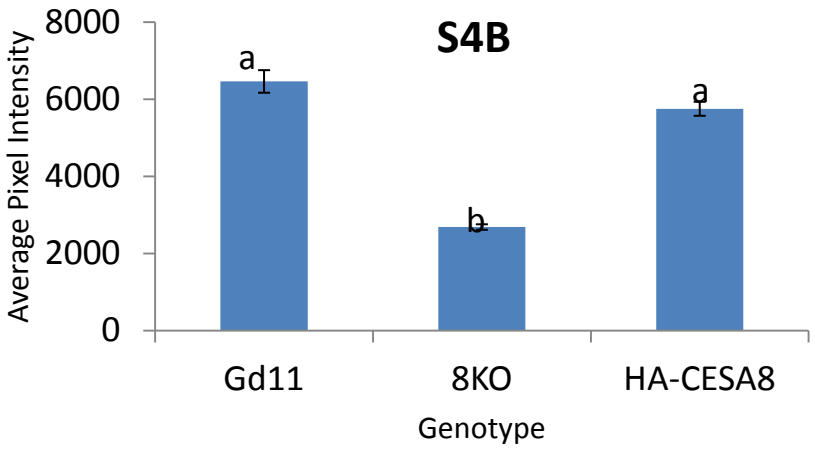

Figure S2: Quantitative analysis of S4B fluorescence intensity in leaf midribs of *P. patens* wild-type (Gd11), *ppcesa8*KO-lox16 (8KO), and *PpCESA8pro::HA-PpCESA8* (HA-CESA8). Fluorescence intensity is significantly lower in *ppcesa8*KO-lox16 compared to wild-type and *PpCESA8pro::HA-PpCESA8*. The *PpCESA8pro::HA-PpCESA8* line was created by transforming the *ppcesa8*KO-lox16 line with the vector driving expression of HA-tagged PpCESA8 using *PpCESA8* native promoter. *PpCESA8pro::HA-PpCESA8* is not significantly different from wild-type indicating that the HA-tagged PpCESA8 successfully restored the function of the native PpCESA8.

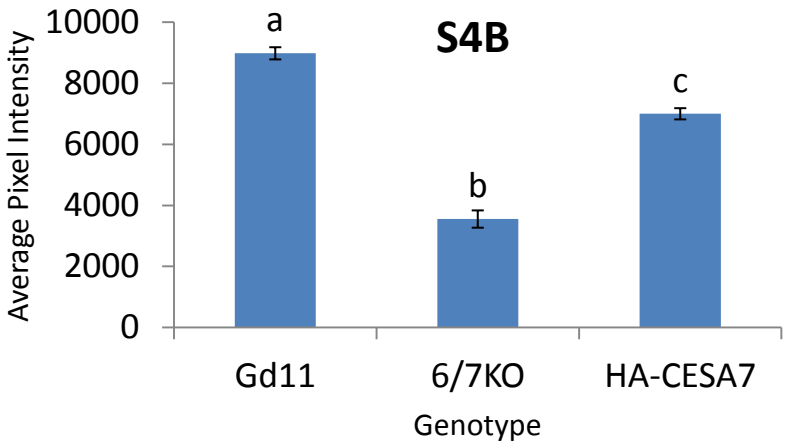

Figure S3: Quantitative analysis of S4B fluorescence intensity in leaf midribs of *P. patens* wild-type (Gd11), *ppcesa6/7*KO-lox23 (6/7KO), and *PpCESA7pro::HA-PpCES7* (HA-CESA7). Fluorescence intensity of wild-type is the highest among the three. *Ppcesa7*KO-lox23 has the lowest fluorescence intensity. *PpCESA7pro::HA-PpCESA7* has an intermediate fluorescence intensity but significantly higher than the intensity of *ppcesa6/7*KO, indicating at least partial rescue by introducing the HA-tagged PpCESA7. The *PpCESA7pro::HA-PpCESA7* line was created by transforming the *ppcesa7*KO-lox23 line with the vector driving expression of HA-tagged PpCESA7 using *PpCESA7* native promoter.